Analysis and Design of Fault Tolerant Axial Flux Permanent Magnet Synchronous Motors

Harold Saavedra Ordóñez

Department of Electrical Engineering

Universitat Politècnica de Catalunya

Thesis submitted in partial fulfillment of the requirements of the degree of Doctor in Electrical Engineering

Barcelona, December 2014

Supervisors

Dr. José Luis Romeral Martínez

Dr. Jordi-Roger Riba Ruiz

Strive for perfection in everything you do, take the best and make it better and if doesn't exist design it

Sir Henry Royce

ACKNOWLEDGEMENTS

I want to thank my supervisors, Prof. José Luis Romeral and Jordi- Roger Riba, for their guidance, support, patience and trust during my studies in the Universitat Politècnica de Catalunya. To the members of MCIA research group, to all of them many thanks for their friendship and support during this time.

Most of all, I owe the greatest debt of gratitude to my family. My parents and brother, without them this wouldn't have been possible. Agradecimientos especiales a la Dra. Martha Cecilia Amaya Enciso que este disfrutando allá donde este.

SUMMARY

Electric vehicles (EVs) are attractive compared to internal combustion engine powered vehicles due to several benefits, including low emissions, higher efficiency, less maintenance costs, stronger acceleration or lower fuel price, among others. EVs require traction motors with especial features, including high efficiency [1], high power and torque density, compactness, precise torque control, extended speed range [2,3] and fault tolerant capability. Sinusoidally fed permanent magnet synchronous motors (PMSMs) are also compatible with adjustable speed ac inverter drives since they can be regulated by applying advanced control techniques, thus allowing enhanced controllability when compared to rectangular-fed brushless dc permanent magnet motors (BLDC) [4].

Axial flux permanent magnet machines (AFPMMs) synchronous motors are disc-shaped and very compact, therefore being a valid solution for direct drive in-wheel applications [5]. The direct drive motor allows simplifying the mechanical structure of the vehicle, thus increasing overall efficiency and minimizing vehicle weight. Due to their disc-like shape, AFPMMs allow different designs, including multiple or single air gaps, with slots or slot less configurations or ironless designs [6]. These types of machines are often classified into internal stator (torus) and internal rotor topologies, depending on the function of the central disk. The torus topology includes both NN and NS configurations, where NS refers to a north pole N facing a south pole S placed at the other side of the stator [7].

Fault tolerance has become an increasingly interesting topic in the last decade, when automation has become more complex. Automotive, together with aerospace, naval, medical and military applications now incorporate a number of machine drives in such a way that the whole system relies heavily upon them. Consequently, when dealing with electric drives used for propulsion, faults can be critical since an uncontrolled output torque may have adverse impact on the vehicle stability, which ultimately can put in risk the passenger's safety. Furthermore a fault tolerant design will increase the reliability on the system; this would be related to the ability to continue the operation at a modest torque to finish the trip, at least reach a repair shop [8].

Electrical motors with more than three phases are usually called multi-phase machines. These systems are distinguished with several benefits which make them proper candidates in applications where safety and reliability is important. Multi-phase motors have the ability of continuing the operation under faulty conditions, since it is only required to change the control algorithm. In comparison with conventional machines, multiphase motors show lower amplitude of currents in each phase, lower torque ripples with higher ripple frequency and reduced operational noise. In fact, five-phase PMSMs produce higher torque (around 15%) and less torque ripple (around 71% less) than initial three-phase PMSMs with the same copper loss [9].

This work focuses on the analysis and optimal electromagnetic design of fault tolerant permanent magnet synchronous motors. The study is mainly based on the research of analytical design procedures and the effect of electrical faults in the motor behavior,

according to the configurations of each machine. The study will be developed by using analytical tools, and validated by applying 2-D and 3-D finite element methods (FEM).

First a brief study about the main achievements regarding the design of fault tolerant machines is made, identifying the possible improvements and main rules of design in this kind of machines.

Then a study focused on the requirements of a fault tolerant design is made, in order to select the appropriate motor configuration. Since the consequences of inter-turn faults can be catastrophic in PMSMs, chapter 3 studies the influence of the winding configuration on the detection of such faults. This detection is based on the analysis of the stator currents and the (zero-sequence voltage component) ZSVC spectra. Several types of winding configurations are selected for analysis i.e. fractional- and integral-slot windings, overlapping- and non-overlapping-windings, single- and double-layer, full- and short-pitch, constant- and variable-pitch windings.

Taking into the fault tolerant tendencies about the redundancy of the system, the study of the effect of inter-turn fault is extended to the five phase machine, thus chapter 3 also deals with a parametric model of the five-phase PMSM that accounts for the effects of inter-turn faults. This parametric model is used to select the harmonic frequencies to be studied to detect such faults. Likewise, the amplitudes of these harmonic frequencies are further analyzed by means of FEM simulations, therefore showing the potential of the proposed system to detect inter-turn faults in their early stage, which is a desirable characteristic for a fault tolerant system.

Chapter 3 also analyzes the demagnetization effect on AFPMM torque. The main objective of this last part is to study the influence of the magnet shape in the performance of an AFPMM working under faulty condition, in order to select the most suitable type of magnet for the design of a fault tolerant machine.

After an exhaustive analysis of the main electromagnetic faults on PMSMs, chapter 4 is focused on the optimal electromagnetic design of an AFPMM. The optimal design is based on a set of analytical equations whose accuracy is validated by means of FEM simulations. Next, to find the optimal solution, the huge set of possible motor solutions is explored by means of computationally efficient optimization algorithms leading to an optimum solution while minimizing the computational burden. The set of analytical equations are solved to obtain the geometrical, electric and mechanical parameters of the optimized AFPMM and several design restrictions are applied to ensure fault tolerance capability, along with the recommended features that have been drawn from the fault analysis study.

Finally, in chapter 4 a dual outer rotor AFPMM with NN configuration for automotive applications is optimized by applying accurate analytical sizing equations and taking into account fault tolerant constraints. For optimization purpose, a multi-objective design strategy is applied, in which the optimization variables are the motor efficiency and power density and ten input geometric and electric parameters are considered, with their respective bounds and constraints. At last the model is verified by applying 3D-FEM simulations and the main performance characteristics are compared.

CONTENTS

LIST OF FIGURES

LIST OF TABLES

ACRONYMS

BLDC: Brushless Direct Current

EMF: Electromotive force

ZSVC: Zero sequence voltage component

AFPMM: Axial flux permanent magnet motor

RFM: Radial flux machine

AFM: Axial flux machines

RFPM: Radial flux permanent magnet

PMSM: Permanent magnet synchronous machine

EV: Electric vehicle

PM: Permanent magnet

DC: Direct current

FCT: Field controlled torus

MMF: Magnetomotive force

WC: Winding configuration

GA: Genetic algorithm

MoGA: Multi-objective genetic algorithm

FEA: Finite element analysis

FEM: Finite element method

FFT: Fast fourier transform

SQP: *S*equential quadratic programming

PWM: Pulse-width modulation

1. INTRODUCTION

This chapter sketches the main lines of investigation on which this thesis research is involved. It introduces the research field of the thesis's contents, details the hypothesis statement and then exposes the main objectives of the work.

With the impulse of global environmental policies, engineers and scientists have been pushed to develop new ways of transportation, thus promoting the use of renewable resources while reducing green-house gases emissions. Consequently, the technologies related to electric vehicles are currently in most of the agendas of academic and industrial research teams. The electrical motor drive is a key part in hybrid and EVs (Electric Vehicles) and the only propulsion system in battery EVs. Traction motors for EVs are different from motors applied in industry. EVs load features include constant torque at low speed operation and constant power at high speed. Motors for EVs must be designed to fulfill several features such as high power, high reliability, high torque density, extended speed range (ratio of maximum speed to base speed usually larger than four), high efficiency over whole work area, shockproof and waterproof among others [1].

PMSMs are currently being widely applied and are being object of an intense research because they accomplish features well suited for new industrial applications as ships traction, or aerodynamic control, and their compatibility with adjustable speed ac inverter drives. Those features present in PMSMs can be summarized in high-speed operation, precise torque control even at low speed, high power to weight ratio, compactness, and high efficiency [2]. One kind of PMSM is the axial flux permanent magnet machine (AFPMM), which due to its characteristic design, allows the electrical motor to be placed inside car wheels or hard drives. The disc shape of the active parts of the motor makes it possible to generate diverse and interchangeable designs, i.e. with single or multiple airgaps, with or without slots or even with a totally ironless armature design [3].

Nowadays, safety is an important factor in the automotive industry. Wheel hub configurations allow independent control of each wheel, thus greatly improving the vehicle stability. However, the introduction of drives containing power electronics jointly with electrical machines also raises the concern about the system reliability and behavior during faults, which, indirectly affects passenger safety.

During the last decade an extensive research work about fault-tolerant operation of three-phase electrical motors and drives has been carried out. The achievements of these works are of special interest for the development of electric vehicles since the electric motor provides all the driving force. From the bibliography it is determined that fault-tolerance can be ensured by using multiphase, and in special five-phase motor drives, with fractional-slot single-layer concentrated windings with physical, thermal, electrical, and magnetic isolation among phases [4]. It has been reported that five-phase machines are intrinsically more advantageous for fault-tolerant operation than three-phase machines are, since in the event of a fault, by using the remaining healthy phases, these machines can offer continue operation [5]. Additional advantages of multiphase motor drives include reduced amplitude and increased frequency of the torque pulsations, reduction of the stator current per phase at the same phase voltage,

reduction of the DC link current harmonics or higher torque per ampere for a given volume of the machine among others [4].

Electric motor manufacturers have always pursued the development of optimized motors, mainly aimed to minimize manufacturing costs and materials, while maintaining overall features and performance. The automotive sector is taking advantage of these improvements, thus enhancing fuel economy in electric and hybrid vehicles and reducing greenhouse gasses emissions. However, the optimal design of electrical machines is a complex issue, since it depends of several constrained design parameters which often are not independent and present nonlinear correlations due to the nonlinear behavior of the active materials. Motor design objectives are often difficult to meet, as for example low-cost and high power density motors with high efficiency are often pursued. Therefore, the optimal design is not unique and a compromised final solution is often selected [6].

Optimization algorithms seek to find the optimal or satisfactory design from a broad set of feasible designs by iteratively analyzing an objective function. Optimization algorithms often analyze the possible values of the design variables, which must be confined within the feasible design space. To this end, the design variables are usually constrained within reasonable values to ensure the achievement of an optimal solution [7]. Optimization algorithms are classified into classical or deterministic and stochastic methods. Whereas the former ones use specific rules to move from one solution to the next one, stochastic algorithms apply probabilistic transition rules, thus usually being faster in locating the final solution [8]. Among stochastic algorithms, genetic algorithms (GA) are applied in a wide spectrum of applications, since GAs are recognized as unbiased optimization methods to sample a large space of solutions [9].

Therefore the objective of this thesis is to analyze the impact of common failures of the in-wheel motors and apply new designs of the electrical machine to achieve improved fault tolerant capabilities. The research first analyzes electromagnetic faults in AFPMMs and the methods to detect such faults. According to the conclusions from this study it proposes a methodology for the electromagnetic design of an AFPMM in order to ensure a safe operation and to minimize the power derating in the event of a fault.

Fig. 1 summarizes the thesis structure.

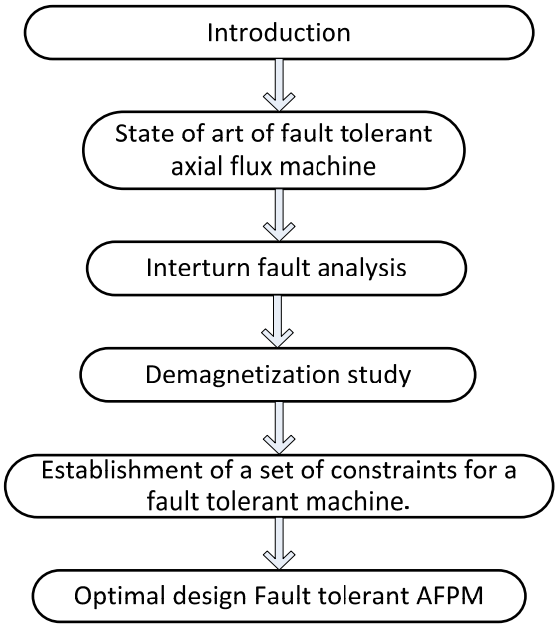

Fig 1. Thesis overview

1.1 OBJECTIVE

The electromagnetic design of a multi-phase axial flux machine and the development of appropriate operational strategies for both healthy and faulty operational conditions while maintaining the required specifications as high as possible for in-wheel motors for electrical vehicles, are the main objectives of the proposed research.

1.2 HYPOTHESIS

An adequate design methodology of a multiphase Axial Flux Permanent Magnet Machine mixing analytical equations, FEM models, with assertive fault tolerant restrictions and appropriate optimization techniques could lead to an optimized special application motor which can provide enough fault tolerant level without losing required power, to avoid self-critical damage and propagation of the fault to nearby devices, thus increasing the reliability and safety level in an electrical vehicle with in-wheel motor configuration.

2. STATE OF THE ART

This section reviews the main characteristics of axial flux machines, stating their benefits for traction applications. It also introduces the main features to take into account in a fault tolerant design, and a review of the different configurations used to assure a fault tolerant characteristic. Finally a comparison between these approaches is carried out and the conclusions about the design guidelines are settled.

2.1 AXIAL FLUX PERMANENT MAGNET MACHINE (AFPMM)

Whereas in radial flux machines (RFM) the airgap is placed in radial direction, in axial flux machines (AFM) the airgap is directed in the axial direction. Additionally, in axial field machines the effective conductors are radially positioned, and the stator and rotor cores are disc-shaped. Conventional radial flux machines have been used almost exclusively since their inventions in 1837 [10].

The history of machine shows that the first machines were axial flux machines although the technology for this kind of machine wasn't improved enough to compete against the radial ones. In 1821, Faraday invented a primitive disc motor which was shaped like an axial flux motor. However, since 1837 when Davenport made the first patent for a RFM, it became the accepted configuration for electrical machines [11].

Careful attention must be given to the design of the rotor-shaft mechanical joint as this is usually the cause of failures in disc type machines [12].

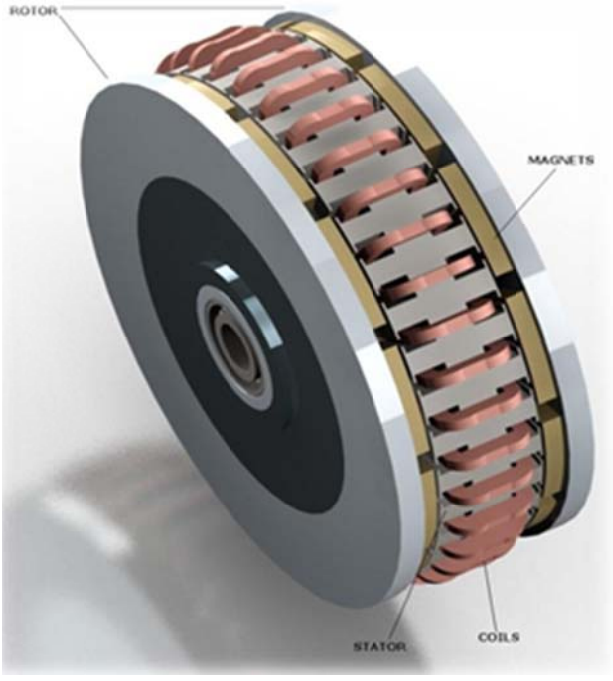

Fig. 2 Axial Flux Permanent Magnet Machine (AFPMM)

- Advantages of AFPMM

The large diameter of the rotor along with its high inertia allows this machine to be used as a flywheel. Since a large number of poles can be accommodated, these machines are ideal for low speed, high torque applications. The disc shape of the active parts of the motor makes it possible to generate diverse and interchangeable designs, i.e. with single or multiple airgaps, with or without slots or even totally ironless armature [13].

- Disadvantages of AFPMM

Whereas the mechanical torque generated by an AFPMM machine is proportional to the diameter raised to the third, in a RFPMM it is proportional to the square of the diameter multiplied by its axial length.

Hence, the benefits of having an axial geometry may be lost as the power level or the geometric ratio of the length to the diameter of the motor is increased [14]. According to [10] the inflexion point is reached when the diameter of the AFPM is two times the length of the RFPM. This limitation is related to single stage machines. However, the power can be increased by stacking several disk machines (stator or rotor) on the same shaft [15].

- Significant Design Parameters in AFPMM

AFPMM machines designed for EV traction require special characteristics. Important parameters which are considered in their design procedure can be summarized as follows [16,17]:

- ✓ Cruising speed range
- ✓ Output power
- ✓ Power to weight ratio
- ✓ Losses and efficiency
- ✓ Heat dissipation capabilities
- ✓ Starting torque
- ✓ Torque to weight ratio
- ✓ Complexity of the rotor and stator structures

The following parameters are the most sensitive design variables which should be considered to maximize the motor performance [18,19]

- The inner and outer radii determine the size of the airgap surface between the stator and rotor of the wheel motor. The airgap surface size greatly

affects the output torque and the motor torque density. Both are important design variables [18].

- The magnet fraction and thickness have a great influence on motor performance, especially the maximum torque, torque ripple, and speed of motor. They are selected as key design variables. The stator tooth fraction has less influence on the maximum torque, and is of little effect on efficiency, ripple, and speed. However, the tooth fraction is an indicator of the crossover area that allows stacking windings in terms of the number of turns and the number of layers. Those determine the maximum allowable magnetomotive force to produce torque. It is therefore selected as a design variable [19].

- The air-gap length is a compromising factor between torque and speed. It is usually made as small as possible to obtain a maximum torque under the constraint of speed limit. Usually, as a first approximation it is set at about 1 mm, which is reasonable for manufacturing as the tradeoff between precision and cost is considered [19].

The number of winding layers, number of turns per tooth, and copper wire diameter determine the value of magnetomotive force, which produces torque but restricts speed [19].The selection of specific parameters values is based mostly in the application requirements and the availability of materials.

2.2 FAILURES IN ELECTRICAL MACHINES

Main faults in electric machines can be divided into:

- Armature Faults

Armature faults are usually caused by winding insulation failure, which frequently happens in the regions where end windings enter the slots. The possible causes of insulation could be due to [20] manufacturing defects, high operation temperature or cooling system malfunction, machine overloading, high voltage transients or vibrations caused by rubbing among others.

Among armature faults there are the ground phase fault and the inter-turn short circuits which are amid the critical faults in electrical machines, since they generate large circulating currents (higher than the rated current) which increase power losses, thus producing excessive heating which may lead to catastrophic failures [21]. In [22] it is stated that by shorting the whole phase through the inverter switches, the short circuit may be confined. However, this procedure is ineffective when a single turn is short-circuited due to its low impedance [22]. It is known that the magnitude of the circulating current depends on the number of shorted turns, their position in the slot and the speed of the machine.

- Permanent Magnetic Faults

For permanent magnet machines, field fault typically refers to a failure in the permanent magnets, where demagnetization is the most common issue. The demagnetization could be uniform over all poles or partial over certain region or poles. Conditions that could cause demagnetization in permanent magnets in a PMSM include [20] high temperature operation, cooling system malfunction, aging or corrosion of the permanent magnets, inappropriate armature current.

- Mechanical faults

Mechanical faults typically refer to bearing failure and eccentricity. The bearing is a mechanical component which consists of two rings and a set of balls rolling between them and it has been recorded as one of the dominant causes for electric machine failure [20]. These failures could be caused by metal fatigue, unbalanced stress, improper installation or Corrosion and contamination among others.

These problems could result in vibrations and noise during machine operation, which are usually measured and processed as diagnosis indicators. Since bearing fault manifests itself as a vibration of rotor and unbalance air gap length, it is sometimes also classified in the eccentricity category [20].Taking into account the electrical motors faults found in reviews and others related publications, Fig. 3 shows the faults distribution in PMSMs according to the main electromechanical fault causes.

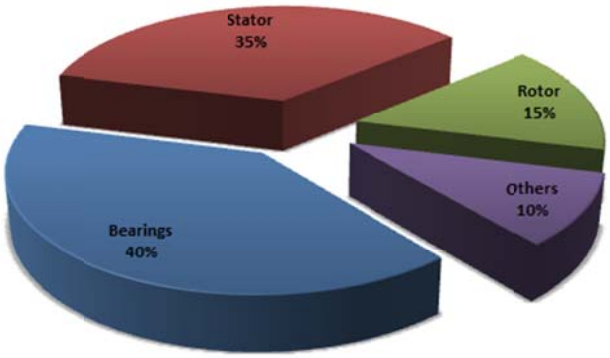

Fig. 3 Faults on PMSM's[23]

2.3 FAULT TOLERANCE IN PMSM

There are different definitions of fault tolerance. In this research, fault-tolerance is defined as the ability of a system to continue operation after a fault in one of the system components has happened. Therefore, in a fault-tolerant system, a single fault in the system does not lead to a system failure [24]. However, the system operation quality may be reduced after a fault. Although according to Fig. 3 there are many potential faults which can occur in a drive system, inevitably within this work the range of faults

under consideration must be restricted. This research focus on stator windings, whose main electromagnetic faults are [25]:

- ✓ Winding short circuit (within a phase)
- ✓ Winding short circuit at the terminals.

As stated in [25] the requirements of an electric machine to be fault tolerant are related to its capability to avoid the propagation of a failure. This includes a previous detection strategy, an isolation of the failure, and the maintenance of (limiting) functionality. Hence, the straightforward solution aims to a redundant and highly isolated system.

But almost all the solutions in machines design are a trade-off, and they depend on the final application, which define the parameters that must be improved. For fault tolerant machines general design lies to one of the following solutions:

- *Complete electrical isolation between phases*

This can be shown to be an essential requirement if continued operation is desired, with either an additional power electronic device or by short-circuiting the winding complete electrical isolation between phases should be performed on both the power converter and the electric machine. For instance, in a star connected system, the voltage in the central point of the star may raise to the DC link voltage, therefore greatly reducing the net torque capability, because a very low current will flow through the windings. The clear alternative is to drive each phase from a separate single-phase bridge. This increases the number of power devices but increases the total power electronic device volt-ampere rating in a less proportion, because each device only needs to withstand the phase voltage rather than the line voltage in star-connected systems [26].

- *Implicit limiting of fault currents*

The most difficult machine fault to accommodate is a winding short-circuit. It is shown that power electronic devices short-circuit failure produces a similar condition to a winding terminal short circuit, except that the fault current flows through the converter as well as the winding. Thus, a phase terminal short-circuit has received particular attention. This leaves two possibilities for dealing with these fault conditions [25].

The first option is to deliberately design the machine with a low per unit inductance; therefore in the case of a short circuit fault, a large fault current will flow through the fault winding. Thus, a winding short-circuit fault will result in a very large winding short-circuit fault current. Consequently, the faulted winding is overheated and subsequently an open-circuit is produced [25].

The second option is to design the machine with a *d* axis per unit inductance approaching 1.0 per unit, so that a phase terminal short circuit will not result in steady state motor currents beyond 1.0 per unit. The thermal limit of the faulted winding will not be exceeded and the short circuit can be accommodated over an extended period [25].

Torque ripple resulting from the short-circuit current in the faulty phase will inevitably be large unless special measures are employed. The second of the above approaches

provides a more reliable fault-tolerant solution, as the first option allows very large per unit fault currents to flow in failed power electronic devices until they turn to open circuit.

- *Magnetic isolation between phases*

Without magnetic isolation, or in other words, if the machine has a large mutual phase-to-phase inductances, the fault currents in one phase induce large voltages in other phases, thus favoring the propagation of the fault [27]. Furthermore, the current flowing in healthy phases supplements the induced voltage in the short-circuited phases due to the magnet magnetomotive force, leading to a worse scenario. [28].

This conclusion shows that for a given un-faulted armature reaction field the single phase short-circuit fault current is substantially greater when there is mutual coupling between phases. It is proved that both the faulted and un-faulted phases perform substantially worse when there is mutual coupling between phases. Therefore the machine should be designed with minimal phase-to-phase mutual coupling, without derating the machine to unacceptable limits [25].

This feature could be found in surface mounted permanent magnet machines, since the airgap flux from the armature reaction is small compared with that generated by the magnets, and a substantial amount of the phase inductance come from the cross-slot leakage flux. The component of magnetic flux from one phase of the stator coils will always link the other phases. Therefore a surface mounted magnet design with a nonmagnetic retaining sleeve combined with relatively deep magnets will greatly reduce the airgap component of the armature reaction field, thus decreasing the mutual coupling among phases [25].

Also in [29] is concluded that the mutual inductances between the phases of an axial flux PM motor are small compared to the self-inductance. The ratio of the gap self-inductance to the mutual inductance is three for the three-phase case.

- *Effective thermal isolation between phases*

When the stator outer surface is well cooled, the dominant temperature rise in the machine is within each slot. By ensuring that each slot contains only a single phase winding the thermal interaction between phases is minimized [25].

- *Physical isolation between phases*

A phase-to-phase fault is especially serious, since it will disable two phases. By placing each winding round in a single tooth, all phase windings are physically separated, thus minimizing the possibility of this kind of fault [25].

- *Number of phases*

The basic criterion used is that the drive should continue to produce rated power in the event of the failure of one phase. Hence, if there are n phases, each phase must be overrated by a fault-tolerant rating factor, F, where $F = n/(n - 1)$. Consequently, if there are three phases, each drive must be overrated by *50%* in order to give full capability when faulted. Clearly, F falls as the number of phases rises, but this must be balanced

against the increasing complexity and cost of a high phase number and the inevitably greater chance of a failure [28].

2.4 CONFIGURATIONS OF FAULT TOLERANT PERMANENT MAGNET MACHINES

In this section summarizes some of the most used configurations used by motor designers in order to achieve fault tolerance in drive systems.

- Memory Motor:

This type of machine can be easily magnetized and demagnetized by using current pulses through the stator windings of short durations without the need for continuous current flow as in the case of typical flux-weakening using a *–Id* current component. This increases machine efficiency [25].

Due to the rotor structure, the load current (*Iq*) cannot demagnetize the magnets. It was also proposed that Al-Ni-Co magnets might be a good choice for this type of machines since they have high remanence (higher power density) and low coercivity (they are easily magnetized and demagnetized). In the limit, the magnets can be fully demagnetized in the case of a fault. One of the key challenges is that the rotor structure is relatively complex and there will be mechanical challenges, especially at high speeds. Another challenge is the control scheme that seamlessly allows magnetizing/demagnetizing of magnets without interrupting the normal machine operation. The machine reaction to transients is another important issue that needs to be addressed. The assumption here is that the power converter is healthy and can be used to inject current pulses to demagnetize the magnets in the event of a fault [30].

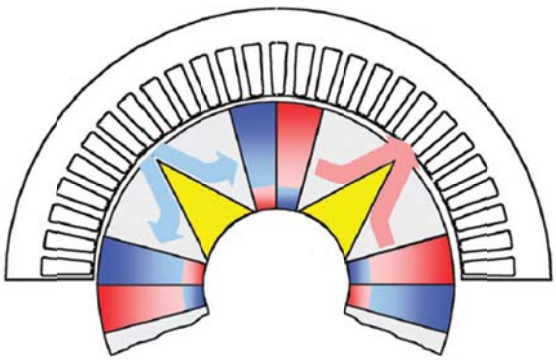

Fig. 4 Memory motors [30].

- Doubly salient and flux switching PM machines

This machine has flux-weakening/fault tolerance capabilities. This topology combines features of switched reluctance machines and brushless DC machines. This type of motor provides improved efficiency, torque density and torque/amp ratio compared to switched reluctance machines and induction machines. It provides cost and fault-

tolerance advantages over brushless PM machines. Another possibility is to have the magnets in the rotor. The machine shown in Fig. 5 has an interior-rotor topology. Another possibility is to have outer-rotor topology, which increases the torque-production capability of the machine [31].

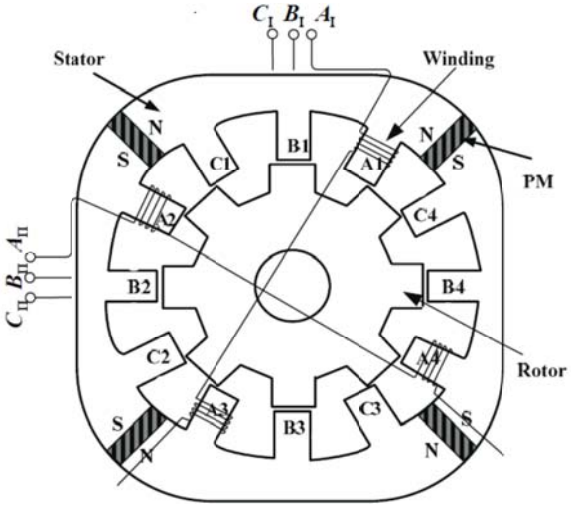

Fig. 5 Doubly salient and flux switching PM machines [31].

- Auxiliary windings

Several ideas involving the use of auxiliary windings on either the stator or rotor sides have been proposed in the literature. Some of these ideas were targeting flux-weakening applications and to the limit completely cancelling the magnet flux in the case of a fault [32].

The excitation current in the auxiliary windings is used to regulate the flux within the machine and to limit or completely cancel the magnet flux when a fault occurs. The disadvantages of this method are the additional weight and power losses due to the auxiliary windings. The auxiliary windings on the rotor side require either brushes with slip-rings or rotating diodes, both of which pose a significant reliability issue. These auxiliary windings will also require a separate power supply [33].

In [34], the use of a toroidal auxiliary DC winding in the stator end region has been proposed (Fig 6). Similar to the previous method, the excitation current in the auxiliary windings is used to regulate the flux within the machine and to the limit completely cancel the magnet under fault occurrence.

This method has the same disadvantages as the previous method. One advantage over the previous method is that the location of the toroid winding allows for a high number of turns and hence a very low excitation current is required to regulate the flux. This helps to reduce the losses and the weight of the auxiliary winding as well as to reduce the burden on the auxiliary power supply.

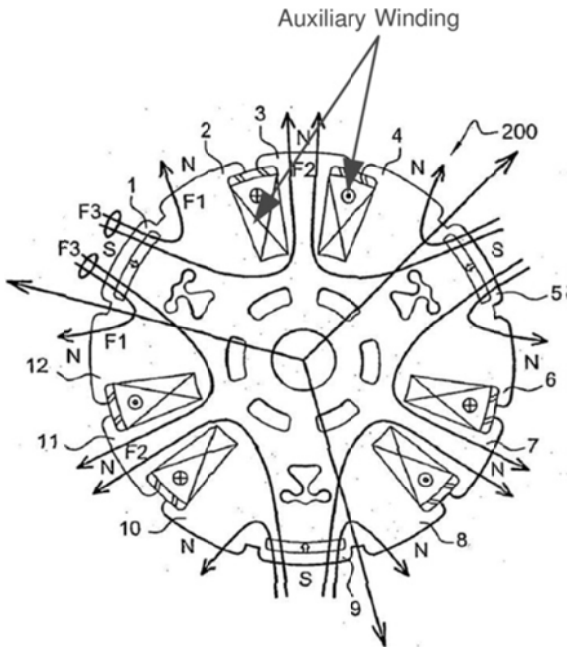

Fig. 6. Auxiliary windings in PMSM [34].

In [35] the auxiliary windings are used in an axial flux machine called Field Control Torus (FCT), where the machine rotor structure is formed by two rotor discs with surface mounted permanent magnets and iron pieces which could act as an electromagnet (Fig 7).

The two disc shaped rotors contain the axially magnetized Nd-Fe-B magnets which are mounted axially on the inner surfaces of the two rotor discs. It should be pointed out that each rotor pole consists of one PM and one iron piece and there exists some space between the magnet and iron piece due to the field winding.

This configuration allows the machine to control the magnetic flux in the airgap by changing the polarization of the iron poles. it means that the excitation of the DC field winding of one polarity tends to increase the flux on both inner and outer portions of the rotor pole thus strengthening the magnetic field and increasing the flux linking the stator armature windings.

Excitation of the field winding with the opposite polarity will decrease the flux in the consequent poles in both inner and outer portions of the rotor disc thereby achieving field weakening.

Simulation results prove that nearly 87% control range can be obtained at no load and a 51% control range can be obtained at full load [35]. It was also observed that the control of the FCT machine could be achieved without any demagnetization risk of the magnets because of the airgap flux control.

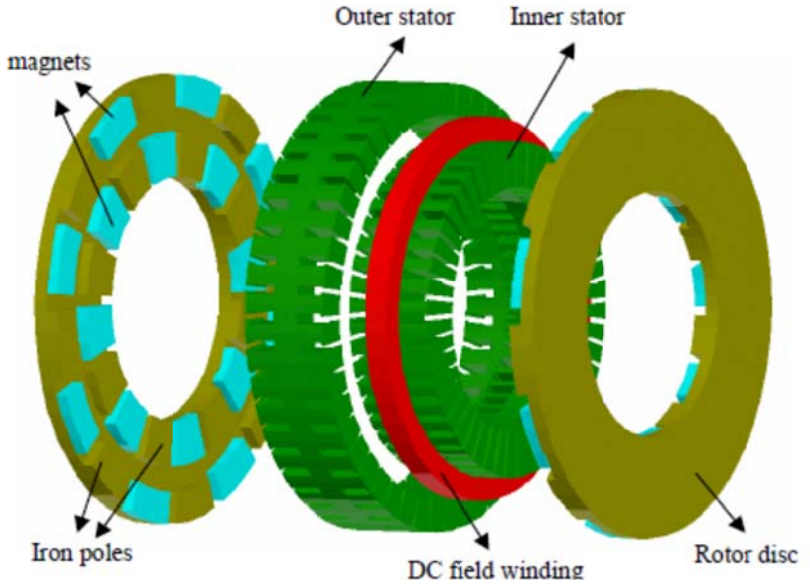

Fig. 7. AFPM with DC winding [35].

- Transverse flux PM machines

Another type of PM machines that has been investigated for fault tolerant drives is the transverse flux PM machines. These machines have good fault-tolerant capability since they offer high inductance, which limits the fault current. On the other hand, transverse flux machines are challenging in terms of manufacturing. They also suffer from low power factor and are unsuitable for applications requiring wide constant power speed ratio [36].

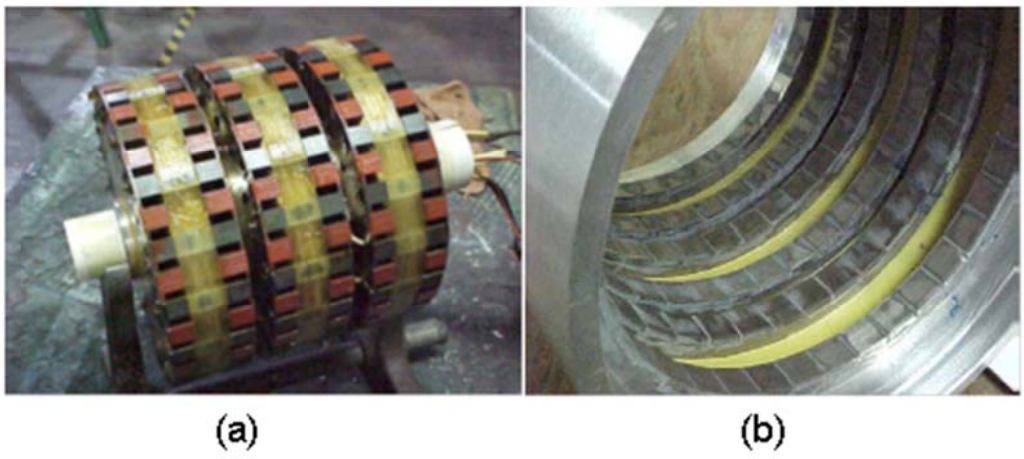

Fig.8. Transverse flux PM machines (a) stator (b) rotor [36].

- Multiphase Machines

Redundancy is a key factor in fault tolerant designs. Redundancy can be attained by increasing the number of phases, i.e. greater than 3. In fact one of the most important properties of multiphase machines is their ability to continue operating after the loss of one (or more) phase(s) without problems, something that cannot be achieved with

conventional machine configurations [36]. Under the faulted phase(s) conditions, the available degrees of freedom that exist in multiphase machines are effectively utilized for an appropriate post-fault operating strategy [37,38].

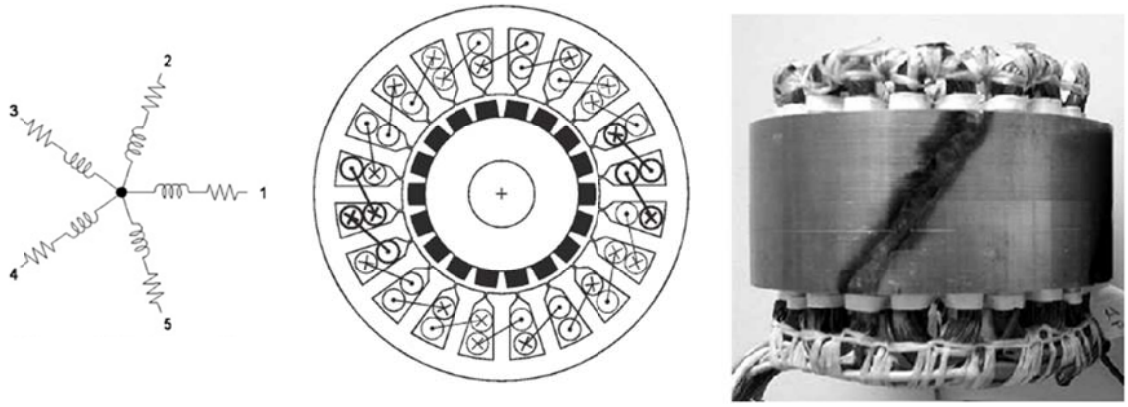

Fig. 9. Five-phase machine 20-slot 18-pole [39].

In a multiphase machine a stator winding can be designed to yield either near-sinusoidal or quasi-rectangular MMF distribution, by using distributed or concentrated windings, for all ac machine types. Also the stator winding of an *n*-phase machine can be designed in such a way that the spatial displacement between any two consecutive stator phases equals $\alpha = 2\pi/n$, in which case a symmetrical multiphase machine results. This will always be the case if the number of phases is a prime number. However, if the number of phases is an even number or an odd number that is not a prime number, stator winding may be realized in a different manner, as *k* windings having *a* subphases each (where $n = a \cdot k$). Typically, $a = 3$ (although $a = 5$ exists as well) and $k = 2, 3, 4, 5 \ldots$, in such a case the spatial displacement between the first phases of the two consecutive *a* subphase windings is $\alpha = \pi/n$, leading to an asymmetrical distribution of magnetic winding axes in the cross section of the machine (asymmetrical multiphase machines) [40].

The basic idea of all fault-tolerant strategies is that a multiphase machine can continue operating, thus generating a rotating magnetic field as long as at least 3 phases remain un-faulted or two if the star neutral point remains accessible. The strategies developed depend to a large extent on the application of the multiphase drive. The simplest case arises in multiphase machines with $n=3 \cdot x$ $(x=1, 2, ..)$ phases, with *k* isolated neutral points. If one phase fails, the complete set of three-phase windings, in which the fault has taken place, is taken out of service. For example, in the case of a six-phase machine with two isolated neutrals, if one phase fails the whole three-phase winding is taken out of service. But this configuration implies a special inverter topology with redundant switches. The machine can however continue to operate without any control algorithm modification using the remaining healthy three-phase winding, of course with the available torque reduced to one half of the rated torque (assuming no increase in the current in the healthy phases).This is a great solution in traction applications [40,41].

Listed below there are some of the advantages of multiphase over three-phase machines:

- ✓ The stator excitation in a multiphase machine produces a field with a lower space-harmonic content, so that the efficiency is higher than in a three-phase machine [42].

- ✓ Multiphase machines are less susceptible than their three-phase counterparts to time-harmonic components in the excitation waveform. Such excitation components produce pulsating torques at even multiples of the fundamental excitation frequency [43].

- ✓ For the given machine output power, the use of more than three phases enables splitting the power among a larger number of inverter legs, thus enabling use of semiconductor switches of lower rating [40].

- ✓ Utilization of multiphase motor drives also enables improvement in the noise characteristics, when compared to three-phase motor drives [44].

There are some experimental approaches to this kind of machines like in [45, 46], where a multi-phase drive was designed, in which each phase was considered as a single module. The effect of each module on the others was minimized. Therefore, in the case of failure of one module, the rest of the system maintains continuous operation. In [25] it is pointed out that the electrical, magnetic, thermal, and physical interaction between the phases should be minimized. Electrical isolation is an essential requirement in the event of a short circuit in the power device or phase winding. Otherwise, the star point in a star connected system may increase to the DC link voltage and there will be no net torque capability. One solution is to supply each phase from a single phase bridge. However, in this case the number of switches will be doubled. Physical separation must be guaranteed by placing each winding round a single tooth. To meet the requirement for magnetic isolation of PM machines, each coil also should be wound around a single tooth, thus eliminating overlapping end-windings [40].

A multiphase fault tolerant strategy clearly needs an inverter topology compatible with the machine design. The fault tolerance in a converter is attained by using redundant power electronics devices. The most used configuration is the additional phase leg fault-tolerant inverter topology, which consists of four inverter legs, as shown in Fig. 10. In this topology, each phase leg contains a series fuse between the upper and lower power devices to isolate the leg.

Each phase winding of the machine is connected to a normally closed side of an electronic switch, while the open terminals of three switches are tied to the center point of the inverter fourth leg. Under normal operation, the fourth leg is not activated. If a fault occurs in any of the inverter phase legs, that leg is isolated by means of the switch, and the phase winding is connected to the additional phase leg and activated. This topology provides rated post-fault power without the overrating of power devices, and the output torque is similar to that of the pre-fault operation without excessive torque ripple. The drawback of this configuration is that it doesn't consider a machine fault, thus in the case of an inter-turn short circuit the drive can't use the additional leg to fed the motor [47].

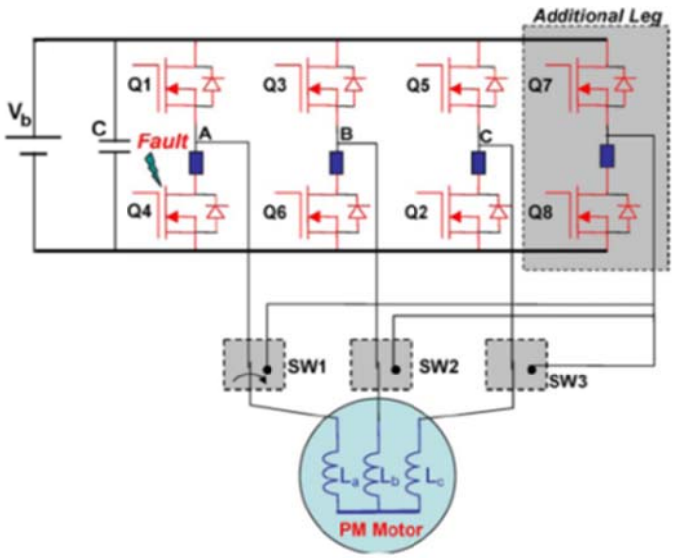

Fig. 10. Additional leg inverter topology with a standard machine [47].

When dealing with multiphase machines a configuration with a neutral point available is the most effective. According to [40], this architecture shows that neutral point gives better characteristics in post-fault operation since the single neutral point enables utilization of all the remaining healthy phases.

The neutral leg inverter fault-tolerant topology consists of four inverter legs; three of which are connected to the phase windings of a PM machine, while the fourth leg is connected to the neutral of the machine, as shown in Fig 11. Each inverter leg consists of two electronic switches with a series connected fuse.

This fuse is used to isolate the leg when a simultaneous short circuit of both devices occurs (shoot through). The machine phase windings and the neutral are connected to their respective inverter legs by means of electronic switches. Under normal operation, the neutral leg is not activated.

If a short- or open-circuit fault occurs in any one of the inverter phase legs, the gate pulses of the healthy device are disabled, and the corresponding phase switch is opened while simultaneously activating the neutral leg. This topology delivers 66.7% rated power during post-fault operation [47].

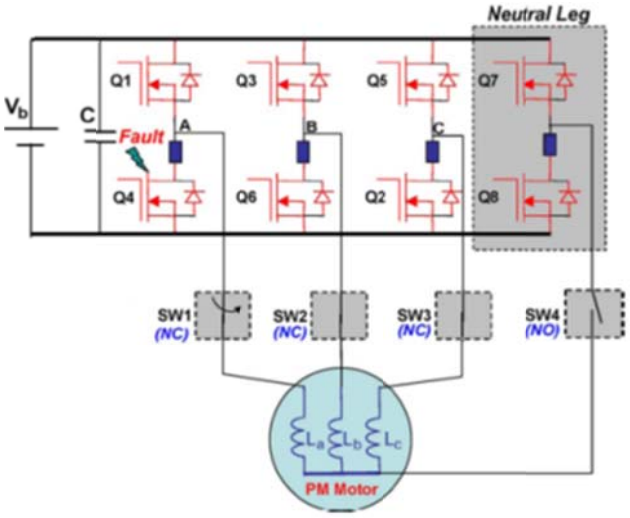

Fig. 11. Three-phase machine with neutral leg inverter [47].

- General comparison of fault tolerant methods applied to PM machines

Table 1 provides a general comparison of the various methods of fault tolerance machine configurations [32]. In the table, a qualitative comparison is done, with the following meaning: '↑' indicates improvement over the average performances, '=' indicates no change or medium performances, and '↓' indicates reduction of performances. This comparison has been made from the fault tolerance point of view. Comparisons regarding others issues could not give the same conclusion.

Table 1. High-level comparison of different fault tolerant methods applied to PMSM's

	Cost	Power density	Reliability	Efficiency	Mature technology
Multiphase machine	↑	↑	↑	↓	↑
Memory motors	=	↓	↓	=	↓
Doubly salient and flux switching pm machines	↑	↓	↑	=	↑
Auxiliary windings	↓	↓	↓	↓	↓
Transverse PM machine	↓	↓	↓	=	↓

As it can be seen in Table 1, the use of a multi-phase machine and the application of a control method from the converter side is the most promising method so far. These systems do not add any additional dead weight under normal condition compared to the other methods, all of which require additional components/weight, which are idle under normal operation.

With regard to the machine design, the essential conclusions are that the machine should have (i) a surface mounted magnet rotor design, (ii) a one per-unit armature self-inductance, (iii) each winding wound around a single tooth and (iv) only one phase winding per slot. The first two conclusions appear to be in conflict because a surface

mounted magnet machine generally has a low per unit reactance. However, the key to achieve these requirements is to design a machine with a large leakage inductance by controlling the depth and width of the slot opening. So the main restriction on any fault tolerant design must achieve a high value of leakage inductance [25].

2.5 OPTIMIZATION APPLIED TO PMSM DESIGN

The field of optimization has grown rapidly during the past few decades. Many new theoretical, algorithmic, and computational contributions of optimization have been proposed to solve various problems in engineering and management. Recent developments of optimization methods can be mainly divided into deterministic and heuristic approaches. Deterministic approaches take advantage of the analytical properties of the problem to generate a sequence of points that converge to a global optimal solution. Heuristic approaches have been found to be more flexible and efficient than deterministic approaches, however, the quality of the obtained solution depends in great amount in the programmer ability to enclose the solutions set. With the increasing reliance on modeling optimization problems in real applications, a number of methods for optimization problems have been presented. Among heuristic algorithms, genetic algorithms (GA) are applied in a wide spectrum of applications, this thesis uses GAs which are recognized as unbiased optimization methods to sample a large space of solutions [48].

In the design of an electric motor, characteristics such as the motor performance, cost, reliability, and manufacturing have to be considered, in order to achieve a market competitive product. Besides a varied set of solutions should be calculated making the design process a multivariable and multimodal problem. Moreover electric machines have a large number of design parameters and most of them behave in a nonlinear way. Therefore obtaining an optimized design is a challenging task because of the high number of sets of possible solutions involved. The joint use of accurate analytical sizing equations combined with the application of optimization algorithms based on artificial intelligence can help researchers and engineers to obtain an improved and faster solution of this complex problem.

When applying optimization algorithms to motor design is of great importance to define the most accurately possible the restriction of the system, in order to avoid unreal solutions and excessive calculation times. Also the number of design variables must be chosen wisely in order to find an suitable solution, if the number of variables is too large the algorithm will consume a lot of time slowing down the design process, on the contrary if minimum variables are chosen, the possible solution will get narrowed and global maximums may not be reached [49].

Since Huang in 1999, developed the sizing equation for AFPMM but did not present the optimized size of the machines, many approaches to an optimized design methodology for AFPMM has been taken. For example, Aydin *et al.* developed optimum-sized AFPMM machines for both TORUS and AFIR topologies, but only two parameters (diameter ratio and air-gap flux density) were considered as optimization variables, with the optimization performed through shape modification [7]. Yang et al, [50] introduces a multi-objective design of an AFPMM seeking a high torque density for an e-scooter,

using an own developed code the optimizer Multi-functional Optimisation System Tool. In [51] Lim et al, derive an algorithm to minimize the cogging torque in AFPMM, the optimization method is based in the niching genetic algorithm, and use FEA as samples generator. Mahmoudi et al, show a design methodology based in genetic algorithms (GA) and FEA, in which pursue to reach a high density topology for a 1 kW AFPMM TORUS [53]. In [54] investigate the torque density of radial, axial and transverse flux machine topologies, using a 10-kW motor as a primarily design. The motors are designed employing in-house analytical dimensioning tools and MATLAB GA multi-objective optimization tool.

2.6 CONCLUSIONS

From the review of the state of the art in fault tolerant electrical machines for traction purposes, the following conclusions can be drawn:

- The axial flux permanent magnet machine is a good candidate for such applications due several appealing characteristics including high power density, high torque at low speed or compact design. In additions, due to the disc shape design of axial flux machines, they are well suited to be used in in-wheel applications.
- Surface mounted permanent magnet machines with the coils winded around a single tooth, and 1 per unit armature reactance, provide an extra degree of fault tolerance capability.
- Multi-phase machines and specifically five-phase machines are especially suited for fault tolerant applications, therefore a five-phase axial flux permanent magnet machine is proposed.
- Since electrical faults are concentrated in the stator, a short-circuit faults are especially harmful, it is highly desirable to select a winding configuration which allows both, detecting such faults while making it difficult its propagation.
- From the bibliographic review it is proved that FEM simulations allow predicting the machine behavior, so they are highly suitable to assist the design of electrical machines. In addition the bibliography shows that the FEM method is also compatible with the optimal design of electrical machines when applying suitable strategies to avoid highly intensive computational loads.

3. ELECTRICAL FAULTS ANALYSIS

After the conclusion achieved in the previous chapter, from an electric design point of view, the only fault whose effects can be minimized with a proper design is a short-circuit fault. Due to this reason, in order to select the most suitable motor configuration for a fault tolerant system, it is highly desirable to study the effect of such kind of fault in a permanent magnet machine. It is well known that short circuits can lead to demagnetization faults in permanent magnet machines, therefore it is also interesting to analyze the magnet shapes more suited to lower the impact of such faults.

The first part of the chapter shows the characteristics of several machines of the same power rating but with different winding configurations. Next, a comparison of the current and ZSVC frequency signatures of the analyzed motors under healthy and faulty condition is described. The second part studies an inter-turn fault in a five phase machine with a fractional winding, where it is proved the adaptability of the fault detection method stated in the first part. Finally, it is modeled an axial flux machine with different sets of magnets shapes and the torque quality is compared, thus selecting the magnet shape most suited to minimize the effects of demagnetization faults.

3.1 INTER-TURN FAULT IN PMSMS

Stator windings short circuits are among the most frequent faults in electrical machines. They are often originated by inter-turn short circuit faults. So, inter-turn short circuits are among the most potentially destructive electrical faults in ac machines. According to [55] inter-turn faults cause most of the insulation failures in electrical motors.

In the case of permanent magnet synchronous motors (PMSMs), the magnitude of the short circuit current is greatly influenced by the actual speed, the number of short-circuited turns and the insulation resistance between the short-circuited turns. In [56] it has been shown that inter-turn faults may generate large circulating currents through the shorted turns which magnitude may be several times that of the rated current. Additionally, this circulating current increases linearly with the actual speed of the PMSM. The circulating currents generate winding overheating, thus compromising the insulation integrity of the neighboring turns. This effect also increases the copper loss in the machine and the permanent magnets temperature, which in turn may produce an increase of the stator currents [57]. Since the line currents are often little affected by this large circulating current [56] it makes difficult the action of the protective overcurrent relays. Therefore, inter-turn faults may progress into severe faults such as coil-to-coil short circuits which in turn may develop into phase-to-phase short circuits and phase-to-ground faults [58]. These faults show a fast evolution, are very destructive and may irreversibly damage the machine insulation. To prevent serious machine damage it is highly desirable their detection at the earliest [59], in order to avoid propagation and allow the system to reconfigure for a fault functioning condition.

Inter-turn short circuit faults typically occur during actual machine operation. Consequently, to detect such faults in their early stage, it is of paramount importance to

perform an online monitoring of some relevant electrical variables and to carry out a fast fault diagnosis of the machine condition [60].

3.1.1 Inter-turn Faults in PMSMs with Different Winding Configurations

For a fault tolerant design, a fault must be detected on time in order to let time to the control drive could to take appropriate actions to minimize the effect of such fault. Extensive research has been developed to detect inter-turns faults in permanent magnet machines, but minimal has been done in order to compare the effect of a fault depending on the winding configuration. In this section a comparison between several windings configurations under faulty conditions is made to determine which one could be the optimal for a fault tolerant design.

It is recognized that PMSMs with stator windings with higher number of slots per pole and per phase (q) generate more sinusoidal MMF distributions and back EMF waveforms, while producing lower torque ripple and power loss [61]. Conversely, fractional-slot non-overlapping windings usually exhibit higher harmonic content in the armature reaction field and a slightly lower winding factor [62]. However, they show appealing features, including short end-turns, minimization of copper volume and Joule loss, as well as reduced manufacturing costs [61].

Table 2 shows the main parameters of the analyzed winding configurations.

Table 2 Summary of the analyzed stator windings configurations

	Analyzed windings configurations (WC)					
Features	**WC1**	**WC2**	**WC3**	**WC4**	**WC5**	**WC6**
Slots/pole/phase (*q*)	1/2	1+1/4	1+1/4	3	3	1
Poles pairs (*p*)	8	4	4	2	2	3
Slots number	24	30	30	36	36	18
Turns per phase	384	200	200	144	144	144
Layer type	Double	Double	Single	Single	Double	Single
Short pitch	No	Yes	No	No	Yes	No
Variable pitch	No	No	Yes	No	No	No
Overlapping windings	No	Yes	Yes	Yes	Yes	Yes
Series-connected stator pole pairs	8	4	4	2	2	3
Symmetric winding	Yes	Yes	No	Yes	Yes	Yes
Number of shorted turns in phase *a*	8	6	6	4	4	4
Ratio between faulty and healthy turns	2.08%	3.0%	3.0%	2.78%	2.78%	2.78%

In order to analyze the effect of inter-turn faults in PMSMs, the stator currents and ZSVC harmonics of different PMSMs with six winding configurations when operating under healthy and faulty stationary conditions (WC are investigated by means of two-dimensional finite element method (2D-FEM) simulations.

To compare the results, all analyzed configurations have the same percentage of shorted turns, which is about 2-3%. It is worth noting that a change in the fault severity may affect the amplitude of some of the harmonic frequencies. However, the characteristic harmonic frequencies already present in the stator currents and ZSVC spectra are not affected. Hence, the conclusions of this study are valid under different fault severities.

As shown in Table 2, the analyzed machines include fractional- and integral-slot windings, overlapping and non-overlapping, single- and double-layer, full- and short-pitch and series-connected coils. However, this work does not analyze parallel-connected coils since the authors of this work found no significant differences in the stator currents and ZSVC spectra between series- and parallel-connected coils. Furthermore this thesis does not analyze delta-connected windings since they are less applied in three-phase PMSMs than wye-connected windings because the third-harmonic currents circulating around the delta-connection generate extra torque ripple and Joule losses [63]. To simulate the short circuit faults, some turns in phase *a* are short-circuited through a fault resistance R_f which models the insulation failure. Its value depends on the fault severity, so when the fault evolves to a full inter-turn short circuit, R_f decreases towards zero. It is shown in Fig. 12, which depicts a particular winding configuration in which each phase comprises three series-connected coils.

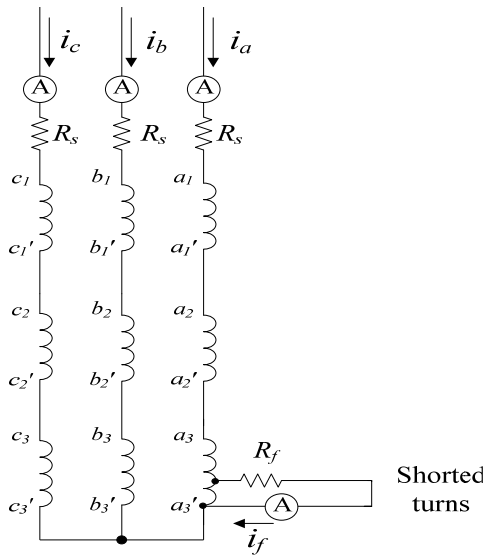

Fig. 12. Diagram of the modified stator windings including the shorted turns, the insulation resistance and the circulating fault current i_f.

The results presented in this section have been obtained by means of 2D-FEM simulations under stationary load and speed conditions. It is worth noting that FEM simulations allow carrying out an accurate analysis of electric motor operating characteristics and therefore designing fault diagnosis schemes for different machine configurations [64].

3.1.1.1 The Detection Method Based On the Stator Currents

According to [56], the severity of an inter-turn short circuit fault increases linearly with the PMSM speed and rises with the percentage of shorted turns in a certain phase. At high speed operation, the circulating current i_f shown in Fig. 12 may be much greater than the rated current. Therefore, it may irreversibly damage the machine if no corrective action is taken. This large fault current originated by inter-turn short circuit faults may have a measurable impact on the stator currents spectra.

As stated in [65], the spectrum of the fault current i_f usually contains the fundamental electrical frequency and its odd multiples, including a significant third harmonic component for a three phase system. The amplitudes of these harmonics are greatly influenced by the permanent magnets geometry [66]. Since the stator currents are affected by the circulating current i_f, a third harmonic component appears in the stator currents spectra [65] and the amplitudes of the odd multiples of the fundamental supply frequency may change. It should be pointed out that this set of fault frequencies emerges in both constant speed and transient conditions. However, under transient speed conditions, the frequency (position or rate) and amplitude of the fault harmonic frequencies may change depending on the motor operating conditions. Consequently in some cases it is difficult to diagnose inter-turn faults from the analysis of the stator currents spectra. For this purpose the ZSVC-based method is also analyzed in this work.

3.1.1.2 The Detection Method Based on the ZSVC

In this section it is assumed that the effects of inter-turn short circuit faults may be detected by monitoring the harmonic content of the ZSVC. As explained, the stator currents spectra may be influenced by the motor drive, thus hindering the diagnosis based on the analysis of the harmonic content of the stator currents. However, when measuring the ZSVC as shown in Fig. 13, this acquisition is decoupled from the motor drive effects [66].

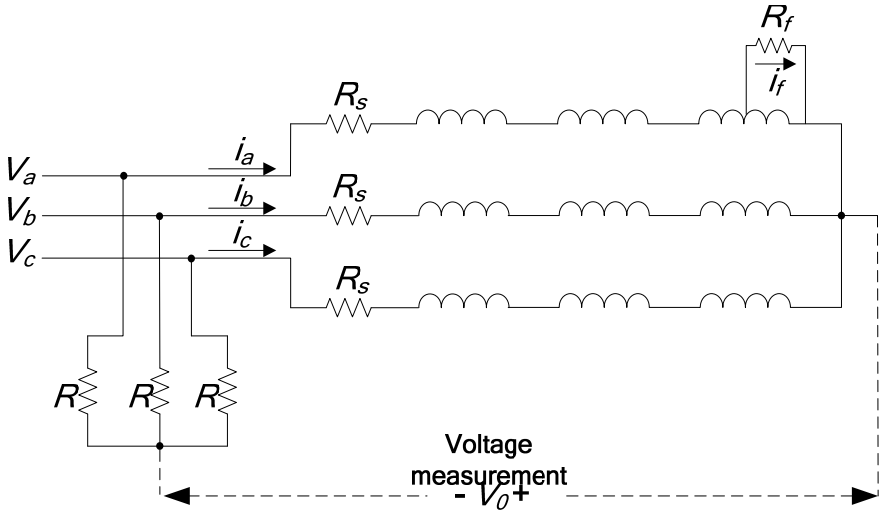

Fig. 13. Strategy applied to measure the ZSVC. Diagram of the PMSM stator including the stator windings connections, the shorted turns in phase *a* and the three-phase resistive network used to generate an artificial neutral point. The analyzed PMSMs have *n* short-circuited inter-turns out of *N* in phase *a*.

Fig. 13 shows the system applied in this section to measure the V_0 ZSVC. From an experimental point of view, a low cost three-phase balanced resistive network must be used to perform this measurement. It creates an artificial neutral point on the drive side. Additionally a voltage sensor is required to measure the V_0 voltage. The span of this sensor should be selected according to the amplitude of the ZSVC, which is usually much lower than the phase-to-neutral voltage. This system may provide enhanced resolution of the harmonic frequencies compared to the method based on the analysis of the stator currents, especially at low speed operation. This fact was corroborated experimentally in [67].

The ZSVC may be expressed as [14],

$$V_0 = \frac{1}{3}\mu R_s i_f + \frac{1}{3}\mu(L+2M)\frac{di_f}{dt} - \frac{d\lambda_{PM,0}}{dt} \quad (1)$$

According to (1), in the case of a PMSM with inter-turn faults, the V_0 ZSVC is greatly influenced by the circulating current i_f, which has a demagnetizing effect [56]. The most contributing term in (1) is the one containing the time derivative of the magnetic flux generated by the permanent magnets [66]. This term presents an important third harmonic component, due to the particular geometry of the rotor magnets. As a consequence, the fundamental frequency of the V_0 ZSVC corresponds to the frequency of the third harmonic of the voltage source. In addition, the first two terms in (1) are also influenced by the circulating fault current i_f. The main component of the fault current spectrum is the fundamental harmonic of the supply frequency [66]. Additionally, the fault current spectrum contains the odd multiples of the supply frequency, including the third harmonic, because of the flux harmonics effects. Therefore, the same harmonics (first, third, fifth and seventh among others) are expected to emerge in the ZSVC spectrum of a faulty machine three phase machine.

3.1.1.3 Comparative Results When Analyzing Different Windings Configurations

In this section the behavior of the six winding configurations (WCs) detailed in Table 2 are analyzed. Both the stator currents and ZSVC spectra of these configurations are obtained by means of 2D-FEM simulations.

All FEM models were performed and simulated using the FLUX-2D® 10.4 software package. The 2D-mesh of all models contains about 8700 triangular elements, as shown in Fig. 14. The speed of all analyzed motors was selected so that the rated electrical frequency was 50 Hz for all motors. Simulations were performed taking into account a sampling frequency of 1.5 kHz and 2048 points were simulated, thus leading to a resolution of 30 points per electric cycle. Therefore, the fast Fourier transform (FFT) of such waveforms provides 1024 points, with a frequency resolution of 0.73 Hz.

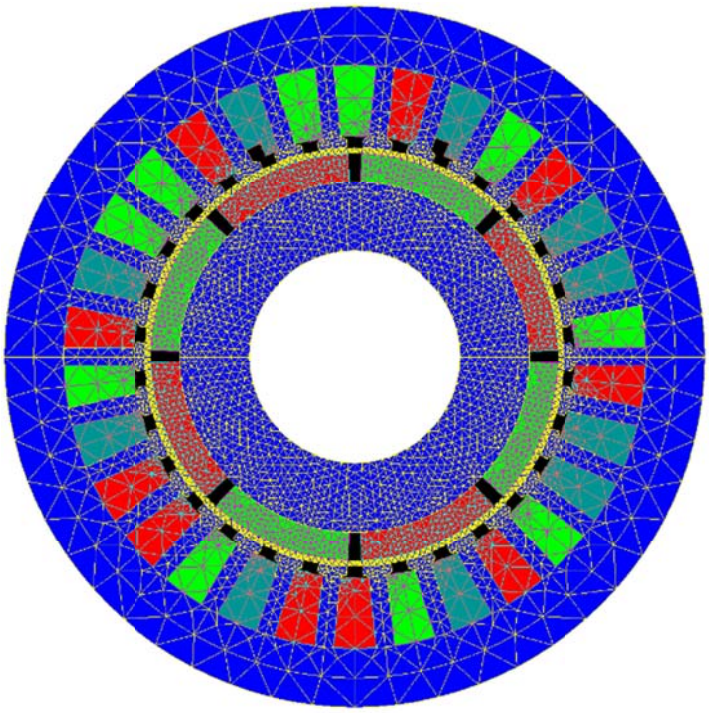

Fig. 14. FEM model of configuration WC3.

A. Series-connected coils

The stator currents spectra of the six healthy and faulty analyzed configurations are shown in Fig. 14, which correspond to the configurations detailed in Table 2. Note that all configurations analyzed have all the coils of a phase winding connected in series.

Results from Fig. 15 clearly show the obvious impact of the winding configurations on the spectral composition of the stator currents. A summary of these results is presented in the following lines:

-. WC1 (q = 1/2, double layer): the amplitudes of the constructive harmonics (fifth and seventh) increase significantly in the case of the faulty motor and new triplen harmonics (third and ninth) appear in the currents spectra.

-. WC2 (q = 1+1/4, constant-pitch): in the case of a faulty PMSM, the constructive harmonics amplitudes (fifth and seventh) increase significantly and new harmonic components multiples of three (third, sixth and ninth) appear in the currents spectra.

-. WC3 (q = 1+1/4, variable-pitch): in the case of the faulty motor, the fifth harmonic current amplitude decreases, but the amplitude of the seventh harmonic increases. Furthermore, new integer harmonics (third, fourth, sixth and eighth) appear in the currents spectra of the faulty motor.

-. WC4 (q = 3, full-pitch): when dealing with a faulty machine, the amplitudes of the constructive harmonics (fifth and seventh) increase, and new triplen harmonics (third and ninth) appear in the stator currents spectra.

-. WC5 (q = 3, short-pitch): in the case of a faulty machine, the fifth harmonic current amplitude increases but the amplitude of the seventh harmonic decreases. In addition,

new triplen harmonics (third and ninth) appear in the stator currents spectra of the faulty PMSM.

-. WC6 (q = 1, full-pitch): in the case of a faulty machine, the fifth and seventh harmonic current amplitudes experiment a slight decrease. New triplen harmonics (third and ninth) appear in the stator currents spectra of the faulty PMSM.

From the results presented in Fig. 15 it is concluded that in the case of inter-turn faults, when dealing with integral- or fractional-slot windings (with either $q < 1$ or $q > 1$), new harmonic components appear in the currents spectra. Within these fault frequencies, important third harmonic amplitude emerges in the currents spectra for all analyzed winding configurations. Therefore, inter-turn faults may be diagnosed through the analysis of the third harmonic component of the stator currents, and provide a suitable configuration for a fault tolerant scheme.

Fig. 16 shows the ZSVC spectra for the six analyzed series-connected winding configurations for both healthy and faulty machines. Results from Fig.16 show the impact of the winding configurations on the ZSVC spectra.

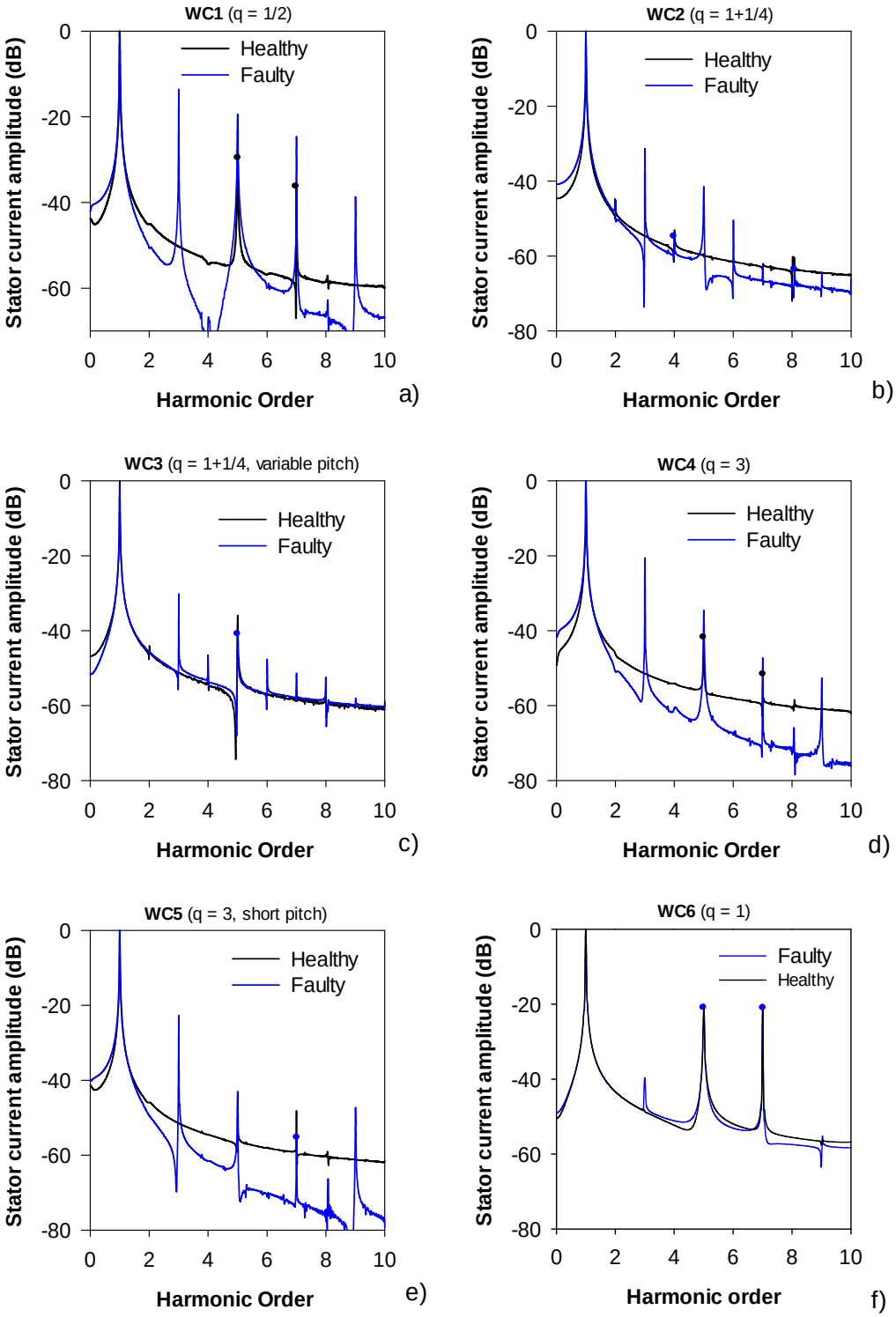

Fig. 15. Stator currents spectra of the analyzed healthy and faulty PMSMs with different series-connected winding configurations. a) WC1. b) WC2. c) WC3. d) WC4. e) WC5. f) WC6. The spectra are normalized with respect to the rated current.

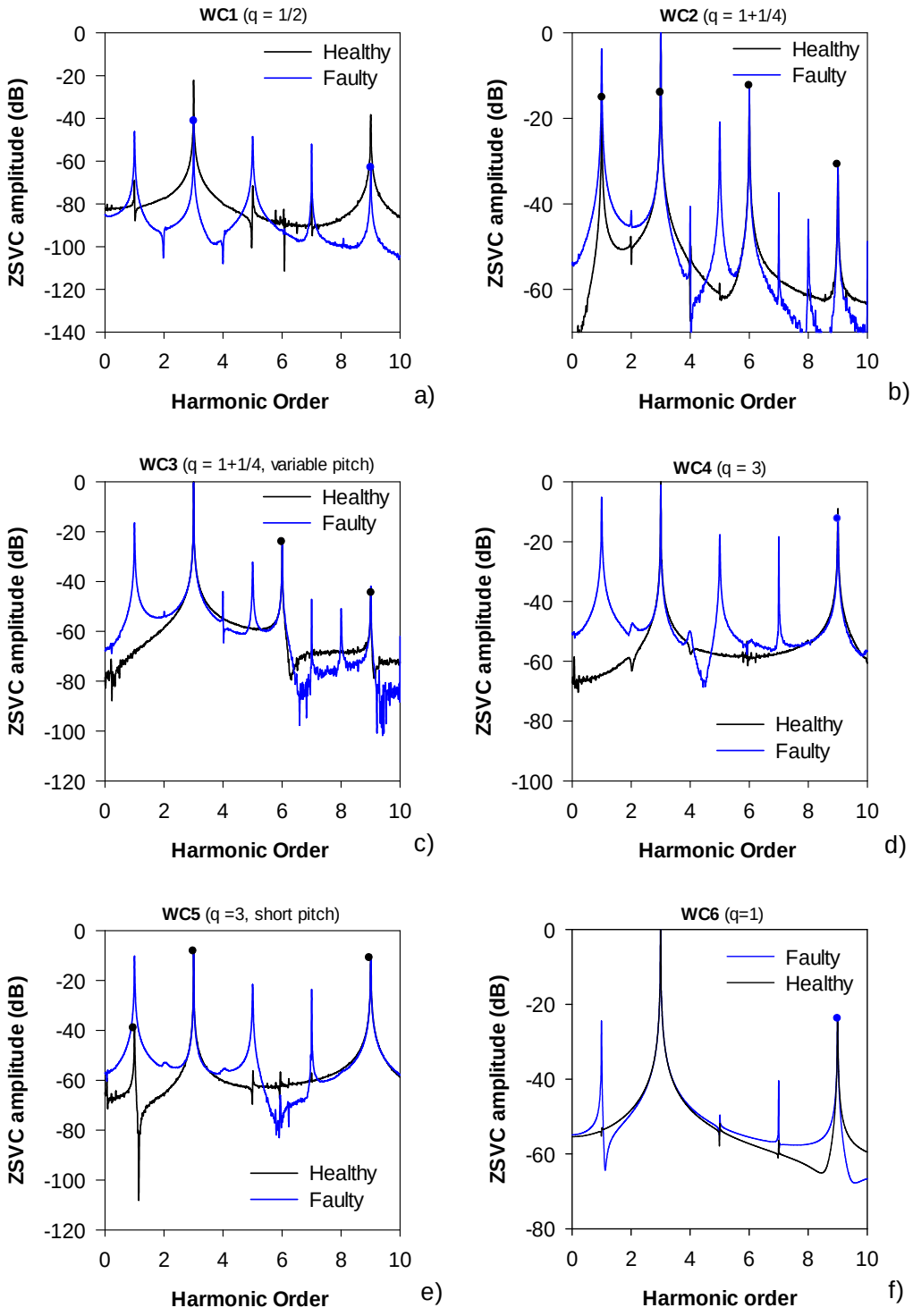

Fig. 16. ZSVC spectra of the analyzed healthy and faulty PMSMs with different series-connected winding configurations. a) WC1. b) WC2. c) WC3. d) WC4. e) WC5. f) WC6. The spectra are normalized with respect to 10% of the phase voltage at the analyzed speed.

A summary of the results presented in Fig. 16 is as follows:

-. WC1 (q = 1/2, double layer): the amplitudes of the ZSVC constructive harmonics (third and ninth) decrease significantly in the case of a faulty PMSM, and new odd harmonics appear in the ZSVC spectrum (fifth and seventh). Furthermore, the first harmonic amplitude experiments a sharp increase.

-. WC2 (q = 1+1/4, constant-pitch): in the case of a faulty PMSM, the constructive harmonics amplitudes (third, sixth and ninth) decrease slightly when compared to those of a healthy machine. Additionally, new harmonic components appear in the ZSVC spectrum (fourth, fifth, seventh and eighth) and the amplitude of the first harmonic experiments a sharp increase.

-. WC3 (q = 1+1/4, variable-pitch): when analyzing a faulty machine, the constructive harmonics amplitudes decrease slightly and new harmonics appear in the ZSVC spectrum (first, fourth, fifth, seventh and eighth).

-. WC4 (q = 3, full-pitch): in the case of a faulty machine, the constructive harmonics amplitudes (third and ninth) decrease slightly. New odd harmonic components appear in the ZSVC spectrum (first, fifth and seventh), which have large amplitudes.

-. WC5 (q = 3, short-pitch): in the case of a faulty machine, the constructive harmonics amplitudes (third and ninth) decrease slightly. New odd harmonics components appear in the ZSVC spectrum (fifth and seventh) and the first harmonic amplitude experiments an important increase.

-. WC6 (q = 3, short-pitch): similarly to the case of a full-pitch motor, in the case of a faulty motor the amplitudes of the constructive harmonics (third and ninth) decrease slightly. In addition, new odd harmonics components appear in the ZSVC spectrum (first and seventh), whereas the amplitude of the fifth harmonic increases.

After analyzing the results presented in Fig. 16, it is concluded that in the case of three phase PMSMs with inter-turn faults and for all the analyzed winding configurations, fifth and seventh new harmonic components emerge in the ZSVC spectrum. Additionally, faulty machines present large first harmonic amplitude when compared with that of the healthy ones. Therefore, by analyzing the amplitude of the first, fifth and seventh ZSVC harmonics, such faults may be detected on time.

B. Current injection through the shorted turns

In order to analyze the mechanism from which new harmonic components appear in both the stator currents and ZSVC, a specific FEM model has been build. As shown in Fig. 17, it consists of a current source that injects a pure sine-wave current, the fault current i_f, which only contains the fundamental harmonic of the voltage supply. Only the WC3 model was simulated, since this configuration presents a broad set of fault harmonics in both the stator currents and ZSVC spectra.

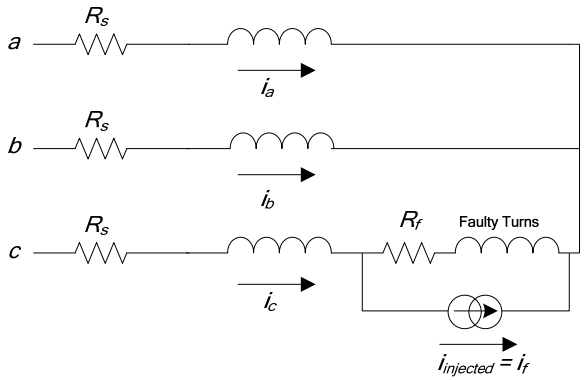

Fig. 17. Injected current through the faulty turns.

As explained, the fault harmonics that emerge in the stator currents and the ZSVC spectra due to inter-turn faults are related to the harmonics of the fault current i_f, which in turn are a consequence of the back EMF waveform.

Fig. 18 shows the back EMF spectrum induced in the six shorted turns of configuration WC3 when a pure sine-wave current is injected as displayed in Fig. 17. It has been simulated when the PMSM acts as a generator under no load conditions. Results from Fig. 18 clearly indicate that the back EMF spectrum induced in the shorted turns contains odd and even harmonics. However, the content of the back EMF spectrum in a complete phase winding may change depending on the configuration and connection type of the stator windings [68].

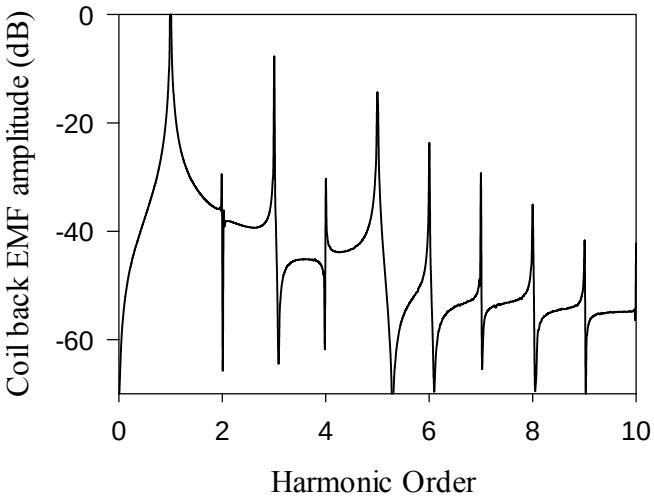

Fig. 18. Back EMF spectrum induced in the faulty turns of configuration WC3 in open circuit conditions as shown in Fig. 17.

Fig. 19 compares the spectrum of the injected sinusoidal current with that obtained from FEM simulations supposing realistic inter-turn short circuit conditions. An important feature of the i_f current when considering realistic fault conditions, is that it contains the same harmonics than those found in the spectrum of the back EMF induced in the faulty turns. Therefore, it may be concluded that the harmonic pattern in the back EMF is transmitted to the fault current i_f.

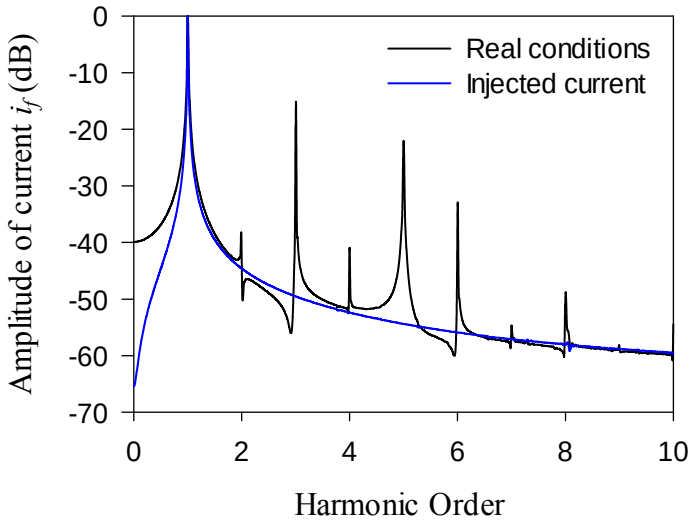

Fig. 19. Injected and real fault current i_f through the faulty turns.

Fig. 20a shows that the stator current spectrum obtained by injecting the sinusoidal current i_f in the shorted-turns does not contain new fault harmonics. It is important to highlight that there is no trace of the third harmonic. However, when considering the real inter-turn fault, the stator current spectrum is more complex and an important third harmonic component emerges. These results indicate that the third harmonic of the stator currents is originated by the third harmonic of the fault current i_f. Similarly, Fig 20b shows that as in the case of the stator currents spectrum, the ZSVC spectrum obtained when injecting a pure sinusoidal current i_f only contains the first harmonic and the harmonics multiples of three. However, when considering a real fault condition, the ZSVC spectrum is more complex since it contains all the harmonic components already present in the back EMF spectrum of the shorted turns.

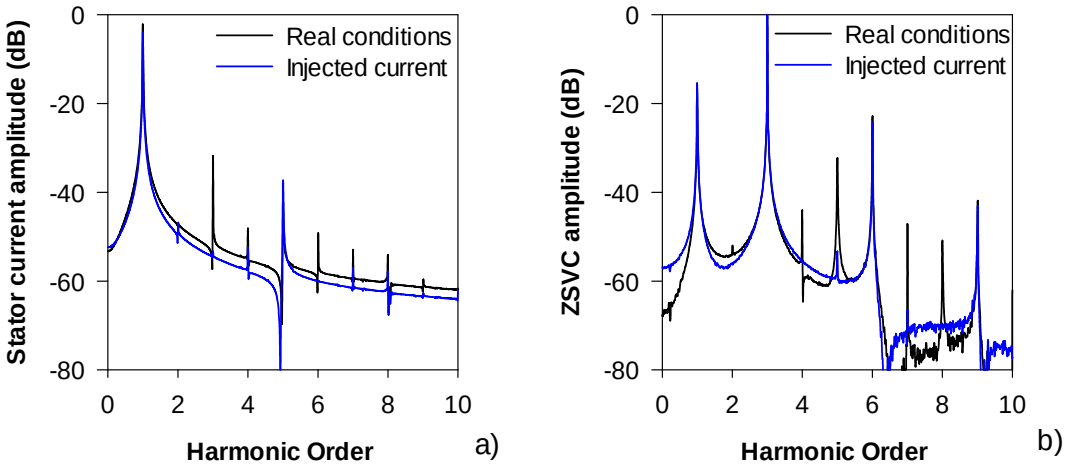

Fig. 20. Stator currents and ZSVC spectra obtained by injecting a sinusoidal current i_f and considering real inter-turn short circuit conditions in configuration WC3. a) Stator currents spectra. b) ZSVC spectra.

Note that the simulations of the faulty PMSM have been conducted using a fault resistance R_f = 0.07 Ω, a value in the range found in [69]. However, this resistance may influence the results presented in this section. Fig. 21 studies its effects by analyzing a

variation from 0.02 Ω to 0.14 Ω It proves that the fault harmonic amplitudes of both the stator currents and ZSVC decrease with increasing values of the fault resistance R_f, thus lowering the sensitivity of the method. However, as shown in Fig. 21, the ZSVC based method is less sensitive to changes in R_f than the system based on the stator currents.

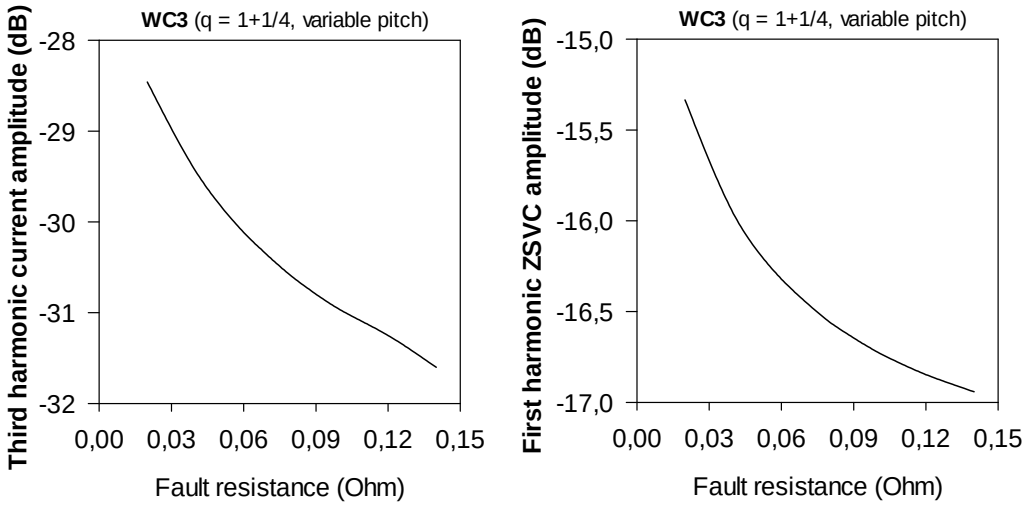

Fig. 21. WC3 configuration. Effect of the fault resistance R_f on the fault harmonic amplitudes. a) Third harmonic amplitude of the stator current. b) First harmonic amplitude of the ZSVC.

3.1.1.4 Experimental Validation of the FEM Model

To validate the FEM model with experimental data a 380-Vac PMSM from ABB manufacturer driven by an ABB DGV-700 power converter was used. This motor has 3 phases, 6 poles, 144 turns per phase, rated speed of 6000 r/min and rated current of 2.9 A and corresponds to WC6. During the experimental tests, both motors are loaded with an identical PMSM that acts as a load, driven by its own power converter.

Fig. 22 shows the experimental and simulated back-EMF spectrum of the analyzed machine when running at 6000 r/min as a generator with the stator windings in open circuit.

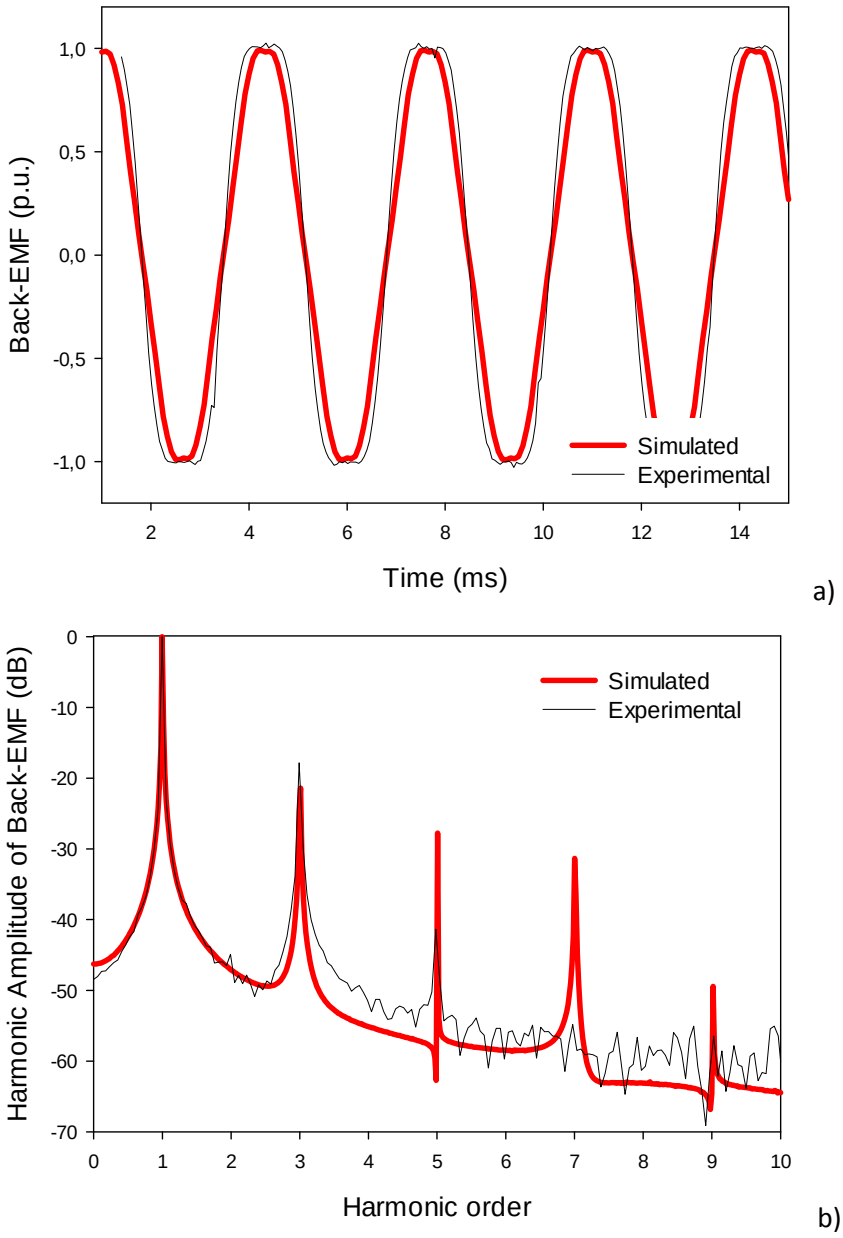

Fig. 22. Back-EMF of a healthy PMSM when operating at 6000 r/min. a) Back-EMF in p.u. versus time. b) Back-EMF amplitude in dB versus frequency.

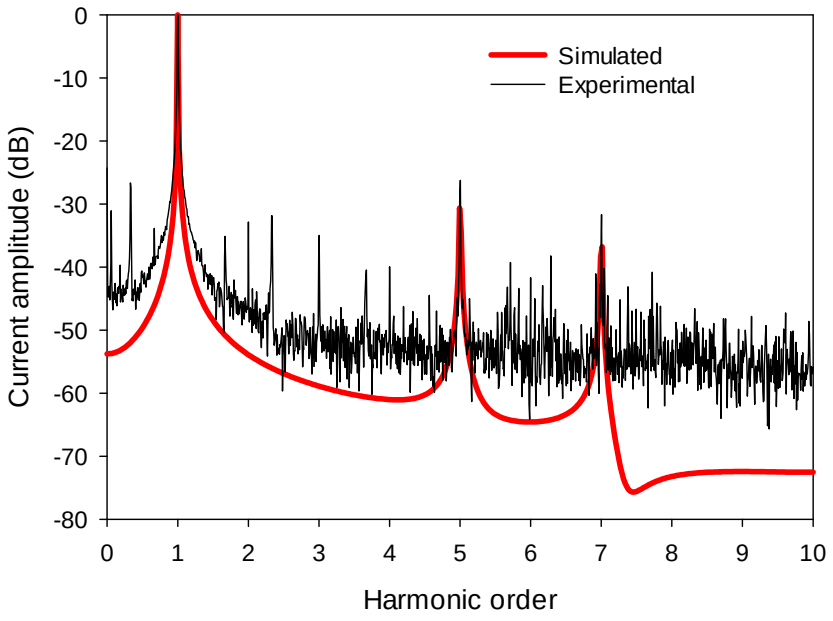

Fig.23. Simulation and experimental results of stator currents spectrum for healthy SPMSM, running at 3000 rpm and rated load.

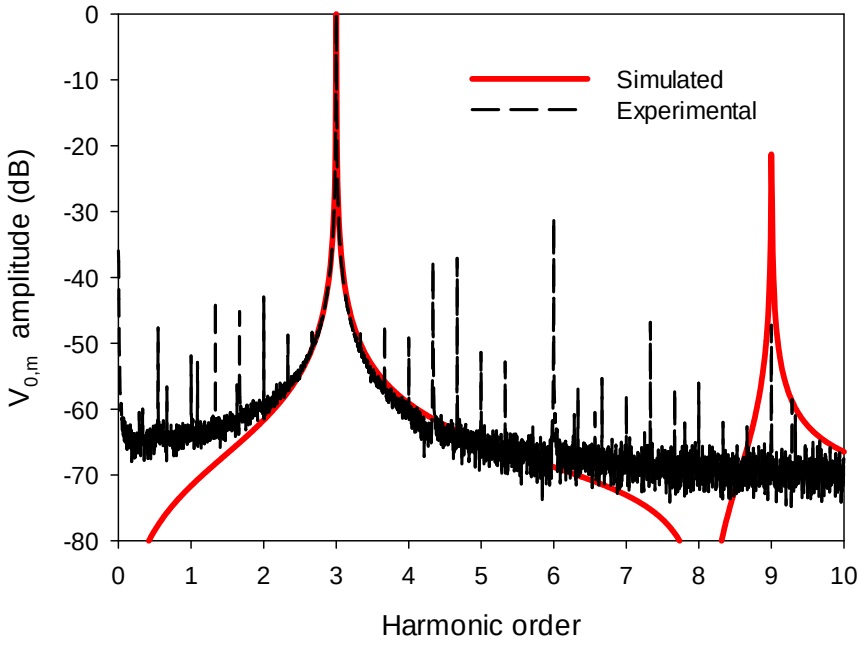

Fig.24. Simulated and experimental ZSVC spectral content of a healthy SPMSMs operating under rated load at 6000 r/min.

Fig 23 and 24 show a good agreement between the simulated and experimental peak values, which proves the validity of the FEM simulations. It must be noted that experimental data contains more harmonic distortion, in part due to the acquisition system and the distortion coming from inverter switching. Simulation and experimental results approve the effectiveness of the methods. It is worth noting that fractional-slot windings (with either with $q < 1$ or $q > 1$) facilitate the short-circuit detection and improve the fault tolerant characteristics of a PMSM drive.

3.1.2 Inter-turn Faults in Five-Phase PMSMs

Multiphase machines are distinguished with several advantages in regards to faulty conditions, which make them proper candidates in fault tolerant applications. Comparing to three-phase machines, multiphase systems have more abilities to work after fault occurrence in one (or even two) of the phases.

This section analyzes the detection of inter-turn short circuit faults in five-phase PMSMs in their early stage, i.e. with only one turn in short circuit by means of the analysis made on the previous section. For this purpose, a parametric model of five-phase PMSMs which accounts for the effects of inter-turn short circuits is developed to determine the most suitable harmonic frequencies to be analyzed to detect inter-turn faults. The amplitudes of these fault harmonic are analyzed in detail by means of finite-elements method (FEM) simulations, which corroborate the predictions of the parametric model. A low-speed five-phase PMSM for in-wheel applications is studied and modeled. This section proves that the ZSVC-based method provides better sensitivity to detect inter-turn faults in the analyzed low-speed application. Results presented under a wide speed range and different load levels show that it is feasible to detect such faults in their early stage, thus allowing applying a fault tolerant strategy to minimize their effects while ensuring a safe operation

3.1.2.1 Model of the PMSM Considering Stator Winding Inter-Turn Faults

The equations of a five-phase PMSM with inter-turn faults expressed in the *abcde* stationary reference frame are presented. These equations are based on the three-phase PMSM model studied at the previous section [70] and are used to identify the most suitable harmonics of the stator currents and the ZSVC to be used as a fault indicator.

By supposing the inter-turn faults located in phase *e,* the equations are as follows,

$$[V_{sf,abcde}] = [R_{sf}] \cdot [i_{sf,abcde}] + [L_{sf}][\frac{di_{sf,abcde}}{dt}] + [e] + [V_0] \quad (2)$$

the matrixes in (2) may be expressed as,

$[V_{sf,abcde}]=[V_a\ V_b\ V_c\ V_d\ V_e\ 0]^t$, $[i_{sf,abc}]=[i_a\ i_b\ i_c\ i_d\ i_e\ i_f]^t$, $[V_0]=V_0[1\ 1\ 1\ 1\ 1\ 0]^t$

$$[R_{sf}]=\begin{bmatrix} R_s & 0 & 0 & 0 & 0 & 0 \\ 0 & R_s & 0 & 0 & 0 & 0 \\ 0 & 0 & R_s & 0 & 0 & 0 \\ 0 & 0 & 0 & R_s & 0 & 0 \\ 0 & 0 & 0 & 0 & R_s & -\mu R_s \\ 0 & 0 & 0 & 0 & \mu R_s & -\mu R_s - R_f \end{bmatrix},$$

$$[L_{sf}]=\begin{bmatrix} L & M_0 & M_1 & M_1 & M_0 & -\mu M_0 \\ M_0 & L & M_0 & M_1 & M_1 & -\mu M_1 \\ M_1 & M_0 & L & M_0 & M_1 & -\mu M_1 \\ M_1 & M_1 & M_0 & L & M_0 & -\mu M_0 \\ M_0 & M_1 & M_1 & M_0 & L & -\mu L \\ \mu M_0 & \mu M_1 & \mu M_1 & \mu M_0 & \mu L & -\mu^2 L \end{bmatrix}, \quad [e]=\frac{d}{dt}\begin{bmatrix} \lambda_{PM,a} \\ \lambda_{PM,b} \\ \lambda_{PM,c} \\ \lambda_{PM,d} \\ \lambda_{PM,e} \\ \mu\lambda_{PM,e} \end{bmatrix},$$

$$\begin{cases} \lambda_{PM,a} = \lambda_{PM,1}\cos(\theta) + \sum_{h=1,3,5\ldots} \lambda_{PM,h}\cos(h\theta - \theta_v) \\ \lambda_{PM,b} = \lambda_{PM,1}\cos\left(\theta - \frac{2\pi}{5}\right) + \sum_{h=1,3,5,\ldots} \lambda_{PM,h}\cos\left(h\theta - \theta_v - h\frac{2\pi}{5}\right) \\ \lambda_{PM,c} = \lambda_{PM,1}\cos\left(\theta - \frac{4\pi}{5}\right) + \sum_{h=1,3,5,\ldots} \lambda_{PM,h}\cos\left(h\theta - \theta_v - h\frac{4\pi}{5}\right) \\ \lambda_{PM,d} = \lambda_{PM,1}\cos\left(\theta + \frac{4\pi}{5}\right) + \sum_{h=1,3,5,\ldots} \lambda_{PM,h}\cos\left(h\theta - \theta_v + h\frac{4\pi}{5}\right) \\ \lambda_{PM,e} = \lambda_{PM,1}\cos\left(\theta + \frac{2\pi}{5}\right) + \sum_{h=1,3,5,\ldots} \lambda_{PM,h}\cos\left(h\theta - \theta_v + h\frac{2\pi}{5}\right) \end{cases} \quad (3)$$

R_s being the stator phase resistance, L the phase self-inductance and M_0 and M_1 the mutual inductances, where the subscript "0" denotes adjacent phases and "1" nonadjacent phases. In addition, the stator zero-sequence flux component generated by the permanent magnets is expressed as $\lambda_{PM,0} = (\lambda_{PM,a}+\lambda_{PM,b}+\lambda_{PM,c}+\lambda_{PM,d}+\lambda_{PM,e})/5$, where h is the harmonic order and $\mu = n/N$ is the ratio between the number of short-circuited inter-turns (n) and the total number of turns in each phase (N). Furthermore, R_f is the resistance that models the insulation failure, whereas i_f is the fault current through the n short-circuited turns.

By adding the first five rows in (2) and taking into account (3), the ZSVC measured between the dc mid-point of the inverter and the center of the stator windings is obtained as shown in (4). Therefore, when considering a five-phase PMSM without neutral conductor it results in,

$$V_0 = \frac{1}{5}\Sigma V + \frac{1}{5}\mu R_s i_f + \frac{1}{5}\mu\left(L + 2M_0 + 2M_1\right)\frac{di_f}{dt} - \frac{d\lambda_{PM,0}}{dt} \quad (4)$$

where $\Sigma V = V_a+V_b+V_c+V_d+V_e$ and $i_a + i_b + i_c + i_d + i_e = 0$.

Commercial PMSMs are fed by electronic inverters which inject ZSVCs in the PMSM. In addition, because the neutral system voltage is not available, the line-to-neutral voltages V_a, V_b, V_c, V_d and V_e are not directly measurable. Fig. 25 shows the stator windings connections, the electronic inverter and a wye-connected resistive network used to measure the ZSVC.

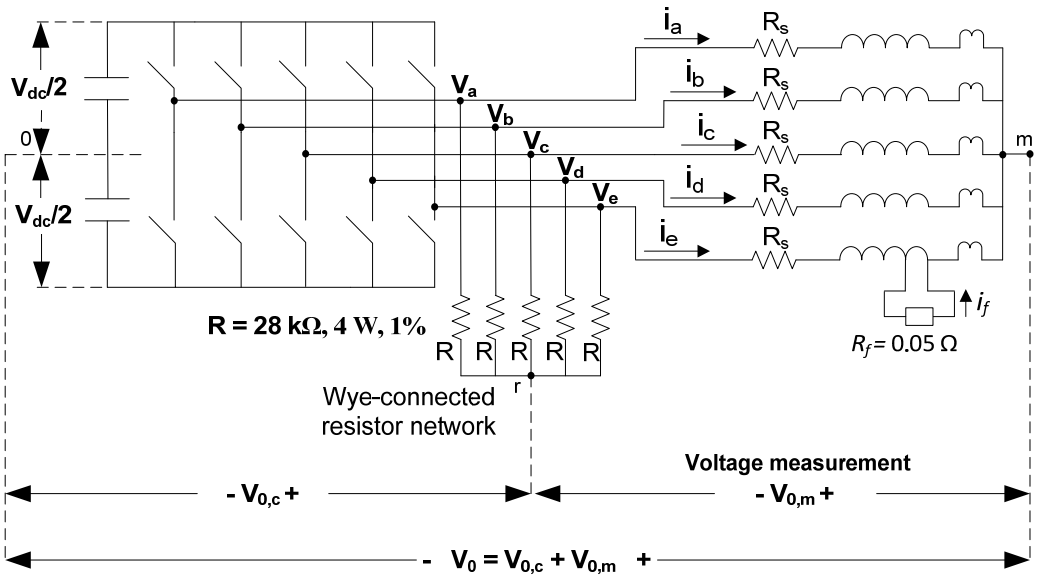

Fig 25. Diagram showing the five-phase PMSM connected to the inverter, the stator windings, the resistor network used to generate an artificial neutral point to measure the $V_{0,m}$ ZSVC, the short-circuited turns, the fault resistance R_f, and the circulating fault current i_f.

To decouple the ZSVC from the drive effects when measured between the central point of a balanced five-phase wye-connected resistor network and the neutral of the stator windings, as used on the three phase PMSM [71,72], thus obtaining $V_{0,m}$. In this case, since $V_{0,c} = (V_a+V_b+V_c+V_d+V_e)/5$, (3) results in,

$$V_{0,m} = \frac{1}{5}\mu R_s i_f + \frac{1}{5}\mu\left(L + 2M_0 + 2M_1\right)\frac{di_f}{dt} - \frac{d\lambda_{PM,0}}{dt} \tag{5}$$

Since the last term in (5) explains the effects of the magnets, it is the most contributing term. This term induces an important fifth harmonic component since the $d\lambda_{PM,0}/dt$ harmonics different than the fifth and its multiples are null. In consequence, the fundamental frequency of the ZSVC corresponds to the fifth harmonic of the electrical frequency. Since the two first terms in (5) are due to the fault current i_f (which main component is the first harmonic), the ZSVC spectrum of a faulty machine must contain a significant first harmonic component. This indicates that inter-turn faults may be detected by analyzing the first harmonic of the ZSVC.

The induction effect of the permanent magnets is the primary source of the fault current i_f. This means that the fault current i_f must contain a fifth harmonic component as occurs with the $V_{0,m}$ ZSVC. Since (2) predicts a link between i_f and the stator currents i_a, i_b, i_c, i_d and i_e, the stator currents spectra must also present a fifth harmonic component originated by the shorted turns. However, the induction effect of the permanent magnets greatly diminishes at low speed operation. In addition it is well-known that the motor drive may influence the stator currents harmonic content [73]. These combined effects may make it difficult to diagnose inter-turn faults by analyzing the fifth harmonic of the stator currents, especially at low speed operation as is the case of in-wheel motor

applications. The magnitude of the short circuit current depends on the number of partially short-circuited turns as well as on their relative position in the slot where the winding is accommodated [74].

The equations system given by (2)-(3) also allows explaining the emergence of a fifth harmonic component in both the neutral and the phase currents when a healthy wye-connected five-phase PMSM has an accessible neutral point which is connected to the dc midpoint of the inverter by means of a neutral conductor. Under these constrains (5) may be rewritten as,

$$i_n\left(R_n+\frac{1}{5}R_s\right)+\frac{1}{5}\left(L+2M_0+2M_1\right)\frac{di_n}{dt}=\frac{1}{5}\Sigma V+\frac{1}{5}\mu R_s i_f+\frac{1}{5}\mu\left(L+2M_0+2M_1\right)\frac{di_f}{dt}-\frac{d\lambda_{PM,0}}{dt} \quad (6)$$

Where $i_n = i_a + i_b + i_c + i_d + i_e$ is the current through the neutral conductor and R_n is its resistance. From (6) it is deduced that the current through the neutral conductor will contain a fifth harmonic component due to the term $d\lambda_{PM,0}/dt$, even when dealing with a healthy machine ($i_f = 0$). This effect is well known and allows corroborating the strength of equations (5) and (6).

3.1.2.2 The Analyzed PMSM and the FEM Models

In this case the analyzed machine was a five-phase radial flux surface-mounted PMSM with outer rotor configuration which is shown in Fig. 26. It has wye-connected stator fractional windings (q<1). This motor was specially designed to be applied in electrical traction systems like electrical bicycles, electrically assisted velomobiles or wheelchairs among others.

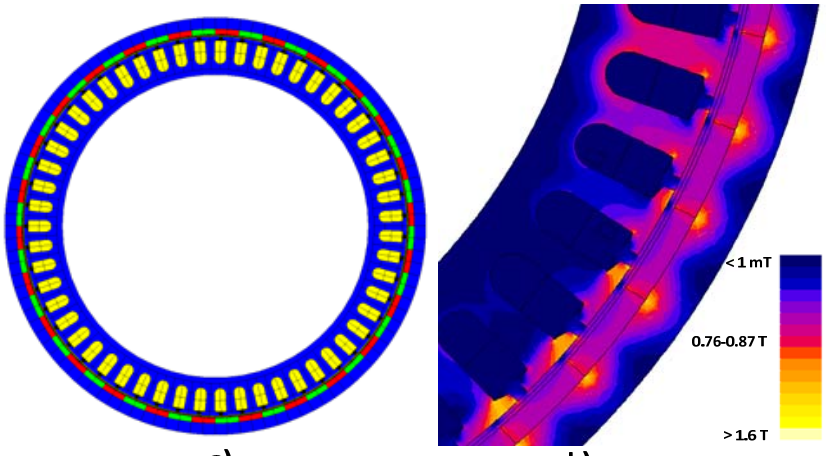

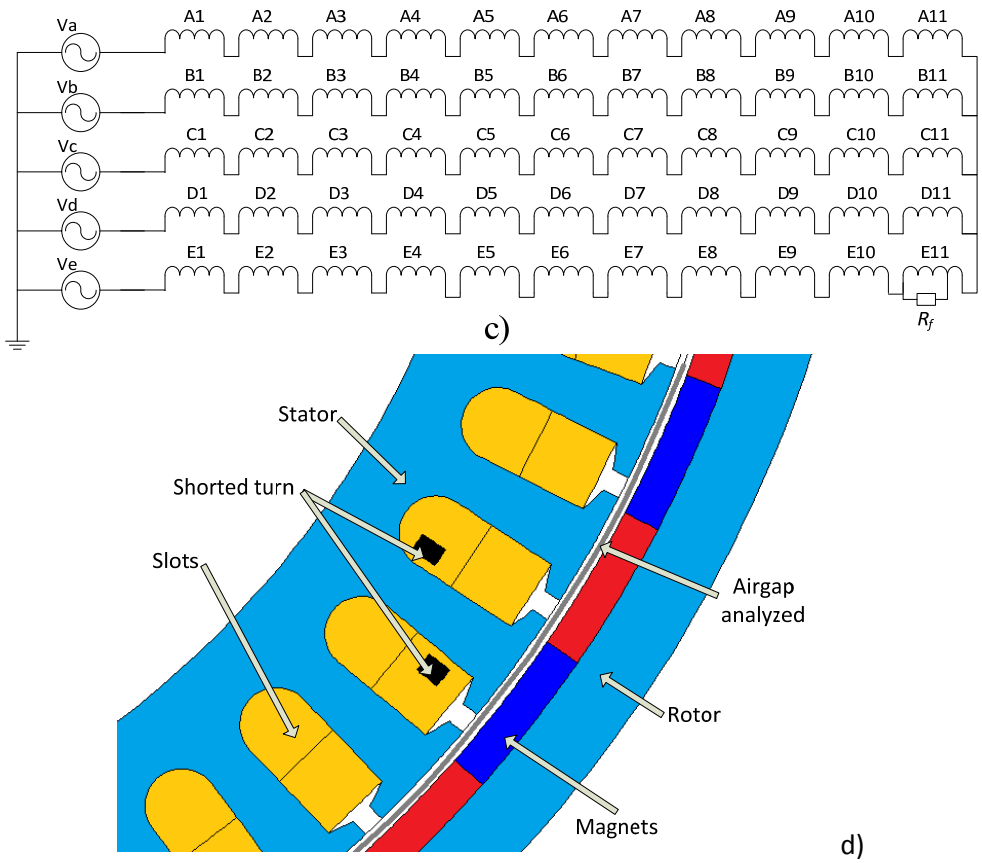

Fig 26. a) Diagram showing section of the stator and rotor. b) Magnetic flux density distribution in a section of the PMSM. c) Connection diagram of the 11 coils in each phase of the stator. d) Location of the short-circuited turn and 2D mesh applied in the FEM simulations.

Simulations of the faulty PMSM have been conducted by using a fault resistance R_f = 0.05 Ω. This value is within the range found in [65]. It is worth noting that the black area shown in Fig. 26 is proportional to the number of short-circuited turns in the slot.

The 2D-FEM model of the experimental PMSM was modeled at Flux Cedrat software package. The model consists of approximately 44000 triangular surface elements and 88692 nodes. All simulations assume balanced sinusoidal line voltages and consider a time step of 0.204 ms (4.9 kHz sampling frequency) and 0.84 s are simulated to obtain 4096 points with a resolution of 30 points/cycle. The FFT leads to an output of 2048 points with a frequency resolution of 1.2 Hz.

The main parameters of the machine dealt with in this work are shown in Table 3.

Table 3. Main parameters of the analyzed PMSM

Outer Rotor Characteristics	
Rated power	1 kW
Rated torque	23 Nm
Rated speed	379 r/min
Outer diameter	220 mm

Axial length	36 mm
Air gap length	1 mm
Number of phases	5
Poles pairs	26
Rated phase voltage	18 V
Max current	10 A
Rated electrical frequency	164 Hz
Resistance per phase	0.1 Ω
Self-inductance per phase	107 µH
Mutual inductance between adjacent phases	15 µH
Mutual inductance between nonadjacent phases	10 µH
Number of stator slots	55
Number of coils per phase	11
Number of turns per coil	10
Number of wires in parallel per turn	10
Number of magnets in the rotor	52
Permanent magnets material	SmCo
Permanent magnets remanence	0.8 T

The faulty machine model supposes only one turn short-circuited out of 110 turns in phase *e*, which is located in the position depicted in Fig. 26.

As stated, short-circuit faults are the only fault that could be overcome by design and for a fault tolerant system is of upmost importance its early detection, in order to allow a drive system to reconfigure. For this purpose this section analyzes the feasibility to detect inter-turn faults when only one turn is short-circuited based on the FEM simulations of the five phases motor.

Fig. 27 shows the stator currents spectra of both a healthy and a faulty machine without neutral return conductor. Results from Fig. 27 clearly show that both healthy and faulty spectra are quite similar, thus being unpractical to diagnose an incipient inter-turn fault from the analysis of the stator currents in this particular machine.

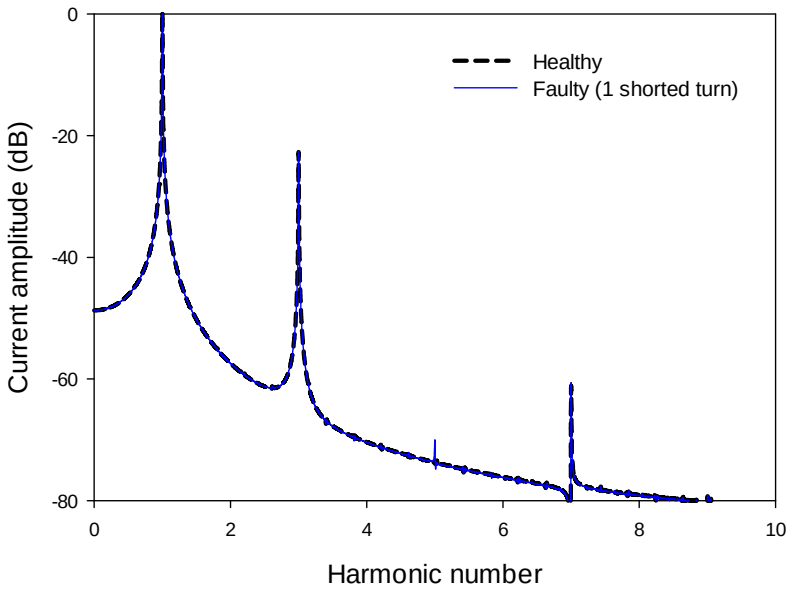

Fig 27. Stator currents spectra of the analyzed healthy and faulty (1 turn in short circuit) PMSMs when operating at rated speed under rated load conditions.

Fig. 28 shows the ZSVC spectra of both, the healthy and faulty machines. Contrarily to the case of the stator currents spectra, the ZSVC show important changes when a faulty turn is simulated, as shown in Fig. 28. As derived from (5), in the case of a faulty machine the influence of the fault current in the ZSVC is reflected in the first harmonic component of the ZSVC. This theoretical result is corroborated by means of the FEM results provided by Fig. 28. In addition, the ZSVC spectrum of the faulty machine also contains third and seventh harmonic components, but with a considerable low amplitude.

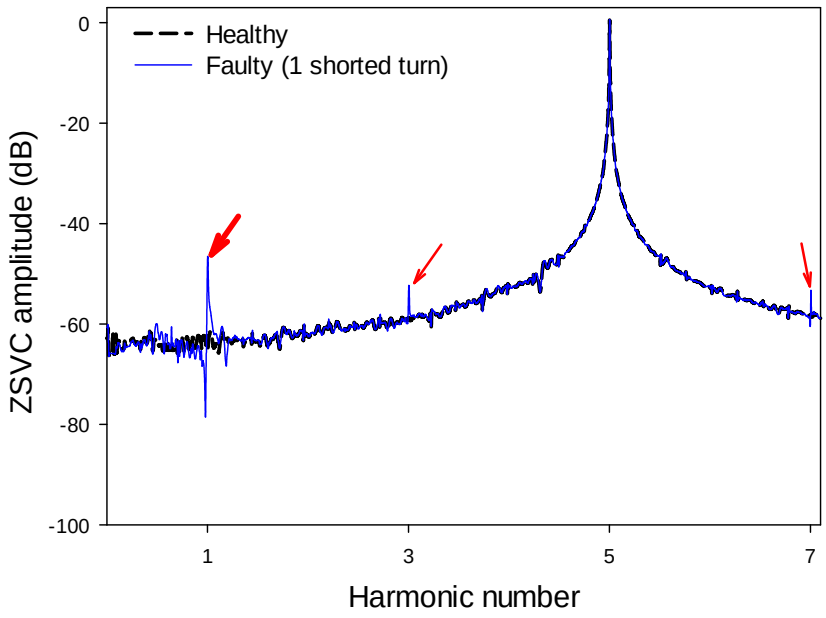

Fig 28. ZSVC spectra of the analyzed healthy and faulty (1 turn in short circuit) PMSMs when operating at rated speed under rated load conditions.

Figs. 29 show the amplitudes of the fifth harmonic of the stator currents for both healthy and faulty (one shorted turn) PMSMs when operating under different speed and load conditions. However, results presented in Fig. 29 show almost no difference between the healthy and faulty conditions of the analyzed machine since both results are virtually superimposed. Therefore, it is concluded that for the analyzed machine, the detection of inter-turn short circuit faults in the very incipient stage is not feasible from the analysis of the harmonic content of the stator currents.

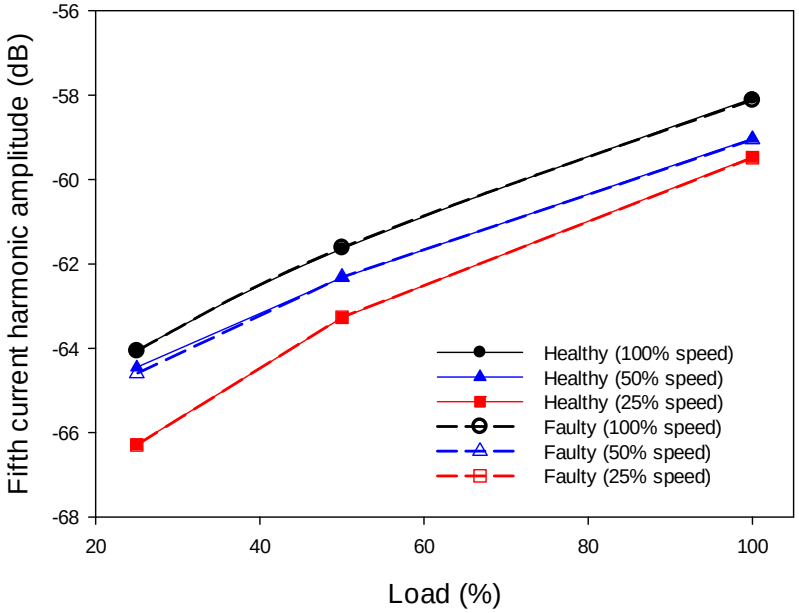

Fig 29. Healthy and faulty (one shorted turn) PMSMs operating under different speed and load conditions. Fifth harmonic amplitude of the stator currents.

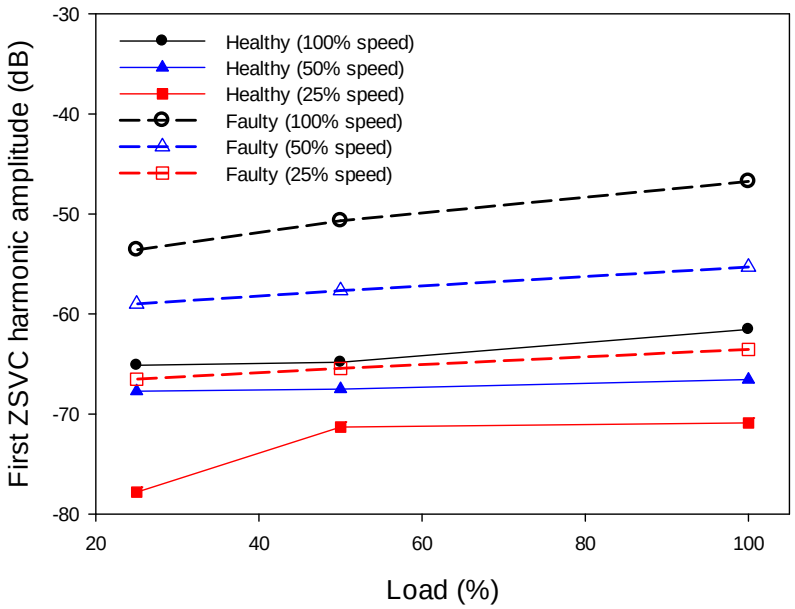

Fig 30. Healthy and faulty (one shorted turn) PMSMs operating under different speed and load conditions. First harmonic amplitude of the ZSVC.

Fig. 30 shows the amplitudes of the first harmonic of the ZSVC for both the healthy and faulty (one shorted turn) PMSMs when operating under different speed and load conditions.

According to the results presented in Fig. 30, the faster the PMSM speed, the higher the amplitude of the first harmonic. However, this amplitude is almost constant for a given load level. In addition, despite of the incipient fault level analyzed, always there is an increment of the first harmonic amplitude of the ZSVC when comparing a faulty motor with a healthy one. For better understanding, results presented in Fig. 30 are summarized in Table 4.

From the results presented in Table 4, it is concluded that in the case of a faulty PMSM with only one short-circuited turn, the amplitude of the first ZSVC harmonic experiments a sharp increment of at least 5.85 dB (the minimum value in Table 4). Therefore, to let some security margin, a threshold value of 4 dB may be used to detect such incipient fault, i.e. one turn in short circuit.

Table 4. First harmonic of the ZSVC amplitude. Difference between faulty and healthy PMSM's.

First ZSVC harmonic			
	100% full load (dB)	50% full load (dB)	25% full load (dB)
100% rated speed	14.81	11.26	7.35
50% rated speed	14.15	9.85	5.85
25% rated speed	11.56	8.71	11.29

It is worth noting that PMSMs are usually controlled in a closed loop mode, so the effect of the controller may be significant. However, as shown in Fig. 31, both the magnetic flux density in the air gap region just in front of the short-circuited turn and the phase currents are virtually not affected by the incipient fault. Therefore, the current loop hardly will perceive any difference between the healthy case and the very incipient fault condition, so no influence of the controller and consequently no distortion of the ZSVC spectrum are expected. However, as shown in Figs. 28 and 30, this incipient fault is clearly reflected in the ZSVC spectrum because of the contribution of the fault current i_f, as explained by equation (5).

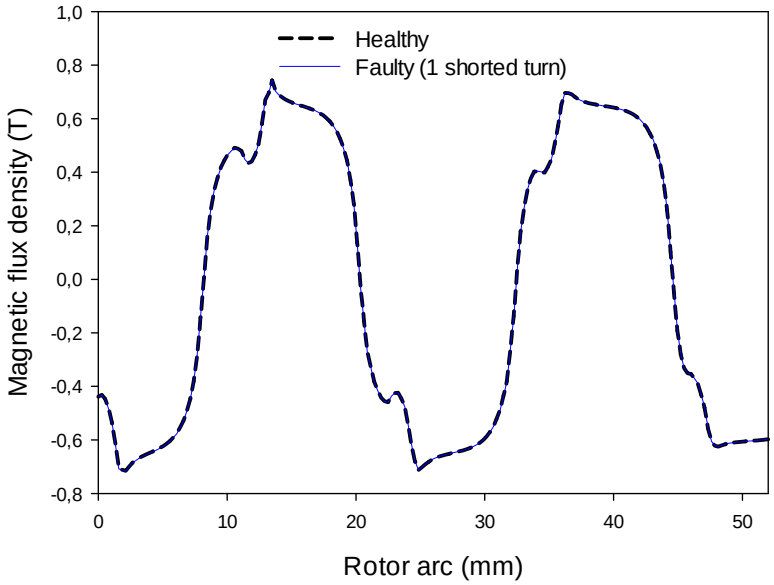

a)

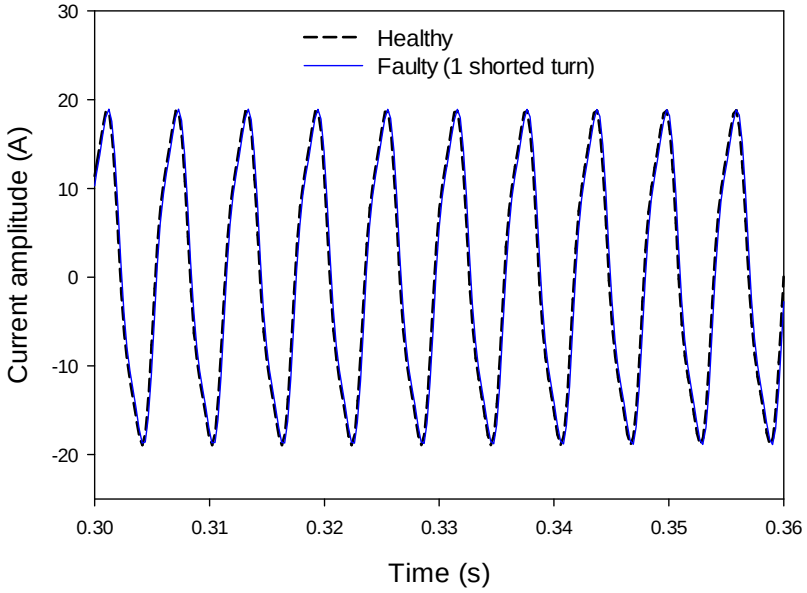

b)

Fig 31. Healthy and faulty (one shorted turn) PMSMs operating under rated speed and load conditions. a) Magnetic flux density in the air-gap region just in front of the faulty slots. b) Stator currents.

From these results it was concluded that a five phase motor with a fractional winding combined with an appropriate ZSCV measure system, could early detect an inter-turn short circuit fault, which is an interesting feature for a fault tolerant system.

3.2 DEMAGNETIZATION IN AFPMM

As stated in the state of art, an inter-turn fault in a PMSM cannot be isolated, since the fault current circulating through the short-circuit coils will be constantly fed by the magnetic flux of the rotating permanent magnets. So it could be expected a possible demagnetization of the permanent magnets of the rotor due to a sudden peak of current circulating by the short-circuited coils. For this reason the effect of the magnets shape on the AFPMM performance under a demagnetization fault has been analyzed by means of 3D-FEM simulations. Furthermore, demagnetization faults in permanent magnet synchronous motors (PMSMs) may generate specific fault harmonic frequencies in the stator currents, output torque and zero-sequence voltage component (ZSVC) spectra, which can affect motor behavior Therefore, these parameters are studied and compared in this section for different magnet configurations to find out the more suitable geometry for safe operation under both healthy and faulty conditions.

3.2.1 THE ANALYZED AFPMM

A 14 kW AFPMM torus which was designed at the MCIA Research Laboratory for validation of the analytical sizing equations and the proposed magnets configurations. This machine has two flat rotor discs made of 40CrMnNiMo8-6-4 plastic mold steel with a suitable hardness distribution and wear resistance. The stator, which contains 36 coils (72 slots), is mounted between the two rotor discs. It is composed of a solid slotted core of M325-35A, in a donut shape. Each coil has 33 turns of enameled wire with 1.5-mm² cross section, maximum current of 90A, 0.1Ω resistance and inductance of 0.575 mH. Each rotor includes twelve NdFeB permanent magnets, which are arranged in an alternating sequence of poles N-S with an NN topology as shown in Fig. 32. The AFPMM torus-NN configuration has been analyzed because it allows connecting the stator windings in a back-to-back configuration, which allows minimizing the end windings length and therefore copper loss.

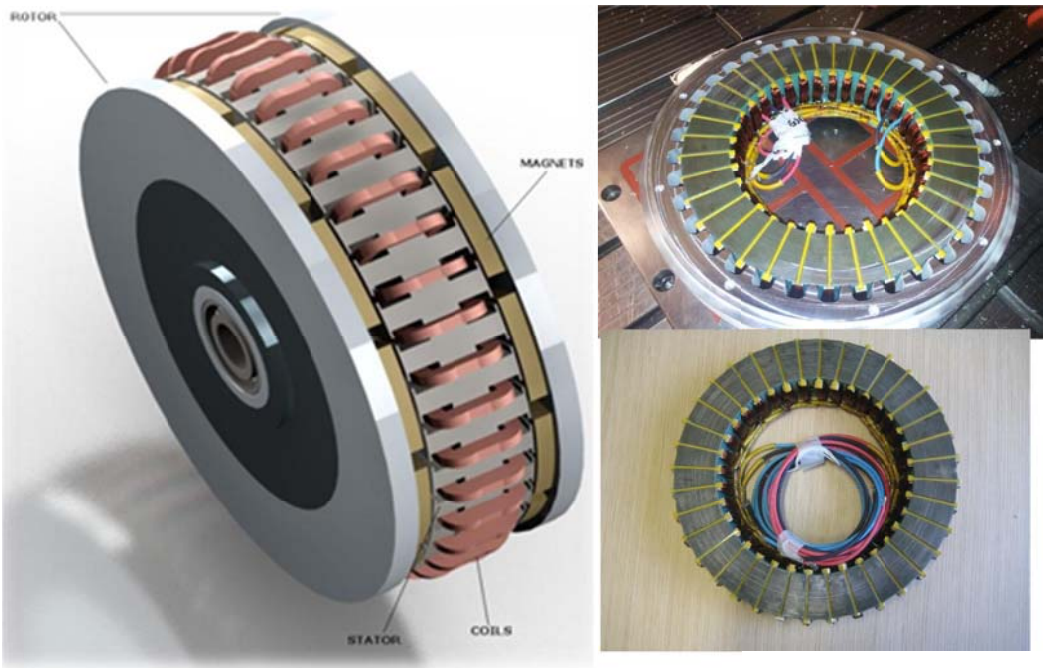

Fig 32. AFPMM torus-NN analyzed in this work.each rotor disc contains 12 magnets in a NN configuration. The stator contains 72 slots connected through back-to-back coils. Each phase winding is composed of 12 coils arranged in three parallel branches with four series-connected coils each.

The machine parameters are given in Table 5. For ease of manufacture, parallel stator slot openings are often employed rather than radial slot openings. When the slot openings are parallel, the ratio of the width of the slot openings to the slot-pitch is not constant. As a consequence, the effective cogging torque waveforms at different radii are different.

Five different magnets configurations were chosen [75], as show in Fig 33. All of them were designed to have the same volume of 1.6×10^{-5} m^3 and are supposed to be made of the same material, NdFeB-35 with remanence B_r = 1.23 T.

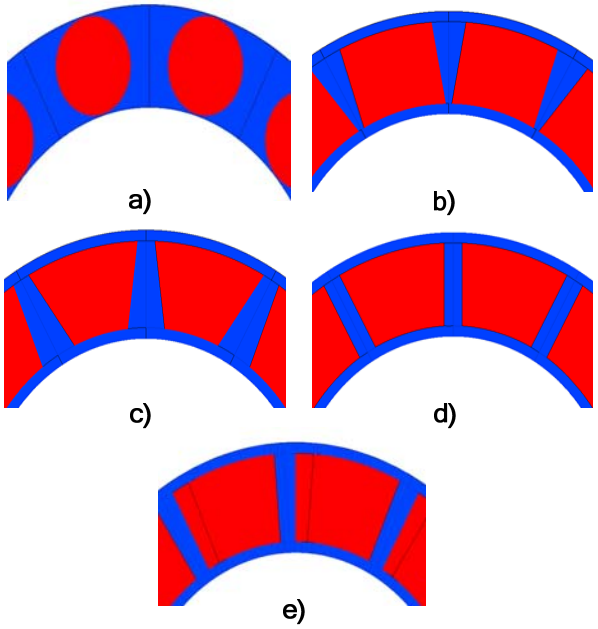

Fig. 33. Analyzed magnets shape. a) Circular magnet. b) Trapezoidal skew. c) Triangular skew. d) Parallel sided. e) Sector or radial magnet shape.

Table 5. Reference machine configuration.

Torus Characteristics	
Rated torque	170 Nm
Rated speed	800 r/min
Max speed	1200 r/min
Number of phases	3
Poles pairs	6
Disc diameter	280 mm
Axial length	120 mm
Airgap length	1.5 mm
Number of slots per side	36
Number of coils per phase	12
Magnets Parameters	
Magnets type	NdFeB-35
Max working temperature (T_{max})	120 ºC
Curie temperature (T_C)	340 ºC
Remanence Flux Density (B_r)	1.23 [T]
Coercivity (H_c)	890 [kA/m]
Thickness	9.1 [mm]

3.2.2 FINITE ELEMENTS MODELING

As it is well known, although radial-flux machines are often simulated by means of two-dimensional finite elements analysis, an axial flux machine must be modeled by means of three-dimensional finite elements methods (3D-FEM) due to its inherent three-dimensional geometry. All the FEM models analyzed have around 220000 tetrahedral volumetric elements, in order to acquire good results accuracy, as displayed in Fig. 34. The AFPMM is modeled with three-dimensional finite-element method and includes all geometrical and physical characteristics of the machine components. Fig. 35, shows the precise location of the fault, the arrows indicates the magnetization direction and the color represents the magnetic flux density. Using this accurate modeling makes it possible to obtain demanded signals for a very high precision analysis. Magnetic flux density, back-EMF, magnetic axial force and cogging torque of the motor were simulated using FLUX-3D V10.4.

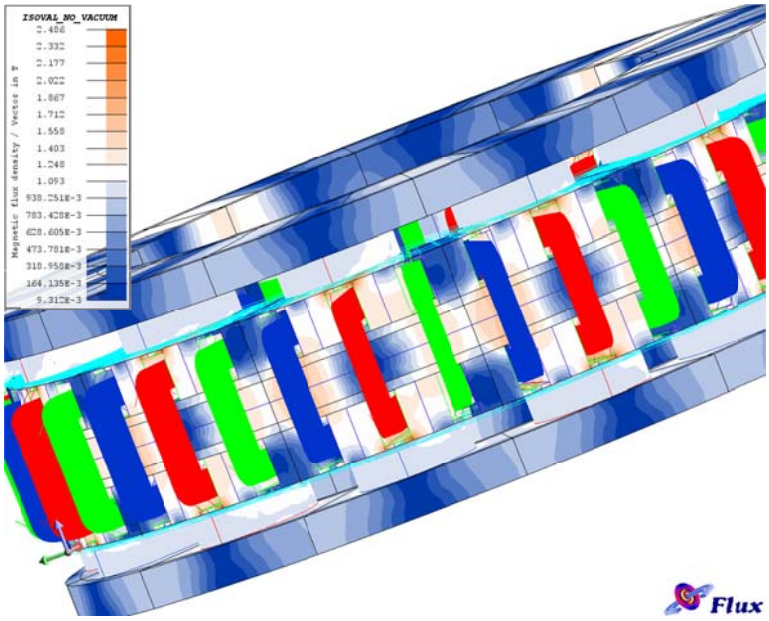

Fig 34. Magnetic Flux distribution on machine.

Fig 35.Demagnetized magnet in green, FEM model.

All the faulty analyzed motors have been simulated by supposing the same demagnetization degree, which correspond to one magnet with half of its normal magnetic remanence (B_{rdemag}=1.23*0.5 [T])

Figs. 36 and 37 show, respectively, the back-EMF waveforms at rated speed and no load con

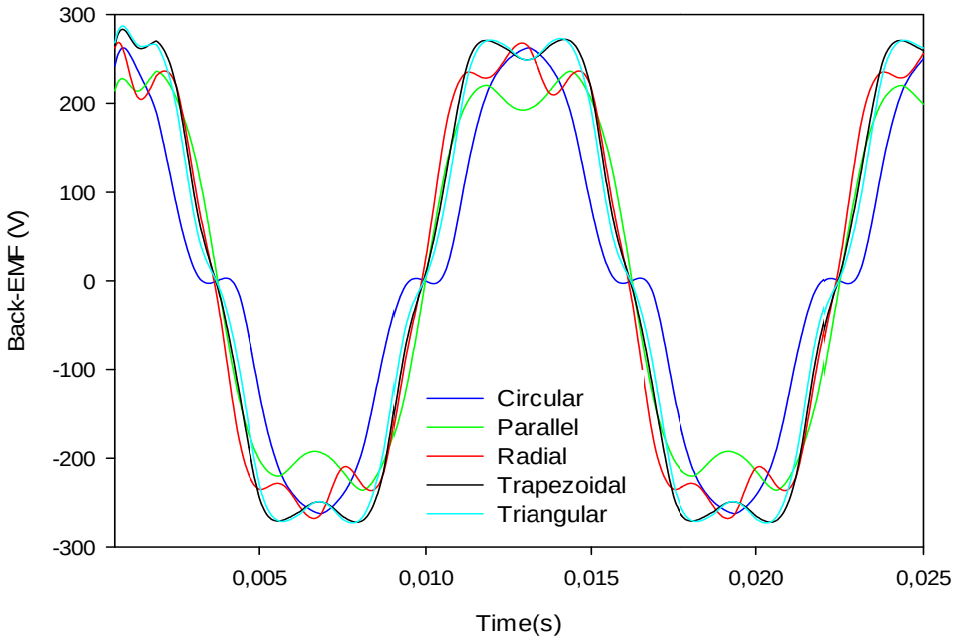

Fig 36. Back-EMF wave of the analyzed magnets configurations at rated speed under no-load conditions.

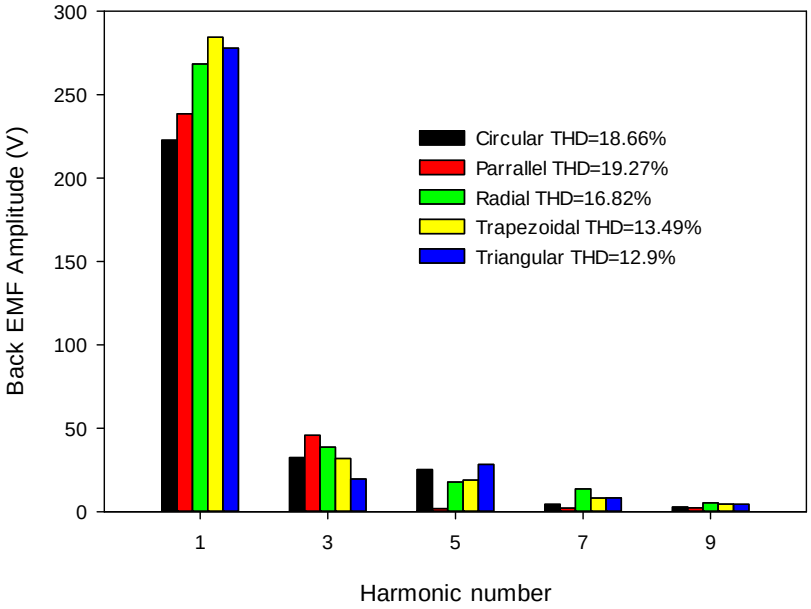

Fig 37. Back-EMF harmonic distribution of the analyzed magnets configurations at rated speed under no-load and healthy conditions.

Albeit the flux density has an impact on the back-EMF shape, the latter is also greatly influenced by the specific windings configuration of the analyzed machine. As shown in Fig. 37, the triangular and trapezoidal magnets configurations are those with less back-EMF harmonic content. This result suggests that these magnets configurations may improve the torque quality generated by the AFPMM, compared with common configurations.

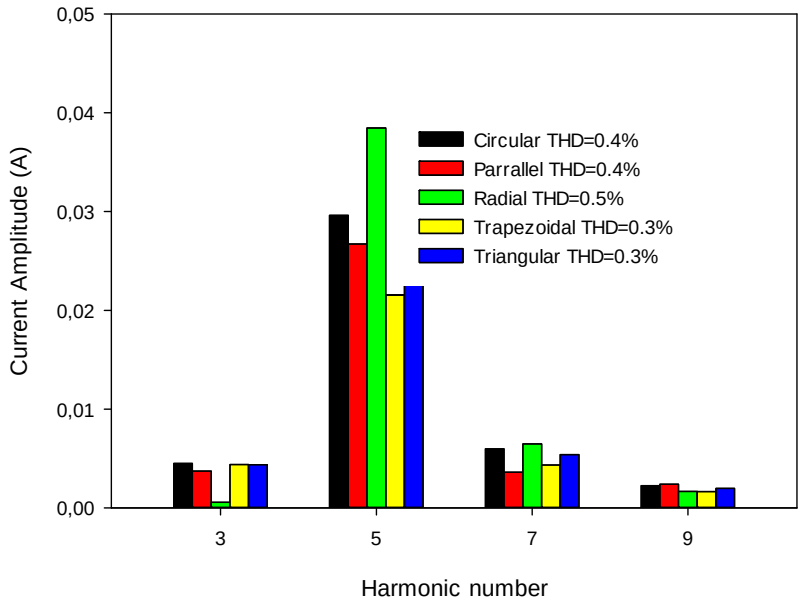

Fig 38. Currents harmonics healthy condition.

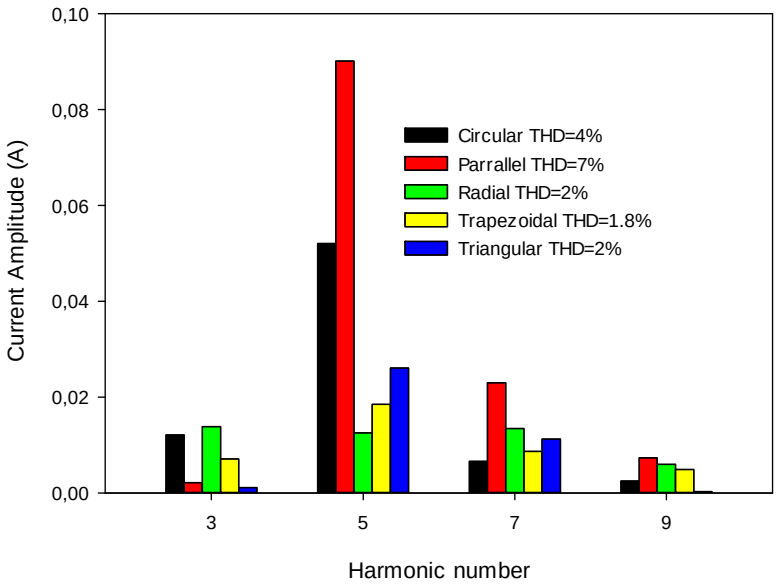

Fig 39. Currents harmonics with a demagnetization of 50%.

Fig 38 and 39 show the currents spectra under healthy and demagnetization conditions, where a noticeable increase of the harmonic amplitude is observed, due to the deformation of the MMF in the airgap caused by the demagnetization.

Fig. 40 to 43 show the torque ripples and the harmonic content of the different analyzed magnets configurations, which corroborates that the radial magnets configuration is that with higher harmonics content whereas the trapezoidal skew configuration is that with lower content, even under demagnetized condition. Therefore, a smoother torque can be attained by using trapezoidal shaped magnets.

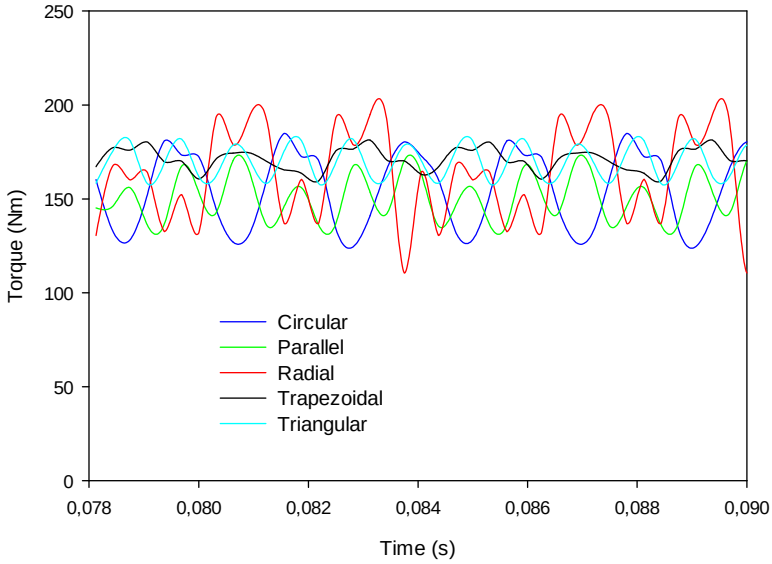

Fig 40. Torque ripples of the analyzed magnets configurations at rated speed and rated load, healthy condition.

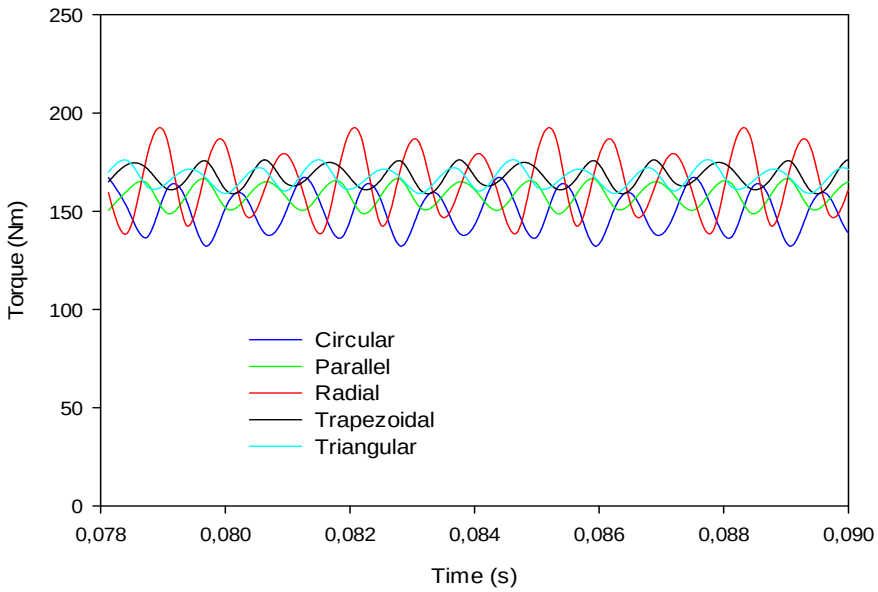

Fig 41.Torque ripples of the analyzed magnets configurations at rated speed and rated load, faulty conditions (demagnetization of 50%).

Figs. 42 and 43 show the torque spectra of the different analyzed magnets configurations, in healthy and faulty condition respectively, although there is a light increase in the total harmonic distortion, the amplitude of most of the harmonics decrease as consequence of demagnetized fault.

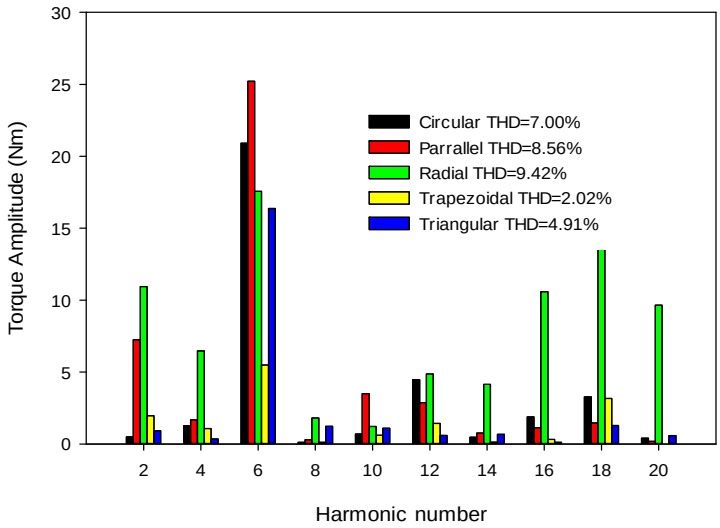

Fig 42. Torque harmonics distribution of the analyzed magnets under healthy condition. The DC component is not displayed in the figure.

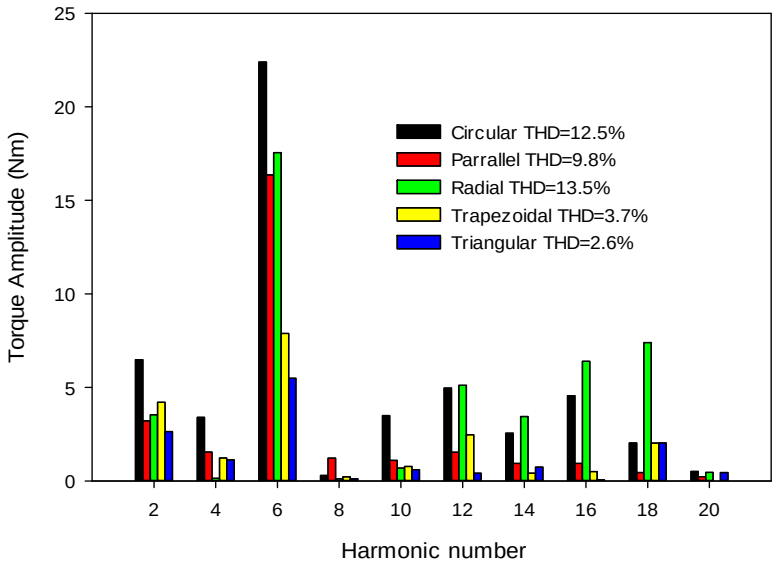

Fig 43. Torque harmonics distribution of the analyzed magnets configurations, with a demagnetization of 50%.

Table 6 summarizes the average torque under healthy and faulty condition, which shows that the configurations with lesser torque ripple (triangular and trapezoidal skew) also lead to higher average torque, even under faulty condition.

Table 6. Comparison of the average torque.

Magnets format	**Average torque healthy (Nm)**	**Average torque faulty (Nm)**
Circular	152	150
Parallel	160	158
Radial	170	165
Trapezoidal	171	168
Triangular	170	167

Fig. 44 and 45, show the ZSVC spectra of the different analyzed magnets configurations. Although under demagnetization condition there is a reduction of the amplitude of some harmonics, the main harmonic (in this case the third) increases by almost 20% in most of the magnet shapes. As mentioned in [67], the correct measurement of the ZSVC could aid to detect a partial demagnetization and inform the control system about the specific performance of the machine.

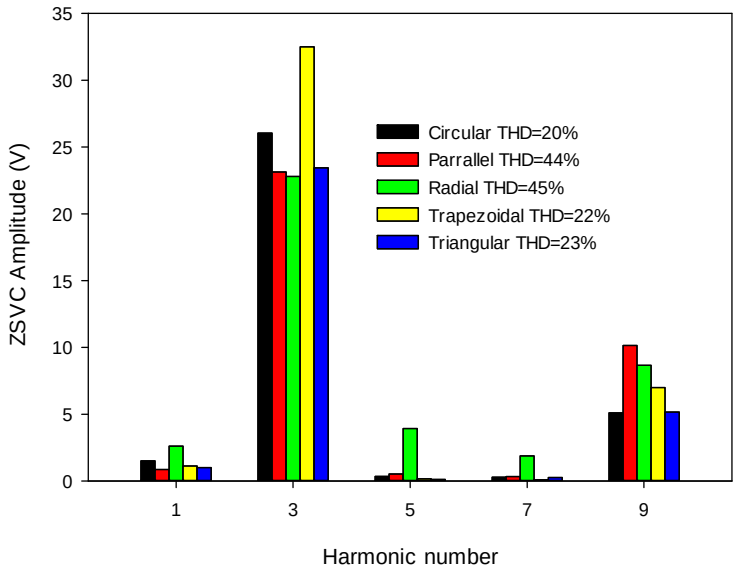

Fig 44. ZSVC harmonics distribution of the analyzed magnets configurations, healthy conditions.

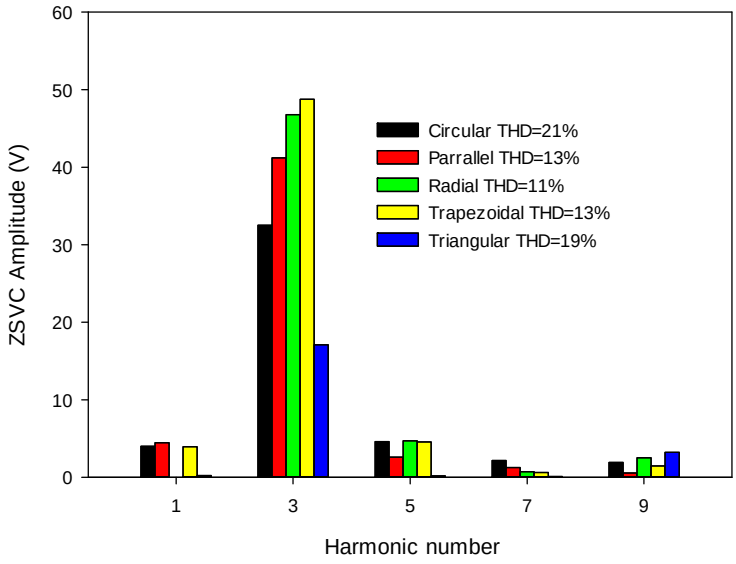

Fig 45. ZSVC harmonics distribution of the analyzed magnets configurations, with a demagnetization of 50%.

3.3 CONCLUSIONS

This chapter has analyzed the effects of short-circuit for both three-phase and five-phase permanent magnet machines, the analysis of the stator currents and ZSVC harmonics to diagnose short-circuit faults when dealing with different winding configurations, as well as the effects of demagnetization faults and the permanent magnets geometry in the machine behavior. The following conclusions can be drawn:

- The method based on the ZSVC to detect short-circuit faults in their early stage has some advantages, specifically sensitivity even at low speed, that the analysis of the stator currents spectra. This conclusion is valid for both three- and five-phase permanent magnet machines.

- When dealing with fractional stator windings with $q < 1$, it is easier to detect short-circuit faults in permanent magnet machines in their early stage. In addition, this type of windings present additional advantages compared to other windings, including reduced cogging torque, less acoustic noise emissions and less vibrations, thus preventing mechanical problems in the bearings.

- The trapezoidal and triangular skew magnets shape provide low torque ripple in both healthy and demagnetization condition, making these magnet shapes the most appropriate in a fault tolerant AFPMM drive system.

4. OPTIMAL DESIGN WITH GENETIC ALGORITHMS

This section describes the process of optimally designing an AFPMM. The main geometric, electric and mechanical parameters of the designed AFPMM are calculated by applying an iterative method based on a set of analytical equations, which are assisted by means of a reduced number of three-dimensional finite element method (3D-FEM) simulations to limit the computational burden. The optimization process of the AFPMM is based on a genetic algorithm, which can be either single-objective or multi-objective. Several fault-tolerance constraints are settled during the optimization process to ensure enhanced fault-tolerance in the resulting motor design. The accuracy of the best solution attained is validated by means of 3D-FEM simulations.

First, a three-phase fault tolerant AFPMM is optimally designed for in-wheel applications used to drive an electrical scooter. A single-objective optimization process is carried out, in which the objective function is the power density. To ensure fault tolerant capabilities, appropriate fault tolerance restrictions are imposed during the design process. Comparisons with available data found in the technical bibliography show the appropriateness of the approach developed in this work.

The next subsection describes the optimal design of a five-phase fault-tolerant axial-flux PMSM. As initial design constraints, it has a TORUS NN configuration and non-overlapping fractional-slot concentrated windings. Unlike the previous design, a multi-objective design strategy is applied, in which the variables to be optimized are the motor efficiency and power density and ten input geometric and electric parameters are considered to be optimized, with their respective bounds and constraints. This is a challenging task, due to the large sets of possible solutions and the non-linear behavior of the electric motor, which provokes intercrossed dependences between the variables to be optimized.

The motor is sized by applying an iterative method based on a set of analytical equations, which allow computing the two output variables from the input parameters values. Next, by applying a multi-objective genetic algorithm (MoGA) approach, the input parameters are modified to find out the Pareto front of the broad set of solutions explored, and from it the best solution attained is identified based on the maximum Euclidean distance to the origin point. To increase the accuracy of the AFPMM design, a further refinement loop is applied, in which the air gap flux density of the solution attained by means of the optimization process based on the analytical equations is substituted with the air gap flux density obtained through 3D-FEM simulations of the same motor.

Once the optimal solution is obtained through the applied procedure, the model is validated by means of a 3D-FEM analysis. For this purpose, the values of four relevant parameters which define the machine performance, obtained through the proposed optimization process and the 3D-FEM model are compared.

4.1 FAULT TOLERANT DESIGN GUIDELINES

An optimization algorithm seeks for a solution in a space limited by the restriction conditions, therefore, those restrictions must be carefully calculated in order to avoid unfeasible solutions and minimize the computational burden. In this section the constraints for the optimal design are established.

Before starting the design process, the following requirements have been established:

- An axial-flux geometry configuration: A compact design is a major need in a wheel hub configuration.
- As for the rotor magnets, the previous results show that trapezoidal skew magnets shape maintains its low torque ripple under both healthy and partially demagnetization conditions, which is indeed a great advantage for fault tolerant applications.
- Ratings for an e-scooter in-wheel design: It is required a rated power of about 2 kW, a base speed between 900 and 1100 r/min, and an electromagnetic torque between 20 and 30 Nm[76]. There are no a priori constraints on the rated value of the voltage and currents.
- A multiphase machine is a must, so a 5 five machine is chosen:
    - Three-phase machines require a high overrating to deal with open-circuit fault, while these machines hardly deal with short-circuit faults. Moving to a higher number of phases seems the best option.
    - The next candidate is thus the four phase-machine, which has not been considered since there are difficulties to cope with the third-harmonic of the emf in normal operation (torque ripple difficult to eliminate with PI control);
    - Five-phase machines possess a good harmonic decomposition.
- A single-layer winding with non-overlapped coils: this requirement is part of the general considerations for the design of fault-tolerant PMSMs [25]. As a loss of two phases is a severe fault, the likelihood of phase-to-phase short-circuit faults is greatly reduced with a physical isolation of the phases. From chapter 3 it was concluded that in a five phase motor with a fractional winding combined with an appropriate ZSVC measurement system an inter-turn short circuit fault could be detected early , which is an interesting feature for a fault tolerant system. However, because of the low winding factor of single-layer windings, the number of pole pairs p should be similar but not equal to the number of slots Q. Therefore, the following relationship between the number of stator slots Q and the number of pole pairs p should be accomplished: $2p = Q \pm 2$.
- Self-inductance of 1 p.u. for the complete fault-tolerant design: as mentioned in the state of art, the design philosophy of fault-tolerant PMSMs is to have independent phases, so the mutual inductances must be as low as possible. This

allows the machine to be operated with faulty windings while limiting the interaction with other phases.

4.2 Optimal Design of a Three-Phase AFPMM

As a previous step before the research and development of a multi criteria optimization procedure, a simplified version of the stochastic GA algorithm is analyzed and, applied to an axial flux three phase PMSM motor. The AFPMM optimized in this section is an in-wheel motor for an urban scooter. Fig. 46 shows the main machine dimensions, imposed by the application, whereas Table I shows the main motor parameters initially considered [52], as well as some of the restrictions considered in the design and optimization processes. The specific configuration of this motor is an internal stator or torus topology, which has two outer rotor discs in a NN configuration. The axially magnetized permanent magnets are glued to both inner faces of the rotor discs. The stator is made of strip wound steel and contains concentrated back-to-back connected windings wounded inside the slots [77].

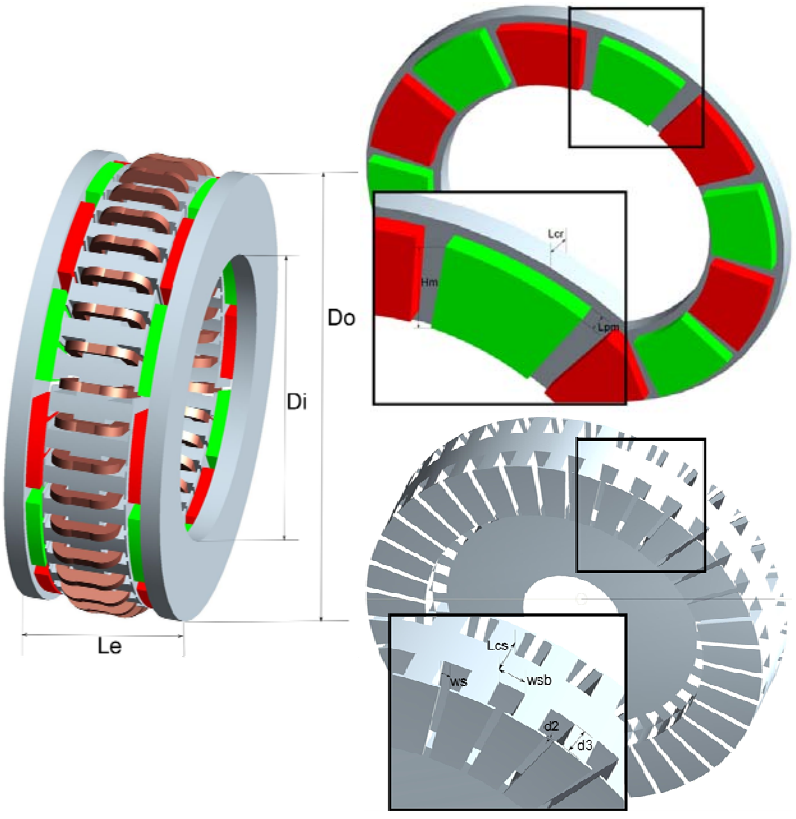

Fig. 46. Motor main dimensions.

These radial windings, which are wounded in the radial direction, are required to produce the electromagnetic torque. Due to the multiple air gaps configuration, the use of back-to-back windings allow minimizing copper losses due to the reduced end windings length when compared with other configurations, thus enhancing overall efficiency [78]. Fig. 47 shows a dual outer rotor AFPMM topology with NN configuration.

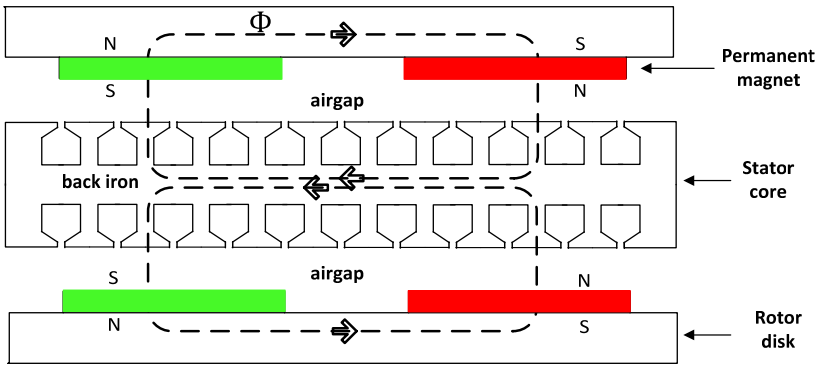

Fig. 47. Dual rotor AFPMM torus topology with NN configuration.

As shown in Fig. 46, trapezoidal magnets are used since this geometry allows minimizing the torque ripple in this kind of machines [78].

Table 7. Main parameters of the analyzed AFPMM.

Dimensional Constraints		
Machine outer diameter	D_o	< 300 mm
Inner to outer diameter ratio	D_i/D_o	0.40 – 0.75
Stator slots	Q	18
Motor effective axial length	L_e	< 200 mm
Air gap length	g	0.5 - 2.5 mm
Air gap flux density	B_g	0.35 – 0.95 T
Material limitation		
Max. stator and rotor core flux densities	B_{cs}, B_{cr}	< 1.5 T
PM remanence	B_r	1.3 T
PM relative permeability	μ_r	1.05
Requirements		
Rated line-to-line voltage	$V_{L\text{-}L}$	< 100 V
Input phase current (peak value)	$I_{s,peak}$	< 20 A
Number of phases	m	3
Number of stators	m_1	1
Output power	P_{out}	1 kW
Base electrical frequency	f_b	50 Hz
Pole pairs	p	8
Motor efficiency	η	> 80%
Electric loading	A_s	10 - 30 kA/m
Air gap flux density	B_g	0.35 – 0.95T

Current density	J_s	3.5 A/mm^2
Ratio of the average to the peak air gap flux density	α_I	0.48
Aspect ratio coefficient	K_l	0.7
Electrical power waveform factor	K_p	0.5
Current wave form factor	K_i	$\sqrt{2}$
EMF factor	K_e	0.692
Copper fill factor	K_{cu}	0.228
Carter coefficient	K_c	0.8
Peak corrected factor of the air gap flux density	K_f	0.8
Leakage flux factor	K_d	2/π

4.2.1 ANALYTICAL SIZING EQUATIONS OF THE AFPMM

In this section the equations to size the AFPMM are described. An analytical expression of the sizing equation for axial flux permanent magnet synchronous machines is given in [52],

$$P_R = \frac{m}{m_1}\frac{\pi}{2}K_e K_i K_p K_l \eta B_g A_s \frac{f}{p}(1-\lambda^2)\frac{1+\lambda}{2}D_o^2 L_e \quad (7)$$

Being P_R is the rated power. The selection of the ratio $\lambda = D_i/D_o$ between the inner and outer diameters is critical in order to optimize machine performance, since it greatly influences the magnetic and electrical loadings. Although according to [10] the maximum value of λ is $\frac{1}{\sqrt{3}}$, in practice λ usually lies between 0.6 – 0.8 to maximize the maximum torque to weight ratio.

The machine total outer diameter D_t is related to the protrusion W_{cuo} of the end windings in the radial direction from the iron core [52] as,

$$D_t = D_O + 2W_{cuo} \quad (8)$$

Protuberances exist in both the axial and radial directions of the AFPMM. Being W_{cuo}, W_{cui} the outer and the inner protrusion in the radial direction of the end winding respectively. The amplitude of the protrusions is related to the stator electrical loading A_s, current density J_s, and copper fill factor K_{cu} as,

$$W_{cuo} = \frac{\sqrt{D_o^2 + \frac{4A_s D_g}{K_{cu}J_s}} - D_o}{2}, \quad W_{cui} = \frac{\sqrt{D_i^2 + \frac{4A_s D_g}{K_{cu}J_s}} - D_i}{2} \quad (9)$$

Where the average diameter is calculated as:

$$D_g = \frac{(D_o + D_i)}{2} \quad (10)$$

The effective stack or axial length of the AFPMM depends on the of rotor and stator axial lengths (L_r, L_s) and the airgap g, which in this case is double due to a torus AFPMM configuration,

$$L_e = L_s + 2L_r + 2g \quad (11)$$

The axial length of the stator is related to the stator core axial length L_{cs} and the amplitude of the protrusions by,

$$L_s = L_{cs} + 1.6W_{cui} \tag{12}$$

Where the axial length of the stator core may be calculated from the flux density in the air gap B_g and in the stator core B_{cs} and the ratio $\lambda = D_i/D_o$ as,

$$L_{cs} = \frac{B_g \pi D_o (1+\lambda)}{B_{cs} 4p} \tag{13}$$

Similarly, the axial length of the rotor L_r may be calculated from the axial length of rotor core L_{cr} and the length of the permanent magnets L_{PM} as,

$$L_r = L_{cr} + L_{PM} \tag{14}$$

$$L_{PM} = \frac{\mu_{r,PM} + B_g}{0.95B_r - \frac{1}{K_d}B_u}(g + W_{cui}) \tag{15}$$

Note that (14) depends on the PM relative permeability and remanent flux density $\mu_{r,PM}$ and B_r, respectively, the flux density B_u at the surface of the PMs, and a flux leakage factor K_d.

The axial length of rotor core L_{cr} may be expressed as:

$$L_{cr} = \frac{B_u \pi D_o (1+\lambda)}{B_{cr} 8p} \tag{16}$$

B_{cr} being the flux density in the rotor core.

Since the PMs are placed in the rotor discs, whereas an AC magnetic flux flows through the stator core, the flux flowing through the rotor core is almost constant. According to [52] there is a link between the electric frequency and the stator core flux density, which may be expressed as,

$$B_{cs} = \begin{cases} 5.47 f^{-0.32}\ \mathrm{T} & f > 40Hz \\ 1.7 - 1.8\ \mathrm{T} & f \leq 40Hz \end{cases} \tag{17}$$

In addition, the rotor core flux density should be within the interval,

$$B_{cr} = 1.6 - 1.8\ \mathrm{T} \tag{18}$$

The air gap flux density in an AFPMM may be expressed as:

$$B_g = K_d B_u \tag{19}$$

For the axial flux machines the electrical loading A, is a function of radius. Its average is:

$$A_s = 2mN_{ph}\frac{I_N}{\pi D_g} \tag{20}$$

Number of slots per phase

$$q = Q/m \tag{21}$$

$$q_{mp} = Q/pm \tag{22}$$

Number of slots per phase per pole

$$n_s = N_{ph}/q \tag{23}$$

Being N_{ph} the number of turns per phase. The airgap inductance is defined by

$$L_g = \frac{n_s^2 \mu_R \mu_0 (D_o^2 + D_i^2) k_d}{8(L_{pm} + 2\mu_R k_c g)} \tag{24}$$

The slot inductance

$$L_s = n_s^2 \left[\frac{\mu_0 d_3}{3w_{sb}} + \frac{\mu_0 d_2}{0.5(w_s + w_{sb})}\right](R_0 - R_i) \tag{25}$$

The phase inductance

$$L_{ph} = 2q_{mp}(L_g + L_s) \tag{26}$$

The slot resistance

$$Rs = \frac{\rho n_s^2 (D_o + D_i)}{2k_c S_q} \tag{27}$$

Being ρ the conductor resistivity. The phase resistance

$$R_{ph} = 2q_{mp} R_s \tag{28}$$

The phase impedance magnitude

$$Z_e = \left|R_{ph} + j\omega L_{ph}\right| \tag{29}$$

Maximum back EMF

$$EMF_{max} = K_e N_{ph} B_g \frac{f}{p}(1 - \lambda^2) D_o^2 \tag{30}$$

Maximum current

$$I_{max} = A_s \pi K_i \frac{(1+\lambda)}{2} \frac{D_o}{2mN_{ph}} \tag{31}$$

Power density can be defined as:

$$P_{den} = \frac{Pout}{\frac{\pi}{4} D_O^2 L_e} \tag{32}$$

Base angular frequency

$$\omega_N = 2\pi f \tag{33}$$

Base value for flux linkage

$$\psi_b = \psi_N = \frac{V_N}{\omega_N} \tag{34}$$

Base value for inductance

$$L_b = L_N = \frac{\psi_N}{I_N} \tag{35}$$

4.2.2 RESTRICTIONS FOR MAXIMIZING FAULT TOLERANCE

To ensure a high level of fault tolerance in electric machines, the phase windings should be arranged in independent modules, i.e. they should avoid as much as possible electric, magnetic, physical and thermal coupling [25]. Magnetic isolation allows minimizing voltages induced in adjacent phases due to a fault current in the damaged phase. In addition, both physical and thermal isolation reduce the risk of faults between phases. Non-overlapping windings provide minimum mutual inductance between phases, thus minimizing interactions between the faulty phase and the others, so they are highly recommended in fault tolerant machines.

The restrictions imposed to ensure a high level of fault tolerance capability in the analyzed three-phase AFPMM are summarized below [79],

- When dealing with single-layer windings, the harmonic content of both the MMF and EMF is higher than in double-layer windings, thus increasing acoustic noise and torque pulsation levels. This problem may be minimized by selecting a suitable slot/pole ratio. The number of stator teeth must be an even multiple of the number of phases to reduce acoustic noise and vibrations, thus extending the service life of the shaft bearings. This results in $Q = 6n$, where n is an integer number [79]. This condition can be expressed as,

$$Q \pm 2 = 2p \tag{36}$$

- To increase the phase inductances and reduce the short circuit currents, the slots in the stator should be deep enough [80]. The phase inductance calculated as $Z_L = EMF/I_s$ must be close to 1 p.u., i.e.

$$Z_{ph} = 2\pi f L_b \tag{37}$$

where the base value of the phase inductance L_b is calculated as,

$$L_b = \frac{\psi_b}{I_{s,N}} \tag{38}$$

And the base value of the flux linkage is defined as,

$$\psi_b = \frac{V_{ph,N}}{\omega_b} \tag{39}$$

$\omega_b = 2\pi f_b$ being the base electrical angular frequency.

Both the air gap and slot impedances L_g and L_s in (24) and (25), respectively, are adjusted during the optimization process to obtain unity phase impedance according to (35).

In order to compare speed and computational load three optimization methods have been applied namely genetic algorithm (GA), *fmincon* and *fminimax,* solvers that already are implemented in the Matlab® environment.

Genetic algorithms (GAs) are a family of mathematical methods widely applied to solve optimization problems both constrained and unconstrained. GAs are search methods based on genetics and natural selection [81] and are being applied in the field of design optimization of electric machines [82]. In this case, GA searches the space of the motor parameters emulating genetic reproduction mechanisms, crossover, and mutation with the objective of obtaining an optimal design. GA recurrently modifies the population of individual solutions by randomly selecting at each step individuals from the current population. Therefore, the GA generates a population of individuals each iteration, the best one approaching a local optimal solution. These selected specimens are the parents

which generate the children individuals for the subsequent generation. This process is repeated over successive generations with the finality of obtaining population individuals evolving toward an optimal solution. GA may be applied to solve different optimization problems which cannot be solved by traditional methods that use the gradient information of optimization since GA doesn't use the gradient information. Therefore, GA may be applied even in problems with highly nonlinear, non-differentiable or stochastic objective functions [83].

In order to generate the next generation of individuals from the current population, GA uses the following rules at each step,

- Individual's selection (parents) for the next generation.
- Crossover operators which usually combine two parents' solutions to generate offspring or children solutions for the next generation.
- Mutation operators which allow maintaining genetic diversity from one generation to the next. They apply random changes to individual parents and to children solutions.

Fig. 48 summarizes the steps involved in the GA method.

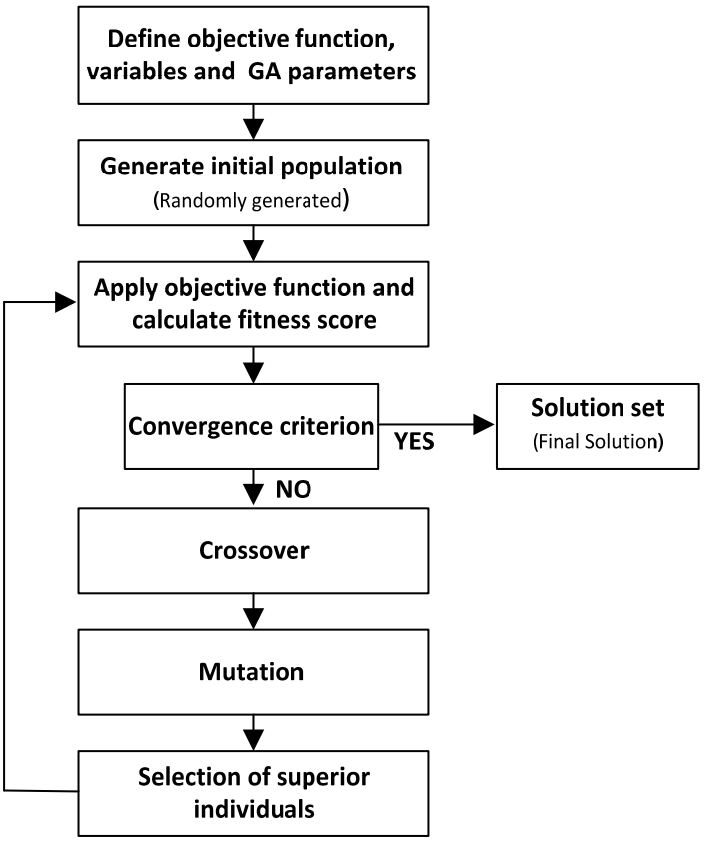

Fig. 48. Steps involved in the GA.

In machine design, there are a considerable number of free parameters. When aiming for an optimal solution, the task becomes extremely complex due to the huge number of possible combinations, unless the number of these free parameters is limited to some

extent. In this design the following eight parameters have been taken as input of the optimization algorithms: inner to outer diameter ratio, air gap flux density, air gap length, electric loading, number of turns per phase, stator slot tip length, slot opening and slot width.

In regards the coding part of the genetic algorithm, these parameters are taken as individuals, and then transformed into a binary string which will form the first chromosome.

In this study, the elitist method is used as the selection operator for scattered crossover. This method of reproduction generates a random binary vector, and then chooses the genes from the first parent in which the vector is a 1 and the genes from the second parent containing a 0, the combination of these genes forming the child.

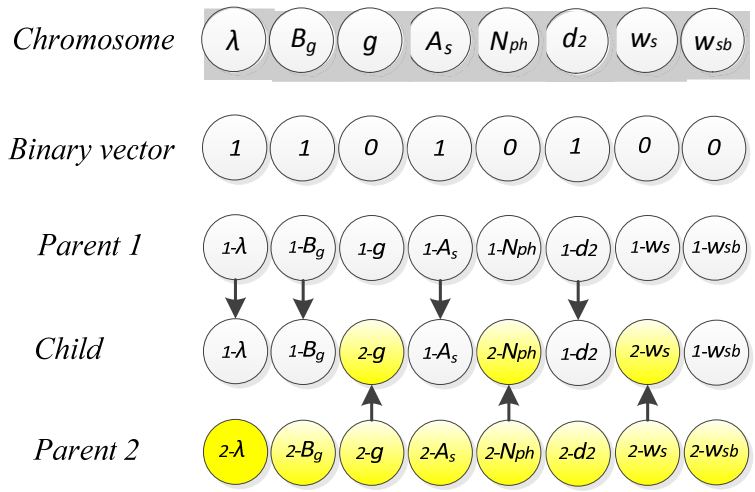

Fig 49. Scattered crossover representation.

The mutation operation randomly generates directions which are adaptive with respect to the last unsuccessful or successful generation. This process is repeated over successive generations with the finality of obtaining population individuals evolving toward an optimal solution.

Two more optimization solvers are used in this first design for comparison purposes, i.e. *fmincon* and *fminimax.* Both functions are included in the Matlab® Optimization Toolbox and can handle linear equalities and inequalities constraints, nonlinear inequality constraint functions and bound constraints.

The *fmincon* solver performs a constrained nonlinear minimization whereas the *fminimax* solver performs a minimax optimization. Both *fmincon* and *fminimax* solvers are sequential quadratic programming (SQP) methods, i.e. nonlinear programming methods which allow solving constrained minimization problems. These quasi-Newton algorithms try to generalize the Newton's method to constrained optimization problems and are able to find local minima of constrained functions. They don’t calculate the Hessian matrix, instead it is approximated by calculating different gradient vectors.

4.2.3 RESULTS

This section shows the results attained by applying the three aforementioned solvers, i.e. *ga*, *fmincon* and *fminimax*. Eight input variables which are shown in Table 8 are the input variables of the optimization algorithms in order to optimize the objective or fitness function, i.e. the power density.

Table 8. Input variables for the optimization algorithm.

Input variables to optimize the fitness function		
Input optimization variables	***Symbol***	**Bounds**
Inner to outer diameter ratio	D_i/D_o	0.40 – 0.75
Air gap flux density	B_g	0.35 – 0.95 T
Air gap length	g	0.5 – 2.5 mm
Electric loading	A_s	10 – 30 kA/m
Turns per phase	N_{ph}	2 – 100
Stator slot tip length	d_2	1 – 4 mm
Slot opening	w_s	1 – 40 mm
Slot width	w_{sb}	2 – 40 mm
Variables involved in linear inequalities		
Variables	***Symbol***	**Inequalities**
Machine outer diameter	D_o	< 300 mm
Motor effective axial length	L_e	< 200 mm
Axial length of permanent magnets	L_{PM}	< 9 mm
Input phase current (peak value)	$I_{s,peak}$	< 20 A

Simulation results presented in this section are compared with those provided in [76]. Results provided by this reference work were tested on laboratory. This comprehensive method allows designing an arbitrary-capacity multi-parameter double-sided AFPMM motor. Table 9 shows the results attained the optimization process when designing a standard AFPMM, i.e. when no fault tolerant restrictions are applied.

Table 9. Results attained when no fault tolerance restrictions are considered.

	Ref. [76]	***fmincon***	***fminimax***	***ga***
P_{den} [W/cm^3]	0.360	0.382	0.382	0.374
D_o [m]	0.1640	0.1642	0.1642	0.1628
N_{ph}	70	70	73	73
A_s [A/m]	15198	15000	15000	15100

g [mm]	1.1	1.0	1.0	1.0
L_e [mm]	–	82.6	82.6	84.5
L_{PM} [mm]	3.6	2.5	2.5	2.7
L_{cr} [mm]	13.0	13.4	13.4	13.2
L_{cs} [mm]	13.0	13.0	13.0	13.0
B_g [T]	0.48	0.46	0.46	0.47
λ[p.u.]	0.58	0.50	0.50	0.49
η[p.u.]	0.915	0.950	0.940	0.948

Values presented in Table 9 show that the results attained by applying the three optimization methods are similar to those presented in [76], thus validating the approach applied. Fig. 50 shows the evolution of the results attained by means of the three studied optimization algorithms.

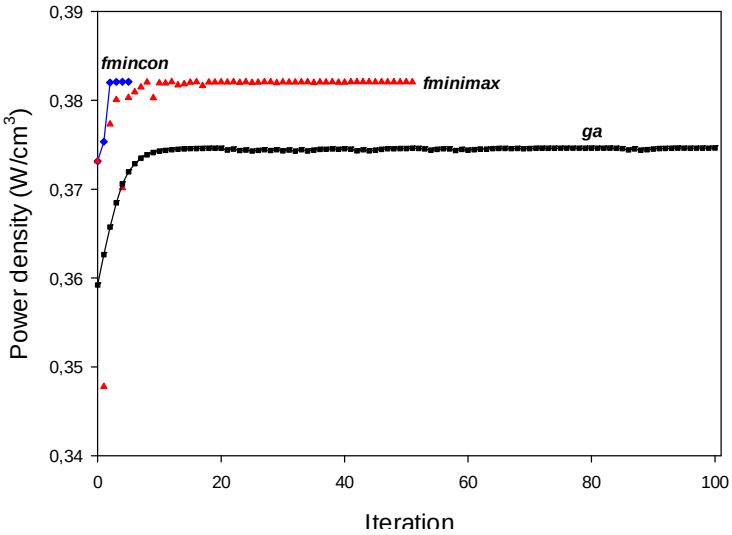

Fig. 50. Fitness function variation when applying the *fmincon*, *fminimax* and *ga* solvers with no fault tolerant restrictions.

According to the results presented in Fig. 50, both *fmincon* and *fminimax* algorithms are faster than *ga* in attaining the optimal solution, and in this specific case they also provide a better solution (higher power density).

Table 10. Results attained considering fault tolerance restrictions.

	fmincon	***fminimax***	***ga***
P_{den} [W/cm^3]	0.331	0.322	0.352
D_o [m]	0.1654	0.1672	0.1637
N_{ph}	73	73	72
A_s [A/m]	15000	14801	15000

g [mm]	1	1	1
L_e [mm]	87.6	87.7	85.4
L_{PM} [mm]	1.8	1.6	2.3
L_{cr} [mm]	11	11	12.4
L_{cs} [mm]	13	13	13
B_g [T]	0.44	0.43	0.45
λ[p.u.]	0.44	0.43	0.46
η [p.u.]	0.84	0.89	0.88

By comparing the results shown in Tables 9 and 10, it is observed that when applying the fault tolerance restrictions the AFPMM's power density unavoidably decreases by a factor less than 8% in the case analyzed. In addition the efficiency also decreases approximately by 7%. In this case the *ga* solver provides the better solution. These results show the effectiveness of the *ga* solver in facing a nonlinear problem such as the fault tolerant design of an AFPMM. It must be noted that both fminimax and fmincon strongly depend on the starting point so generally these algorithms converge to a local minima when dealing with highly nonlinear optimization problems. This is the case of the fault tolerant design of an AFPMM

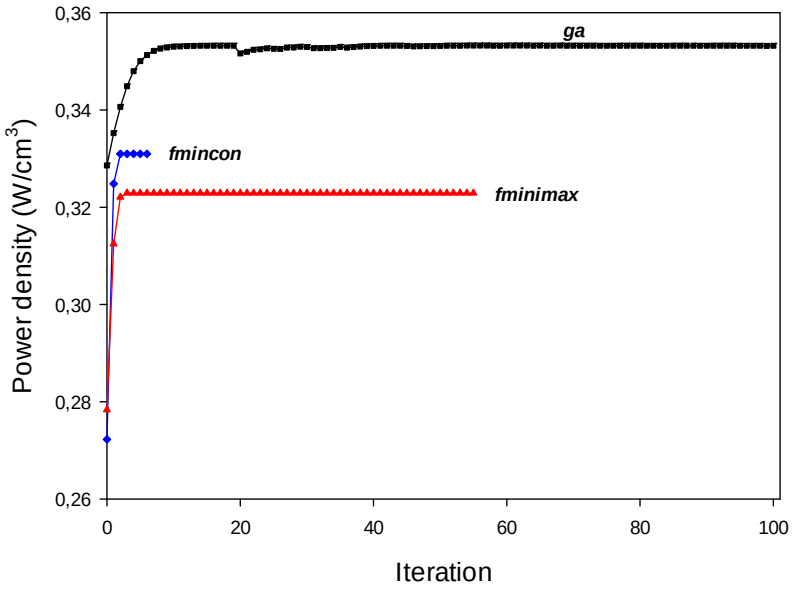

Fig. 51. Fitness function variation when applying the *fmincon*, *fminimax* and *ga* solvers with fault tolerant restrictions.

4.3 MULTI-OBJECTIVE OPTIMAL DESIGN OF A FIVE-PHASE FAULT-TOLERANT AFPMM

In this section a five-phase AFPMM synchronous machine is selected to be optimally designed. This kind of actuator is known to be very convenient for some specific applications such as direct drive in-wheel applications due to the high power and torque densities [84]. It is worth noting that direct drive machines simplify the vehicle mechanical structure, thus the overall vehicle efficiency and weight are minimized. The studied machine has a torus geometry containing an internal stator and two outer rotor disks, which include the magnets. The rotor disks present a NN configuration, i.e. a north pole N facing another north pole N, which is placed at the other side of the stator [82]. Fig. 52 shows the AFPMM dealt with.

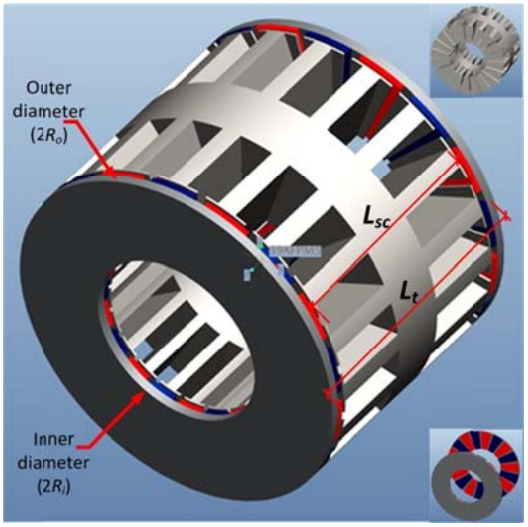

Fig. 52. Dual rotor AFPMM torus topology with NN configuration.

The stator core of the AFPMM is made of strip wound steel and includes concentrated back-to-back connected windings, which are wounded inside the slots in the radial direction [82]. Back-to-back windings allow enhancing the overall machine efficiency, since they offer reduced end windings length, thus presenting lower copper losses. In addition, both rotors contain permanent magnets with trapezoidal geometry to minimize the torque ripple [78].

Non-overlapping windings provide minimum mutual inductance between phases, thus minimizing interactions between the faulty phase and the others, so they are highly recommended in fault-tolerant machines. In addition, the design should ensure low mutual coupling among phases to limit the effect of the short circuit in one phase on other phases. The use of concentrated stator windings (i.e. windings encircling a single stator tooth, thus eliminating end-winding overlap among phase windings) offer several advantages compared to distributed windings, including a reduction of the copper volume of the end windings, which is especially significant when the axial length of motor is small, thus minimizing copper losses and improving the motor efficiency [85] compared to stator windings with integer number of slots per pole and per phase. They also allow reducing the total length of the machine and manufacturing costs since

concentrated windings are easier to realize. Finally, an important advantage is that compared to distributed windings, concentrated windings tend to provide higher inductance when the magnetic flux linkage is the same, which allows extending the flux-weakening region [86].

Since in this particular design the fault-tolerance is a must, a concentrated non-overlapping fractional-slot single-layer winding has been selected, as shown in Fig. 53, since it provides enough magnetic and electric insulation to avoid a major propagation of a short circuit in the event of a short circuit fault.

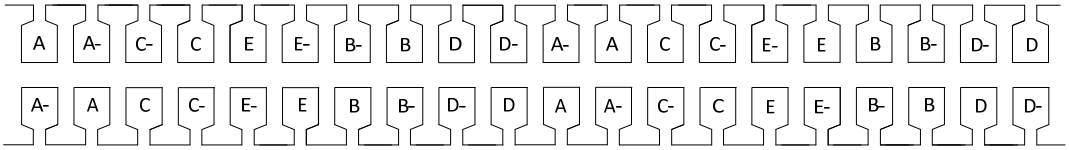

Fig. 53. Layout of the fractional-slot single-layer concentrated winding structure.

4.3.1 SIZING EQUATIONS OF THE FIVE-PHASE AFPMM

This section develops the sizing equations to design the five-phase AFPMM as described in [63]. The mechanical and electrical speeds in rad/s are, respectively,

$$\omega_m = \frac{\pi}{30} \cdot \frac{f}{p} \tag{40}$$

$$\omega_e = p \cdot \omega_m \tag{41}$$

f and *p* being, respectively, the electrical frequency and the number of pole pairs. The torque can be obtained from the output mechanical power as,

$$T_{out} = \frac{P_{out}}{\omega_m} \tag{42}$$

The number of slots per pole and per phase is,

$$q = \frac{Q}{2 \cdot p \cdot m} \tag{43}$$

Q being the number of slots and *m* the number of phases. The coil-pole fraction is defined as,

$$\alpha_{cp} = \frac{2\mathrm{p}}{Q} \tag{44}$$

The angular pole and slot pitches are as follows,

$$\theta_p = \frac{\pi}{p} \tag{45}$$

$$\theta_s = \frac{2\pi}{Q} \tag{46}$$

The slot pitch in electrical radians is,

$$\theta_{se} = \frac{2\pi}{Q} \cdot p \tag{47}$$

The inside and outside pole pitches are,

$$\tau_{pi} = R_i \theta_p \tag{48}$$

$$\tau_{po} = R_o \theta_p \tag{49}$$

R_i and R_o being, respectively, the inner and outer rotor radius. The inside and outside coil pitches are, respectively,

$$\tau_{ci} = \alpha_{cp}\tau_{pi} \tag{50}$$

$$\tau_{co} = \alpha_{cp}\tau_{po} \tag{51}$$

And the inner slot pitch is calculated as,

$$\tau_{si} = R_i\theta_s \tag{52}$$

The distribution factor required to calculate the winding factor is as follows,

$$k_d = \frac{\sin(\pi/2m)}{q\cdot\sin(\pi p/Q)} \tag{53}$$

When q is a fractional number less than 1, the pitch factor K_p can be defined as the ratio between the vectorial and the arithmetic sum of the EMFs per coil side [10],

$$K_p = \sin\left(\frac{\pi p}{Q}\right) \tag{54}$$

In addition the skew factor is,

$$k_s = 1 - \frac{\theta_{se}}{2\pi} = 1 - \frac{p}{Q} \tag{55}$$

And the magnet fraction is,

$$\alpha_m = \tau_m/\tau_p = 1 - \frac{2\cdot p\cdot\tau_f}{\pi(R_o - R_i)} \tag{56}$$

where τ_m and τ_f are, respectively, the permanent magnet and spacer widths shown in Fig. 54.

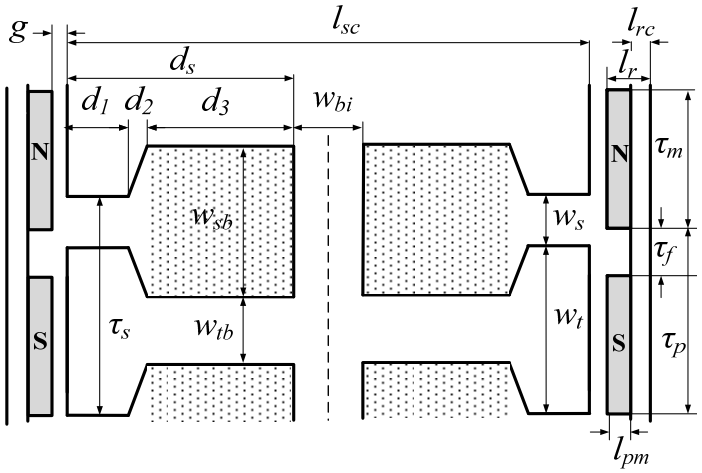

Fig. 54. Sketch of the stator and rotor dimensions.

The permanent magnet leakage factor is,

$$k_{ml} = 1 + \frac{4l_{pm}p}{\pi^2\mu_R\alpha_m(R_i+R_o)}\,ln(1 + \pi\frac{g}{\tau_f}) \tag{57}$$

Being l_{pm} the permanent magnet length. The effective air gap to calculate the Carter coefficient is,

$$g_c = 2g + \frac{l_{pm}}{\mu_R} \tag{58}$$

And the Carter coefficient is calculated as,

$$k_c = \left[1 + \frac{1}{\frac{\tau_{si}}{\omega_s}(5\frac{g_c}{\omega_s}+1)}\right]^{-1} \tag{59}$$

where w_s is the slot opening, as show in Fig. 3. The air gap area is as follows,

$$A_g = \frac{\pi(1+\alpha_m)}{4p}(R_o^2 - R_i^2) \tag{60}$$

The average value of the air gap flux density is,

$$B_g = \frac{C_\theta}{1+\mu_R k_c k_{ml}/P_c} B_r \tag{61}$$

B_r being the remanence of the permanent magnets and C_θ and P_c, respectively, the flux concentration factor and the permeance coefficient,

$$C_\theta = \frac{2\cdot\alpha_m}{1+\alpha_m}, \qquad P_c = \frac{l_{pm}}{2gC_\theta} \tag{62}$$

The air gap flux is calculated as,

$$\phi_g = B_g A_g \tag{63}$$

The stator back iron width is,

$$w_{bi} = \frac{B_g \tau_{po}}{2B_{max}k_{st}} \tag{64}$$

k_{st} being the lamination stacking factor. The stator tooth width calculated at the inner radius is,

$$w_{tbi} = \frac{B_g \tau_{pi}}{2N_{sm}B_{max}k_{st}} \tag{65}$$

B_{max} being the maximum allowable flux density in the stator yoke. The slot bottom width is,

$$w_{sb} = \tau_{si} - w_{tbi} \tag{66}$$

The slot aspect ratio at the bottom width,

$$\alpha_{si} = \frac{w_{sb}}{w_{tbi}+w_{sb}} \tag{67}$$

The shoe depth split between d_1 and d_2,

$$d_1 = \alpha_{sd} w_{tbi} - d_2 \tag{68}$$

α_{sd} being the shoe depth fraction, which is defined as,

$$\alpha_{sd} = \frac{d_1+d_2}{w_{tb}} \tag{69}$$

The number of turns per slot is,

$$n_s = int\left(\frac{E_{max}}{2pk_d k_p k_s B_g q \omega_m (R_o^2 - R_i^2)}\right) \tag{70}$$

The peak value of the back-EMF,

$$E_{max} = 2pk_d k_p k_s B_g q \omega_m n_s (R_o^2 - R_i^2) \tag{71}$$

The peak value of the slot current,

$$I_s = \frac{T_{out}}{2pk_d k_p k_s B_g q(R_o^2 - R_i^2)} \quad (72)$$

The peak value of the phase current is,

$$I_{ph} = \frac{I_s}{mn_s} \quad (73)$$

The conductor slot depth is obtained from the area required to fit the conductors according to the allowable current density,

$$d_3 = \frac{I_s}{k_{cp} w_{sb} J_{max}} \quad (74)$$

Assuming rectangular slots, the slot area is,

$$A_s = w_{sb} d_3 \quad (75)$$

The conductor current density is

$$J_c = \frac{I_s}{k_{cp} A_s} \quad (76)$$

where k_{cp} is the slot fill factor, typically less than 70% (set to 50%) and A_{load} is the stator electrical loading, which can be calculated as,

$$A_{load} = 2mn_s \frac{I_{ph}}{\pi(R_o + R_i)} \quad (77)$$

According to Fig 54, the stator tooth height is,

$$d_s = d_1 + d_2 + d_3 \quad (78)$$

AFPMMs present protrusions in both the axial and radial directions, whose magnitude depends on the stator electrical loading A_{load}, current density J_C, and copper fill factor k_{cp}. The inner protrusions along the axial length can be calculated as [52],

$$W_{cui} = \sqrt{R_i^2 + \frac{A_{load}(R_{i+R_O})}{k_{cp} J_c}} - R_i \quad (79)$$

The effective stack or axial length of the AFPMM depends on the rotor and stator axial lengths as,

$$l_t = l_s + 2l_r + 2g \quad (80)$$

From manufacturer's experience, the effective axial length of the stator is related to the stator core axial length and the amplitude of the inner protrusions W_{cui} as,

$$l_s = l_{sc} + 1.6W_{cui} \quad (81)$$

Where the minimum value of the axial length of the stator core also may be calculated from the flux densities in the air gap B_g and in the stator core B_{sc} and the geometric ratio $\lambda = R_i/R_o$ as,

$$l_{sc,min} = \frac{\pi B_g R_o (1+\lambda)}{2B_{sc} p} \quad (82)$$

This minimum value of $l_{sc,min}$ is imposed to avoid a possible saturation and extra losses in the stator laminations. The new stator axial length is then computed from the total slot depth and the stator yoke width as,

$$l_{sc} = 2d_s + w_{bi} \geq l_{sc,min} \quad (83)$$

Since the value of l_{sc} calculated in (83) must be greater or equal than that in (82) to avoid stator laminations saturation, when $l_{sc} < l_{sc,min}$ the value of w_{bi} must be increased to satisfy (83), so it starts a new iteration from (64). The axial length of the rotor l_r is calculated from the axial length of the rotor core l_{rc} and the length of the permanent magnets l_{pm} as,

$$l_r = l_{rc} + l_{pm} \tag{84}$$

The axial length of the rotor core l_{rc} may be expressed as,

$$l_{rc} = \frac{\pi B_g R_o (1+\lambda)}{4 C_\theta B_{rc} p} \tag{85}$$

B_{rc} being the flux density in the rotor core. It is worth noting that B_{rc} is almost stationary since it is mostly due to the permanent magnets placed in the rotor discs, whereas the ac magnetic flux mainly flows through the stator core.

The peak flux density in the slots is,

$$B_{s,max} = \frac{\mu_o I_s}{w_s} \tag{86}$$

The slot resistance is,

$$R_s = \frac{\rho n_s^2 (R_o - R_i)}{A_s k_{cp}} \tag{87}$$

And the end-turn resistance is calculates as,

$$R_e = \frac{\rho n_s^2 \pi (\tau_{co} - \tau_{ci})}{4 A_s k_{cp}} \tag{88}$$

The phase resistance is obtained from the slot and end-turn resistances as,

$$R_{ph} = 2 N_{sp} (R_s + R_e) \tag{89}$$

The air gap inductance,

$$L_g = \frac{n_s^2 \mu_o \mu_R \theta_c k_d (R_O^2 - R_i^2)}{4 (l_{pm} + 2 \mu_R k_c g)} \tag{90}$$

The slot leakage inductance, is

$$L_s = n_s^2 (R_o - R_i) \left[\frac{\mu_o d_3}{3 w_{sb}} + \frac{\mu_o d_2}{(w_s + w_{sb})/2} + \frac{\mu_o d_1}{w_s} \right] \tag{91}$$

and the end-turn inductance,

$$L_e = \frac{n_s^2 \mu_o \tau_{co}}{16} ln \left(\frac{\tau_{co}^2}{4 A_s} \right) + \frac{n_s^2 \mu_o d_1}{16} ln \left(\frac{\tau_{ci}^2 \pi}{4 A_s} \right) \tag{92}$$

Finally, the total phase inductance is,

$$L_{ph} = 2 N_{sp} \left(L_s + L_g + L_e \right) \tag{93}$$

Both the slot opening w_s and the slot depth d_3 have a great impact on the leakage inductance, since when the first one lowers and/or the last one rises, the slot leakage inductance L_s in (91) increases. Under fault conditions, a high inductance limits the rate of change of the current while increasing the amount of time available to detect such a fault. However, as a high inductance increases the electric time constant, it makes the motor more difficult to drive. As a result, a tradeoff exists.

The Joule losses in the stator conductors are,

$$P_{Jl} = mR_{ph}I_{ph}^2 \tag{94}$$

The total core losses are,

$$P_{cl} = \rho_{bi}V_{st}p_{spec} \tag{95}$$

Where ρ_{bi} is the lamination mass density, p_{spec} is specific loss of the steel laminations dealt with (see Fig. 55), and V_{st} is the volume of the stator steel laminations, which is calculated as,

$$V_{st} = 2k_{st}\left[\pi\left(R_o^2 - R_i^2\right)(w_{bi} + d_s) - QA_s(R_o - R_i)\right] \tag{96}$$

k_{st} being the stacking factor of the magnetic core.

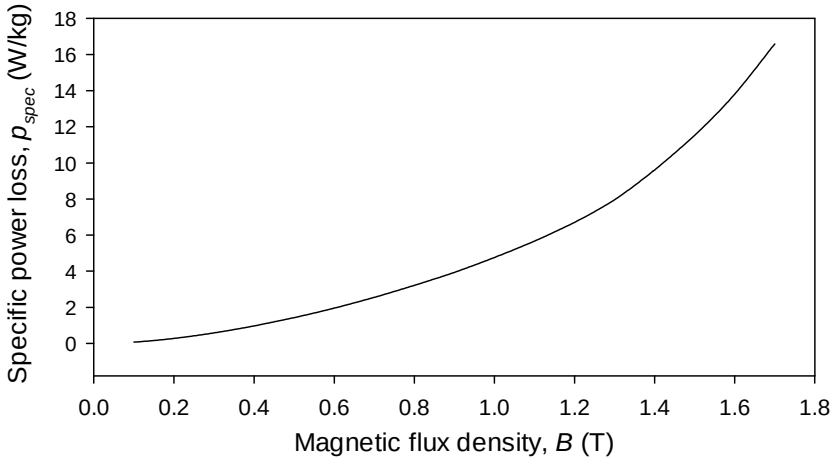

Fig. 55. M330-35A steel laminations, specific core loss versus magnetic flux density at 165 Hz.

And the overall efficiency is,

$$\eta = \frac{T\omega_m}{T\omega_m + P_{Jl} + P_{cl} + P_{sl}} \tag{97}$$

Where P_{sl} are the stray losses, which are mainly composed of friction, windage, and other minor components. This design assumes P_s as 1% of the output power [87]. Finally, the power density is calculated from the mechanical output power P_{out} and the AFPMM volume as,

$$P_{den} = \frac{P_{out}}{\pi R_0^2 l_t} \tag{98}$$

As explained, multiphase machines are well suited for fault-tolerant applications. However, to further improve fault-tolerant capability, other requirements must be fulfilled, including magnetic, electrical, physical and thermal isolation among phases [25] to minimize the possibility of phase-to-phase faults occurrence. This condition may be achieved by using non-overlapping single-layer fractional-slot concentrated windings around each tooth [80] because in this configuration the phase windings are arranged in independent modules. Whereas magnetic isolation minimizes the voltages induced in adjacent phases due to a fault current in the faulty phase, physical and thermal isolation allows reducing the risk of occurrence of faults between nearby phases. Finally, to ensure electrical isolation among phases it is also highly desirable to connect each phase to a distinct single-phase full-bridge PWM converter since each power switch has to withstand the phase voltage instead of the line voltage in star-connected systems [85].

4.3.2 THE MULTI-OBJECTIVE OPTIMIZATION PROCESS

Multi-objective optimization problems involve optimizing simultaneously more than one objective function, where often trade-offs between conflicting objectives must be taken. Electric motors are known to be complex and non-linear systems but in most optimal motor designs, a single-objective function is selected [88]. Typical objectives are minimum cost, highest efficiency or minimum weight. An electric machine is usually defined by a rather large number of parameters, including geometric dimensions, material characteristics, winding configurations [81] and some constrains. Therefore, to achieve an optimal design of the AFPMM it seems reasonable to apply a multi-objective approach based on a genetic algorithm (GA) since GAs are mathematical methods well-suited for solving constrained and unconstrained single- or multi-objective optimization problems.

Due to the quite large number of parameters involved in the design process of an electric machine, to limit the complexity and computational burden of the optimization process it is required to identify a reduced set of parameters which most significantly affects the performance of the analyzed machine [81]. This final approach deals with ten parameters whose values are changed during the optimization process, which are shown in Table 12. These parameters are coded into binary strings forming the chromosomes. The elitist scattered crossover operation is applied, which at each generation produces a random binary vector from which the genes of both parents are combined to form the offspring. Next, the mutation process is applied, by which the GA creates small random variations in each bit of the chromosomes, providing genetic diversity and enabling GA to search for wider spaces. The whole process is repeated until a stablished tolerance criterion is achieved, this could be either the ratio of change between consecutive solutions or the maximum number of generations which is previously settled.

4.3.3 MODEL REFINEMENT THROUGH 3D-FEM ASSISTANCE

Once an optimal solution has been obtained by means of the optimization method based on the in the sizing equations of the five-phase AFPMM (step 1 in Fig. 56), and in order to improve the accuracy of the final design attained, a further refinement is carried out with the help of 3D-FEM simulations of the optimized motor (step 2 in Fig. 56). However, it is well known that 3D-FEM simulations have a high computational burden, so the number of simulations must be minimized.

Therefore, a 3D-FEM model of the AFPMM is generated from the solution attained in step 1. Since the air gap flux density B_g is one of the major design parameters in determining the AFPMM performance, the value of B_g obtained in step 1 is compared with the one obtained by means of the 3D-FEM model. In the case of discrepancy, a next iteration is started by adjusting the B_g value in (61) to that obtained in the FEM simulation, therefore calculating a new solution of the AFPMM design. This process is iterated until the error between the B_g value obtained by means of the optimization process based on the analytical equations and the B_g value obtained through the 3D-FEM simulations is less than a specified tolerance. However, even attaining the pre-established B_g value, it does not ensure to fulfill the design specifications such as output power and torque, or power density among others, so a final validation of the obtained design is highly desirable, this is achieved by the 3D-FEM model simulated under several

conditions. It is worth noting that with only three iterations of this last loop, the convergence was attained. Fig. 56 shows the final optimal design process flowchart applied.

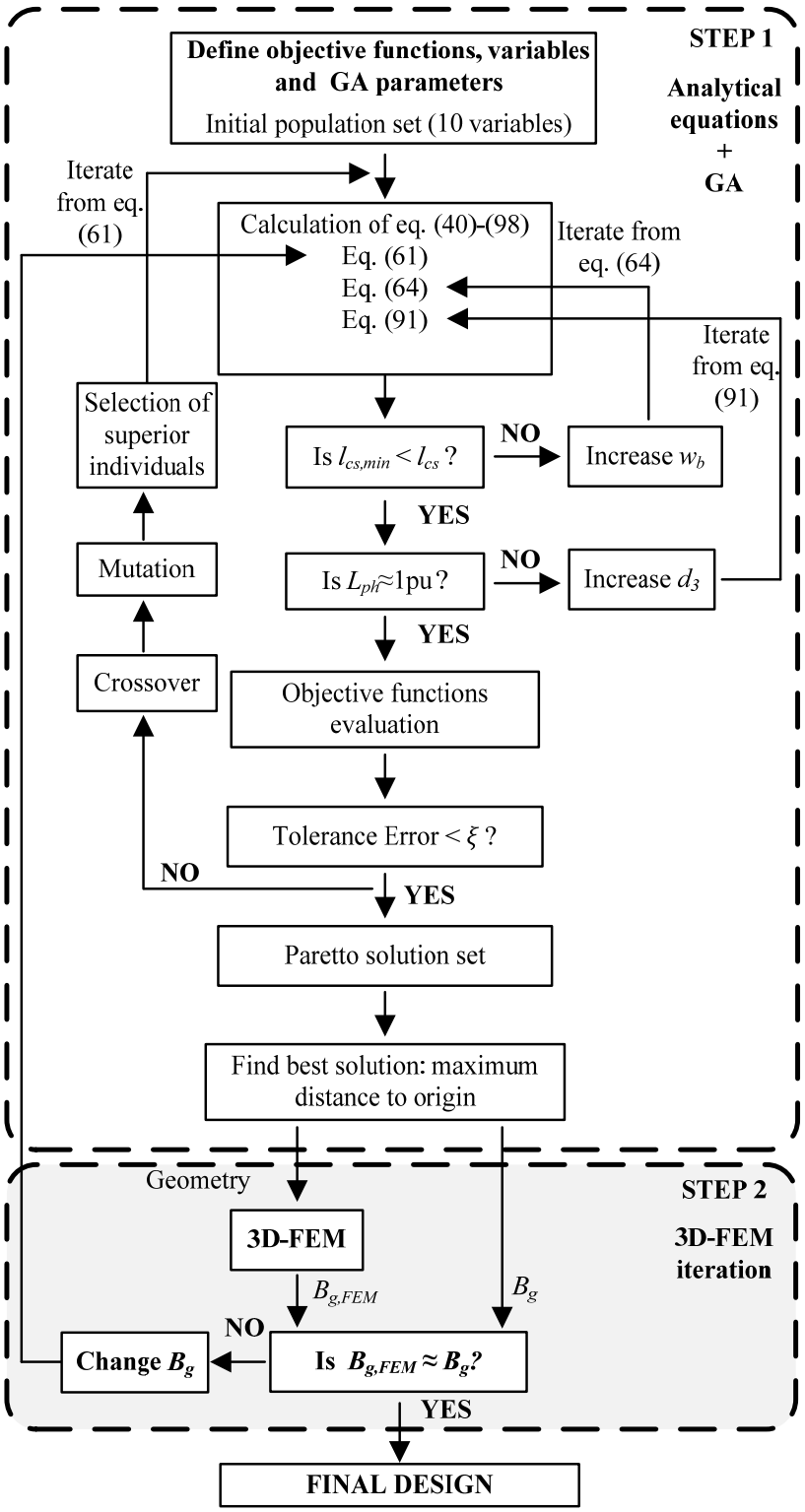

Fig. 56. Design process flowchart

4.3.4 RESULTS

There are some fixed parameters whose values don't change during the optimization process, which are detailed in Table 11. They include the desired output power, base speed, number of phases, pole pairs, number of slots, and desired flux density in the stator and rotor cores, which greatly determine the AFPMM size and performance, as well as the main properties of the materials dealt with.

Table 11. Fixed parameters and requirements of the five-phase AFPMM.

Quantity	***Symbol***	**Magnitude**
Output power	P_{out}	2000 W
Base speed	N	1100 rpm
Output torque	T_{out}	17.36 Nm
Number of phases	m	5
Base electrical frequency	f	165 Hz
Pole pairs	p	9
Number of slots	Q	20
Laminations width	S_{lw}	0.35mm
Saturation flux density	B_{sat}	1.5 T
Slot fill factor	k_{cp}	0.5
Laminations type	*M330-35A*	-
Lamination stacking factor	k_{st}	0.95
Steel laminations mass density	ρ_{steel}	7600 kg/m^3
Wire insulation thickness	W_i	0.5-2 mm
Conductors material	*Copper*	-
Conductors conductivity at 25ºC	ρ_{cu}	16.78 nΩ·m
Permanent magnets mass density	ρ_m	7400 kg/m^3
Permanent magnets relative permeability	μ_r	1.05
Permanent magnets remanent flux density	B_r	1.3 T
Flux density in the stator core (peak value)	B_{sc}	1.8
Flux density in the rotor core (peak value)	B_{rc}	1.7

The input or design variables, i.e. these variables whose values are changed during the optimization phase to explore the whole set of possible solutions, are shown in Table 12. The number of design variables is usually a tradeoff between model accuracy and complexity due to the large number of possible combinations to be analyzed during the

optimization process. Due to this tradeoff, this design deals with ten design variables which greatly impact the AFPMM performance.

Table 12. Design variables of the five-phase AFPMM.

Quantity	***Symbol***	**Magnitude**
Machine inner radius	$x(1)= R_i$	0.03-0.1 m
Machine outer radius	$x(2)= R_o$	0.06-0.2 m
Magnet spacer width	$x(3)= \tau_f$	1-5 mm
Magnet thickness	$x(4)= l_{pm}$	2-9 mm
Air gap length	$x(5)= g$	0.5-1.5 mm
Slot tip length	$x(6)= d_1$	1-4 mm
Slot tip shoe length	$x(7)= d_2$	1-2 mm
Slot width/opening	$x(8)= w_s$	2-10 mm
Peak value of the back-EMF	$x(8)= E_{max}$	24-60 V
Maximum conductor current density	$x(10)= J_{max}$	2-5 A/mm^2

The multi-objective optimization process considers two objective functions, i.e. the AFPMM power density and efficiency.

The main parameters of the MoGA applied include a population size of 1400 individuals, the maximum number of generations is 200, the probability of crossover is 0.8 and the probability of mutation is 0.01.

Fig 57 shows all solutions explored by the MoGA algorithm and the Pareto front. From all this set of solutions, the one maximizing the Euclidean distance to the origin point is selected as the best solution.

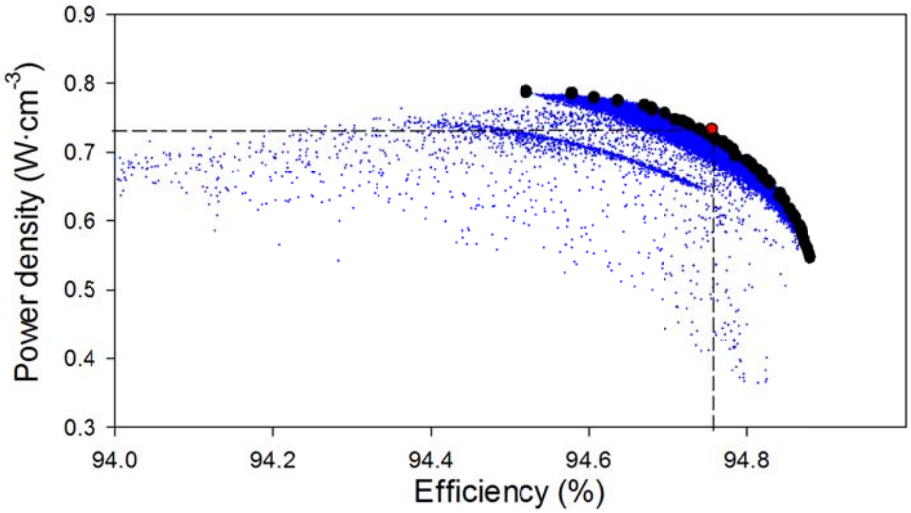

Fig. 57. Analyzed solutions and Pareto front of the fitness function obtained by applying the MoGA solver.

Table 13 summarizes some of the main parameters of the best solution attained by means of the MoGA approach.

Table 13. Results attained by applying fault-tolerance restrictions.

Quantity	***Symbol***	**Magnitude**
Power Density	P_{den}	72931 W/m^3
Efficiency	η	94.75%
Rotor outer radius	R_o	0.10 m
Rotor inner radius	R_i	50 mm
Number of turns per phase	N_{ph}	52
Air gap length	g	0.9 mm
Axial length of machine	l_t	87 mm
Magnet thickness	l_{pm}	4 mm
Rotor thickness	l_{cr}	15.2 mm
Stator thickness	l_{cs}	48.1 mm
Phase inductance	L_{ph}	1.1 mH
Phase resistance	R_{ph}	0.007 Ω
Air gap flux density (peak value)	B_g	0.689 T
Current per phase (peak value)	I_{ph}	18.5 A
EMF per phase (peak value)	E_{max}	4.4

4.4 FINITE ELEMENT VALIDATION MODEL

As it is well known, although radial-flux machines are often simulated by means of two-dimensional finite elements analysis, an axial flux machine must be modeled by means of three-dimensional finite elements methods (3D-FEM) due to its inherent three-dimensional geometry. Therefore, an accurate three-dimensional FEM model of the analyzed AFPMM with around $1.4 \cdot 10^6$ tetrahedral volumetric elements was carefully prepared in the Flux-Cedrat® environment. This model includes all geometrical and physical characteristics of the machine components, including the electric circuit. Using this modeling system it is possible to obtain diverse type of electric and magnetic quantities of the AFPMM obtained through the optimization process with very high accuracy, thus allowing verifying the excellent motor performance obtained by means of the method applied in this thesis. The motor was supplied by means of five balanced voltage sources (72º phase shift between two consecutive phase voltages).

Fig 58 plots the 3D-FEM model along with the permanent magnets and a partial view of the 3D-mesh applied in the FEM simulations.

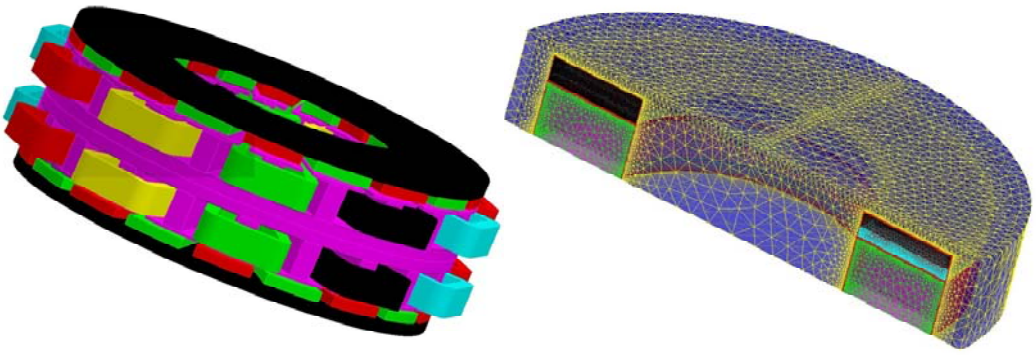

Fig. 58**.** Three dimensional model and mesh.

Fig. 59 shows the magnetic flux distribution within the AFPMM analyzed where it is proved that the flux density in the rotor laminations is almost stationary.

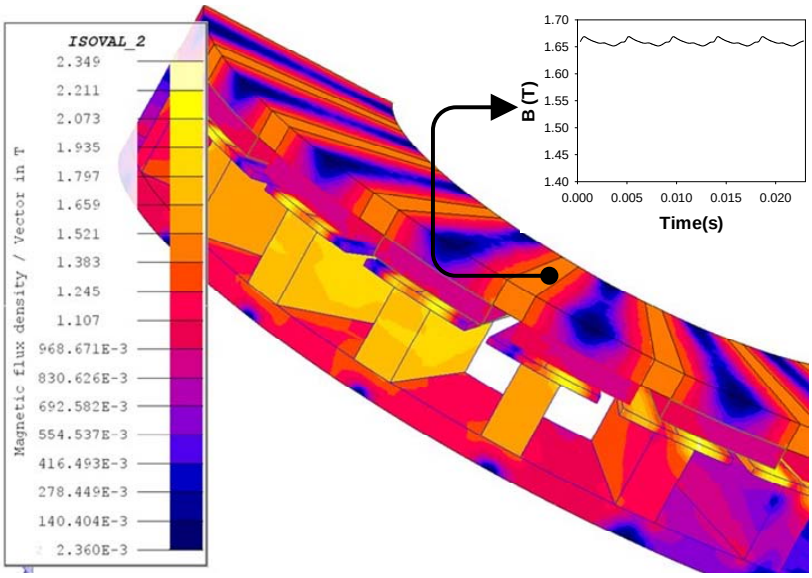

Fig. 59. 3D-FEM results. Flux density distribution.

Fig. 60 shows the output torque, back-EMF and phase inductance obtained through 3D-FEM simulations.

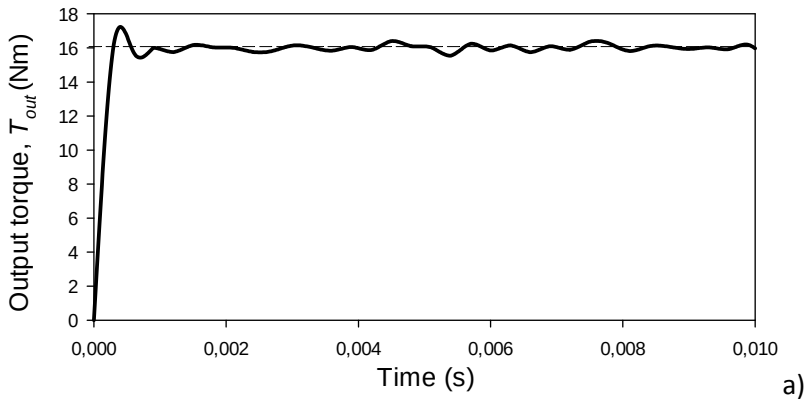

a)

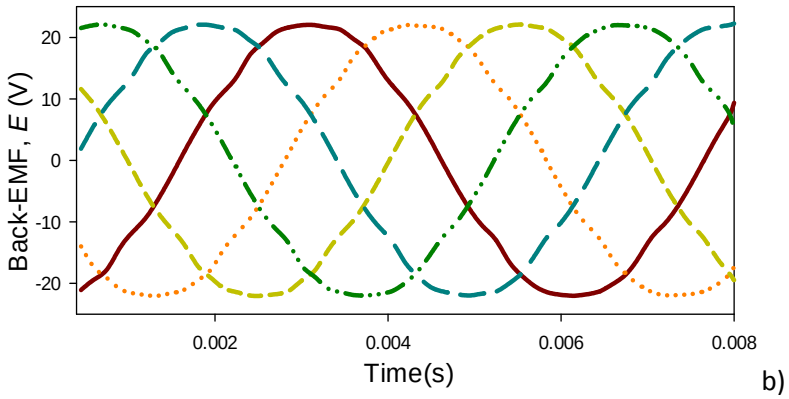

Fig. 60. 3D-FEM results. a) Output torque versus time. b) Phase back-EMF.

Table 14 compares some of the important parameters of the AFPMM calculated by means of the design method applied in this work and by the 3D-FEM approach. These results corroborate the accuracy and usefulness of the applied optimization design method.

Table 14. Comparative results

Quantity	**Optimization method**	**3D-FEM**	**Relative error**
B_g, air gap flux density (peak value)	0.689 T	0.711T	3.19%
T_{out}, output torque	17.36 Nm	15.70 Nm	9.56%
E_{max}, back-EMF (peak value)	21.59 V	22.04 V	3.75%
L_{ph}, phase inductance	1.10 mH	1.14 mH	3.64%

As shown in table 14 a small relative error is obtained. It must be said that this result where obtained after 3 major iterations from the bigger loop explained in Fig. 56. This methodology could lead to a faster design due to the combination of FEM results directly in an optimization loop.

4.5 CONCLUSIONS

This chapter has performed an optimal design of two machines, a three-phase and a five-phase fault tolerant AFPMM by applying a set of analytical equations and both, a single- and a multi-objective optimization approach based on a genetic algorithm. The following conclusions can be drawn:

- Genetic algorithms are well-suited mathematical methods to assist the design process of electrical machines, since they allow dealing with a high number of

input or design variables, whose values are changed during the optimization phase to explore the whole set of possible solutions.

- When applying fault-tolerant restrictions, the power density of the AFPMM obtained tends to decrease. However, by using genetic algorithms in the design stage this effect is minimized.
- The design process has been assisted by means of a hybrid method combining a set of analytical equations and 3D-FEM simulations, taking care of reducing the demanding computational burden due to an intensive use of 3D-FEM simulations.

5. CONCLUSIONS AND CONTRIBUTIONS

In this thesis three-phase and multi-phase permanent magnet motors have been studied and designed because they are well-suited for applications requiring high reliability. Specifically, the thesis has been focused in the optimal design of fault-tolerant axial flux machines for traction applications.

In order to select a fault tolerant system in electrical drives, a first approach deals with the fault analysis. In this thesis the study was focused to electromagnetic faults, and specifically to analyze the effects of short-circuits, since this fault is the only one that can be overcome by choosing an appropriate design. Although inter-turn short circuit faults have been analyzed in different works, our main focus was to study several winding configurations to analyze their behavior when operating under the effect of such fault. This study allows selecting the winding configuration that could deal better with such dangerous regime of working. The study concludes that a fractional winding facilitates the detection of such a fault, which is an interesting characteristic to take into account in a fault tolerant design of electrical machines.

On the other hand, an additional objective was to select the best magnet shape according to their performance under healthy and faulty conditions in order to draw conclusions to assist the design process of a fault tolerant machine. For this purpose the airgap flux density, the back-EMF, the average torque and the torque ripple of an AFPM torus-NN machine with five magnet shapes have been analyzed. The results obtained by means of 3D-FEM simulations have shown that the trapezoidal skew configuration is the magnet shape that presents both lower torque ripple and highest average torque of all analyzed magnet configurations under healthy state and partially demagnetization conditions.

After the fault analysis was done and some important design restrictions where established, an optimization process to design an in-wheel electric motor for an electric scooter was carried out. Concretely, a three-phase axial flux permanent magnet synchronous motor was optimized by applying a set of sizing analytical equations which deal with the main geometrical, electric and mechanical parameters that define the machine, in which the objective function to be maximized was the power density. Comparisons with optimized motors data found in the technical literature show the accuracy of the applied approach since similar power densities were achieved in comparison with previous designs, even when applying fault tolerant constraints. As expected, the efficiency was somewhat lowered in a fault tolerant machine mainly due to inductance constraint, because to achieve such high values of inductance an oversized stator is a must, although this could be overcome with an improved refrigeration system. In addition, fault tolerance conditions were added to the optimization process in order to provide the new motor with enhanced fault tolerance capability, since it is required in safety-critical applications.

In the last section of this thesis, a five-phase fault-tolerant axial-flux permanent magnet synchronous motor was designed by applying a multi-objective optimization approach based on a genetic algorithm. The design process was assisted by means of a hybrid method combining a set of analytical equations and 3D-FEM simulations, taking care of reducing the demanding computational burden due to an intensive use of 3D-FEM

simulations. Some fault-tolerance requisites taken from previous studies were considered during the optimization process to ensure further fault-tolerance capability. Two objective functions (the power density and efficiency of the machine) were considered in the multi-objective optimization process. The accuracy of the sizing method was validated by means of three-dimensional finite element simulations, which showed great accuracy when comparing four relevant parameters that define the machine performance. Results presented in this work showed the feasibility of the applied method to optimally design electric motors with enhanced fault tolerance capability

The contributions can be summarizing as:

- It has been analyzed the behavior of the motor under electromagnetic faults (short circuits) in both healthy and faulty conditions.
- It is proposed a method to detect inter-turn short-circuits by analyzing the third harmonic of the stator currents and, depending on the winding configuration, the ninth harmonic may also be analyzed to this end. Additionally, the first, fifth and seventh harmonics of the ZSVC may be monitored to detect inter-turns faults for all analyzed winding configurations. This information may be useful to design improved fault detection schemes and assure the fault tolerance of the drive.
- It is proposed a particular trapezoidal shape of the magnets, to improve the motor operation under healthy condition, and also to minimize the loss of performance under faulty operation, as a way to improve the fault tolerance of the drive.
- It is proposed a couple of design restrictions (number of slots per phase and pole less than 1 and trapezoidal magnets) for a configuration of a multiphase axial flux machine in order to achieve a certain degree of fault tolerance without compromising the high power density.
- It has been developed a methodology for the optimal design of a five-phase AFPM by means of a hybrid system combining analytical equations and 3D-FEM simulations, which has been scarcely analyzed in the technical literature, with special focus on the design of fault-tolerant motors.

5.1 LIST OF PUBLICATIONS

- **Journals**

- H Saavedra, J. Urresty, J Riba, L. Romeral, “Detection of Interturn Faults in PMSMs with Different Winding Configurations" Energy Conversion and Management. Volume 79, March 2014.
- H. Saavedra, J.-R. Riba, L. Romeral, "Detection of Inter-turn Faults in Five-Phase Permanent Magnet Synchronous Motors," Advances in Electrical and Computer Engineering, vol. 14, no. 4, pp. 49-54, 2014, doi:10.4316/AECE.2014.04008
- H. Saavedra, J.-R. Riba, L. Romeral, “Multi-objective Optimal Design of a Five-Phase Fault-Tolerant Axial Flux PM Motor “ submitted to Advances in Electrical and Computer Engineering.

- **Congresses**

- Urresty, J.-C.; Riba, J.-R.; Saavedra, H.; Romeral, L., "Detection of inter-turns short circuits in permanent magnet synchronous motors operating under transient conditions by means of the zero sequence voltage," *Power Electronics and Applications (EPE 2011), Proceedings of the 2011-14th European Conference on* , vol., no., pp.1,9, Aug. 30 2011-Sept. 1 2011
- Harold Saavedra, Jordi-Roger Riba and Luis Romeral,"Magnet Shape Influence on the Performance of AFPMM in a Torus Configuration" International Conference on Power Engineering, Energy and Electrical Drives. POWERENG 2013.
- Harold Saavedra, Jordi Riba, L. Romeral, “Inter-turn Fault Detection in Five-Phase PMSMs. Effects of the Fault Severity” IEEE International Symposium on Diagnostics for Electric Machines, Power Electronics and Drives. SDEMPED 2013.
- H. Saavedra, J.-R. Riba, L. Romeral, Magnet shape influence on the performance of AFPMM with demagnetization, IEEE Industrial Electronics Society (IECON), 2013.
- H. Saavedra, Jordi Riba, L. Romeral, “Optimal Design of a Three-Phase AFPM for In-Wheel Electrical Traction”, IEEE International Electric Vehicle Conference, IEVC 2014.

- **Collaborations in motor fault analysis and FEM simulations**

- Urresty, J.; Riba, J.; Saavedra, H.; Romeral, J., "Analysis of demagnetization faults in surface-mounted permanent magnet synchronous motors with symmetric windings," *Diagnostics for Electric Machines, Power Electronics & Drives (SDEMPED), 2011 IEEE International Symposium on* , vol., no., pp.240,245, 5-8 Sept. 2011
- Urresty, J.; Riba, J.; Romeral, L.; Saavedra, H., "Analysis of demagnetization faults in surface-mounted permanent magnet synchronous with inter-turns and phase-to-ground short-circuits," *Electrical Machines (ICEM), 2012 XXth International Conference on* , vol., no., pp.2384,2389, 2-5 Sept. 2012
- Hernandez-Guiteras, J.; Riba Ruiz, J.-R.; Saavedra, H., "Redesign of a spherical corona shield for UHV substation connectors," *Power Engineering, Energy and*

Electrical Drives (POWERENG), 2013 Fourth International Conference on , vol., no., pp.384,389, 13-17 May 2013

- R. Salehi Arashloo, M. Salehifar, H. Saavedra, L. Romeral, Efficiency Evaluation of Five-Phase Outer-Rotor Fault-Tolerant BLDC Drives under Healthy and Open-Circuit Faulty Conditions", AECE journal – Advances in electrical and Computer Engineering, vol. 14, May. 2014.

5.2 FUTURE WORK

Regarding the design of PMSM fault-tolerant motors, there are several aspects that should be further investigated. Specially, a good thermal analysis must be performed to allow us to determine the maximum available current in different operating modes. This analysis can be used to size the frame and duty cycle of the machine while operating under faulty conditions, and also can affect to design details.

Besides, mechanical analysis to know the forces and deformations in motor body, axis and bearings has to be performed as well. Under faulty conditions, and depending on the motor design, resulting electromechanical forces can force to modify the electromagnetic design, then affecting the optimal procedure proposed in this thesis.

All of these considerations should be verified on an experimental prototype, considering all electromagnetic, thermal and mechanical constraints, as a practical application of methodology of this Thesis.

Finally, the methodology here proposed could be extended to new motor types, as the emergent synchronous reluctance and hybrid permanent magnet assisted motors.

REFERENCES

[1] P. Van den Bossche, The Electric Vehicle: “raising the standards”, doctoral thesis, Vrije Universiteit Brussel, Faculty Toegepaste Wattenschappen Vakgroep Electrotechniek en Energietechniek, April 2003.

[2] Z.Q. Zhu, D. Howe, "Electrical machines and drives for electric, hybrid, and fuel cell vehicles," Proceedings of the IEEE , vol.95, no.4, pp.746-765, April 2007.

[3] M. Aydin, S Huang, T.A. Lipo, “Axial flux permanent magnet disc machines: a review”, Proc. of EPE PEMC’04.

[4] L. Parsa, H. A. Toliyat, “Sensorless Direct Torque Control of Five-Phase Interior Permanent-Magnet Motor Drives,” IEEE Trans. Ind. Appl., vol. 43, no. 4, July/Aug. 2007.

[5] A. Mohammadpour, S. Mishra, and L. Parsa, “Fault-Tolerant Operation of Multiphase Permanent-Magnet Machines Using Iterative Learning Control,” IEEE Journal of Emerging and Selected Topics in Power Electronics, vol. 2, no. 2, pp. 201-2011, June 2014.

[6] G. Cvetkovski, P. Lefley, L. Petkovska, S. Ahmed, “Optimal Design of a Novel Single Phase PM BLDC Motor Using Genetic Algorithm,” 15th International Power Electronics and Motion Control Conference, EPE-PEMC 2012 ECCE Europe, Novi Sad, Serbia, 2012.

[7] K. Zaplatilek, J. Leuchter, "System Optimization Using a Parallel Stochastic Approach," Advances in Electrical and Computer Engineering, vol. 13, no. 2, pp. 73-76, 2013

[8] L. Liberti, Se. Kucherenko, Comparison of deterministic and stochastic approaches to global optimization, International Transactions in Operational Research, vol. 12, no. 3, pages 263–285, May 2005

[9] M. Tabassum and K. Mathew, A Genetic Algorithm Analysis towards Optimization solutions, International Journal of Digital Information and Wireless Communications, vol. 4, no.1,pp. 124-142, 2014

[10] J. F. Gieras, R. Wang, and M. J. Kamper, Axial Flux Permanent Magnet Brushless Machines, 2004: Kluwer.

[11] C. C. Chan,"Axial-field electrical machines: Design and application", IEEE Trans. Energy Convers., vol. 2, no. 2, pp.294-300, 1987.

[12] D. N. Mbidi, K. van der Westhuizen, R.-J. Wang, M. J. Kamper and J. Blom "Mechanical design considerations of a double-stage axial-flux PM machine", Conf. Rec. 35th IEEE IAS Annu. Meeting, pp.198-201, 2000.

[13] F. Sahin. “Design and development of a high-speed axial-flux permanent-magnet machine”, PhD thesis, Eindhoven University of Technology, May (2001).

[14] A. R. Millner, "Multi-hundred horsepower permanent magnet brushless disc motors ", Proc. IEEE Appl. Power Electron. Conf. (APEC'94), pp.351-355 , 1994.

[15] E. Bomme, A. Foggia, T. Chevalier, "Double air-gaps permanent magnets synchronous motors analysis," Electrical Machines, 2008. ICEM 2008. 18th International Conference on Machines, vol., no., pp.1-5, 6-9 Sept. 2008

[16] M. Aydin, et al., "Design, Analysis and Control of a Hybrid Field Controlled Axial Flux Permanent Magnet Motor," IEEE Transactions on Industrial Electronics, 2010.

[17] T.-S. Kwon, S.-K. Sul, L., Alberti, and N. Bianchi, "Design and Control of an Axial Flux Machine for a Wide Flux-weakening Operation Region," in Record of the 42nd Industry Applications Conference, IAS 2007 IEEE, New Orleans, LA, pp. 2175-2182, Sept. 23-27, 2007.

[18] Y. Yee-Pien, L. Jia-Yuan, X. Xian-Yee, "Design and application of axial-flux permanent magnet wheel motors for an electric vehicle," AFRICON '09, pp.1-5, 23-25 Sept. 2009.

[19] L. Cheng-Tsung, L. Shih-Chao, JFD. Zamora, C. Tsung-Shiun, "Optimal operational strategy design of a single-sided permanent magnet axial-flux motor for electrical vehicle application," Industry Applications Conference, 2003. 38th IAS Annual Meeting. Conference Record of the , vol.3, no., pp. 1677- 1683 vol.3, 12-16 Oct. 2003

[20] D. Yao, S. Xiaodong, M. Krishnamurthy, "Health monitoring, fault diagnosis and failure prognosis techniques for Brushless Permanent Magnet Machines", Vehicle Power and Propulsion Conference (VPPC), pp.1,7, 6-9 Sept. 2011.

[21] J.-C. Urresty, J.-R. Riba, and L. Romeral, "Diagnosis of Interturn Faults in PMSMs Operating Under Nonstationary Conditions by Applying Order Tracking Filtering," IEEE Trans. Power Electron., vol. 28, no. 1, pp. 507-515, Jan. 2013.

[22] P. Arumugam, T. Hamiti, C. Gerada, "Analytical Modeling of a Vertically Distributed Winding Configuration for Fault Tolerant Permanent Magnet Machines to Suppress Inter-Turn Short Circuit Current Limiting," in Proc. IEEE International Electric Machines & Drives Conference IEMDC2011, 2011, pg. 371-376.

[23] M. Delgado, Contributions to Electromechanical Systems Diagnosis by Means Data Fusion Techniques l, doctoral thesis, Universitat Politècnica de Catalunya Electronic Engineering Department, October 2012.

[24] H. Polinder, H. Lendenmann, R. Chin, W.M. Arshad, "Fault tolerant generator systems for wind turbines," Electric Machines and Drives Conference, 2009. IEMDC '09. IEEE International , vol., no., pp.675-681, 3-6 May 2009

[25] B:C. Mecrow, A.G. Jack, J.A. Haylock, J. Coles, "Fault-tolerant permanent magnet machine drives," Electric Power Applications, IEE Proceedings - , vol.143, no.6, pp.437-442, Nov 1996

[26] C. Jahns, Thomas M.; , "Improved Reliability in Solid-State AC Drives by Means of Multiple Independent Phase Drive Units," Industry Applications, IEEE Transactions on , vol.IA-16, no.3, pp.321-331, May 1980

[27] A.G. Jack, B.C. Mecrow, 'Safety critical drives for aerospace applications'. Proceedings of the ICEM 1994, Paris, 1994, Vol. 1, pp. 91-96.

[28] A.G. Jack, B.C. Mecrow, J.A. Haylock, "A comparative study of permanent magnet and switched reluctance motors for high-performance fault-tolerant applications," Industry Applications, IEEE Transactions on , vol.32, no.4, pp.889-895, Jul/Aug 1996

[29] P.R. Upadhyay, K.R. Rajagopal, B. Singh, "Effect of armature reaction on the performance of an axial-field permanent-magnet brushless DC motor using FE method", Magnetics, IEEE Transactions on , vol.40, no.4, pp.2023,2025, July 2004.

[30] V. Ostovic, "Memory motors," Industry Applications Magazine, IEEE , vol.9, no.1, pp. 52- 61, Jan/Feb 2003

[31] L. Yuefeng; T.A. Lipo, "Sizing and optimal design of doubly salient permanent magnet motors", Sixth International Conference on Electrical Machines and Drives, pp.452-456, 8-10 Sep 1993.

[32] A.M. El-Refaie , "Fault-tolerant permanent magnet machines: a review," Electric Power Applications, IET , vol.5, no.1, pp.59-74, January 2011

[33] W.L. Soong, N. Ertugrul, "Field-weakening performance of interior permanent magnet motors," Industry Applications Conference, IEEE , vol.1, no., pp.416-423 vol.1, 2000

[34] J. A. Tapia , D. González , R. Wallace and A. Valenzuela "Axial flux surface mounted PM machine with field weakening capability", Int. Conf. Electrical Machines, ICEM'2004.

[35] M. Aydin, H. Surong, T.A. Lipo, "A new axial flux surface mounted permanent magnet machine capable of field control," Industry Applications Conference 37th IAS, vol.2, pp. 1250- 1257, 2002

[36] J.F. Gieras, 'Performance characteristics of a transverse flux generator'. IEEE Int. Conf. on Electric Machines and Drives, pp. 1293–1299, 2005.

[37]C. Smith, S. Williamson, and C. G. Hodge, "High torque dense naval propulsion motors," in Proc. IEEE IEMDC, pp. 1421–1427, Madison, WI. 2003.

[38]G. Aroquiadassou, H. Henao, S. H. Kia, and G. A. Capolino, "A spectral method of speed ripple analysis for a fault-tolerant six-phase squirrel cage induction machine," in Proc. Int. SDEMPED, Vienna, Austria, 2005, pp. 217–222. 2005.

[39]N. Bianchi, S. Bolognani, M.D. Pre, "Impact of Stator Winding of a Five-Phase Permanent-Magnet Motor on Postfault Operations," Industrial Electronics, IEEE Transactions on , vol.55, no.5, pp.1978-1987, May 2008

[40]E. Levi, "Multiphase Electric Machines for Variable-Speed Applications," Industrial Electronics, IEEE Transactions on , vol.55, no.5, pp.1893-1909, May 2008

[41]S. Mantero, A. Monti, and S. Spreafico, "DC-bus voltage control for double star asynchronous fed drive under fault conditions," in Proc. IEEE PESC, Galway, Ireland, pp. 533–538, 2000.

[42]C. Hodge, S. Williamson, A.C. Smith, ‘Direct drive marine propulsion motors’. Proc. Int. Conf. on Electrical Machines ICEM. Bruges, Belgium, CD-ROM paper 087 5. 2002.

[43]S. Smith, ‘Developments in power electronics machines and drives’, IEE Power Eng. J, 16, pp. 13–17, 2002.

[44] A.N. Golubev, S.V. Ignatenko, ‘Influence of number of stator-winding phases on the noise characteristics of an asynchronous motor’, Russ. Electr. Eng., ,vol 71, pp. 41–46, 2000.

[45]G. Jack, B. C. Mecrow and J. A. Haylock, “A comparative study of permanent magnet and switched reluctance motors for high performance fault-tolerant applications,” IEEE Transactions on Industry Applications, vol. 32, pp. 889-895, 1996.

[46]J. A. Haylock, B. C. Mecrow, A. G. Jack, and D. J. Atkinson, “Operation of a fault tolerant PM drive for an aerospace fuel pump application,” IEE Proceedings of Electric Power Applications, vol. 145, pp. 441 – 448, Sept. 1998.

[47]M. Naidu, S. Gopalakrishnan, T. W. Nehl, "Fault-Tolerant Permanent Magnet Motor Drive Topologies for Automotive X-By-Wire Systems", IEEE Transactions on Industry Applications, vol. 46, no. 2, March/April 2010

[48]M. Tabassum and K. Mathew, A Genetic Algorithm Analysis towards Optimization solutions, Int. Journal of Digit, Inf. Wirel. Commun. vol.4, no. 1, pp. 124–142, 2014.

[49]R. S. Devendran, A. Vacca, Optimal design of gear pumps for exhaust gas after treatment applications, Simul. Model. Pract. Theory, vol. 38, pp. 1–19, 2013.

[50]Y. Yee-Pien, L. Chung-Han, H. Po-Chang, "Multi-objective optimal design of an axial-flux permanent-magnet wheel motor for electric scooters”, Electric Power Applications, IET, vol.8, no.1, pp.1,12, January 2014

[51] L. Dong-Kuk, W. Dong-Kyun, K. Il-Woo, R. Jong-Suk, J. Hyun-Kyo, "Cogging Torque Minimization of a Dual-Type Axial-Flux Permanent Magnet Motor Using a Novel Optimization Algorithm”, IEEE Transactions on Magnetics, vol.49, no.9, pp.5106,5111, Sept. 2013

[52]S. Huang, J Luo, F. Leonardi, T. A. Lipo, “A Comparison of Power Density for Axial Flux Machines Based on General Purpose Sizing Equations”, IEEE Trans. Energy Conv., vol. 14, vo. 2, pp. 185-192, June 1999

[53]A. Mahmoudi, S. Kahourzade, N. A. Rahim, and W. P. Hew, “Design, Analysis, and Prototyping of an Axial-Flux Permanent Magnet Motor Based on Genetic Algorithm and Finite-Element Analysis,” IEEE Trans. Magn., vol. 49, no. 4, pp. 1473-1492, April 2013.

[54] J. Pippuri, A. Manninen, J. Keranen, K. Tammi, "Torque Density of Radial, Axial and Transverse Flux Permanent Magnet Machine Topologies", Transactions on Magnetics, IEEE, vol.49, no.5, pp.2339,2342, May 2013

[55] S. Grubic, J. M. Aller, L. Bin, T.G. Habetler. “A Survey on Testing and Monitoring Methods for Stator Insulation Systems of Low-Voltage Induction Machines

Focusing on Turn Insulation Problems". IEEE Trans Ind Electron, vol. 55, pp. 4127– 4136, 2008.

[56] J.C. Urresty, J.R. Riba, L. Romeral. "Detection of Stator Winding Inter-Turn Faults in Surface-Mounted Permanent Magnet Synchronous Motors by means of the Zero-Sequence Voltage Component". Electr Power Syst Res, vol. 89, pp. 38-44, 2012.

[57] S. Ruoho, J. Kolehmainen, J. Ikaheimo, A. Arkkio. "Interdependence of Demagnetization, Loading, and Temperature Rise in a Permanent-Magnet Synchronous Motor". IEEE Trans Magn. vol. 46, pp. 949–953, 2010.

[58] F. Briz, M. Degner, P. Garcia, A. Diez. "High-Frequency Carrier-Signal Voltage Selection for Stator Winding Fault Diagnosis in Inverter-Fed AC Machines". IEEE Trans Ind Electron, vol. 55, pp. 4181–4190, 2008.

[59] A. Gandhi, T. Corrigan, L. Parsa. "Recent Advances in Modeling and Online Detection of Stator Interturn Faults in Electrical Motors". IEEE Trans Ind Electron. vol. 58, pp.1564-1575. 2011.

[60] L. Hao, Y. Sun, A. Qiu, X. Wang. "Steady-State Calculation and Online Monitoring of Interturn Short Circuit of Field Windings in Synchronous Machines". IEEE Trans Energy Convers; vol. 27, pp. 128–138. 2012.

[61]A.M. El-Refaie, "Fractional-Slot Concentrated-Windings Synchronous Permanent Magnet Machines: Opportunities and Challenges". IEEE Trans Ind. Electron; vol. 57, pp. 107-121, 2012.

[62] J. Wu, Q. Zhu, D. Staton, M. Popescu, D. Hawkins. "Subdomain Model for Predicting Armature Reaction Field of Surface-Mounted Permanent-Magnet Machines Accounting for Tooth-Tips". IEEE Trans Magn,vol. 47, pp. 812-822, 2012.

[63] D.C. Hanselman, Brushless Permanent-Magnet Motor Design, Second Edition. Mc. Graw-Hill, New York; 1994

[64] C. Ruschetti, C. Verucchi, G. Bossio, C. De Angelo, G. García. "Rotor demagnetization effects on permanent magnet synchronous machines", Energy Convers. Manage., vol. 74, pp.1-8, 2012.

[65] L. Romeral, J.C. Urresty, J.R. Riba, A. Garcia, "Modeling of Surface-Mounted Permanent Magnet Synchronous Motors With Stator Winding Inter-Turn Faults". IEEE Trans Ind Electron, vol. 58, pp. 1576–1585. 2011.

[66] J.C. Urresty, J.R. Riba, L. Romeral. "Diagnosis of Inter-Turn Faults in PMSMs Operating Under Non-Stationary Conditions by applying Order Tracking Filtering". IEEE Trans Power Electron, vol. 28, pp. 507-515. 2013.

[67]J.C. Urresty, J.R. Riba, M. Delgado, L. Romeral, "Detection of demagnetization faults in surface-mounted permanent magnet synchronous motors by means of the zero-sequence voltage component". IEEE Trans Energy Convers, vol. 2, pp.42–51, 2012.

[68] Y. Huang, J. Dong, L. Jin, J. Zhu, Y. Guo. "Eddy-Current Loss Prediction in the Rotor Magnets of a Permanent Magnet Synchronous Generator with Modular

Winding Feeding a Rectifier Load". IEEE Trans Magn. vol. 47, pp. 4203-4206, 2011.

[69] B.-G. Gu, J.H. Cho, I. Jung. "Development and analysis of interturn short fault model of PMSMs with series and parallel winding connections", IEEE Trans Power Electr 2014, vol. 29, no. 4, pp. 2016-2026, 2011.

[70]J.-C. Urresty, J.-R. Riba, L. Romeral, "Diagnosis of Interturn Faults in PMSMs Operating Under Nonstationary Conditions by Applying Order Tracking Filtering," IEEE Trans. Power Electron., vol. 28, no. 1, pp. 507-515, Jan. 2013.

[71]J.-C. Urresty, J.-R. Riba, M. Delgado, L. Romeral, "Detection of demagnetization faults in surface-mounted permanent magnet synchronous motors by means of the zero-sequence voltage component," IEEE Trans. Energy Convers., vol. 27, no. 1, pp. 42–51, Mar. 2012

[72]R. M. Tallam, T. G. Habetler, R. G. Harley, "Transient model for induction machines with stator winding turn faults," IEEE Trans. Ind. Appl., vol. 38, no. 3, pp. 632–637, May-June 2002

[73]W. Le Roux, R. G. Harley, T. G. Habetler, "Detecting faults in rotors of PM drives," IEEE Ind. Appl. Mag., vol. 14, no. 2, pp. 23–31, March-April 2008.

[74]J.-C. Urresty, J.-R. Riba, L. Romeral, "A Back-EMF Based Method to Detect Magnet Failures in PMSMs," IEEE Trans. Magn., vol. 49, no. 1, pp. 591-598, Jan. 2013

[75]M .Aydin, M. Gulec, "Reduction of Cogging Torque in Double-Rotor Axial-Flux Permanent-Magnet Disk Motors: A Review of Cost-Effective Magnet-Skewing Techniques With Experimental Verification", IEEE Transactions on Industrial Electronics, , vol.61, no.9, pp.5025,5034, Sept. 2014

[76]A. Mahmoudi, S. Kahourzade, N. A. Rahim, and W. P. Hew, "Design, Analysis, and Prototyping of an Axial-Flux Permanent Magnet Motor Based on Genetic Algorithm and Finite-Element Analysis," IEEE Trans. Magn., vol. 49, no. 4, pp. 1473-1492, April 2013

[77]M. Aydin, S. Huang, T.A. Lipo, "Design and 3D electromagnetic field analysis of non-slotted and slotted TORUS type axial flux surface mounted permanent magnet disc machines," Electric Machines and drives Conference, 2001. IEMDC 2001. IEEE International , pp.645-651, 2001

[78]H. Saavedra, J.-R. Riba, L. Romeral, "Magnet shape influence on the performance of AFPMM with demagnetization," IEEE Industrial Electronics Society, IECON 2013, pp.973,977, 10-13 Nov. 2013

[79]P. Zheng , Y. Sui , J. Zhao , C Tong , T.A. Lipo, and A. Wang, "Investigation of a Novel Five-Phase Modular Permanent-Magnet In-Wheel Motor," IEEE Trans. Magn., vol. 47, no. 10, pp. 4084-4087, Oct. 2011

[80]J.A. Haylock, B.C. Mecrow, A.G. Jack, D.J. Atkinson, "Operation of fault tolerant machines with winding failures," IEEE Trans. Energy Convers., vol. 14, no. 4, pp. 1490–1495, 1999

[81]Y. Duan, D. M. Ionel, “A Review of Recent Developments in Electrical Machine Design Optimization Methods With a Permanent-Magnet Synchronous Motor Benchmark Study,” IEEE Trans. Ind. Appl., vol. 49, no. 3, pp. 1268-1275, May/June 2013

[82]R. Benlamine, F. Dubas, S-A. Randi, D. Lhotellier, C. Espanet, “Design by Optimization of an Axial-Flux Permanent-Magnet Synchronous Motor Using Genetic Algorithms,” International Conference on Electrical Machines and Systems, Busan, Korea, pp. 13-17, Oct. 26-29, 2013.

[83]K Brandisky, D Sankowski and R Banasiak, I Dolapchiev, “ECT sensor optimization based on RSM and GA”, COMPEL: The International Journal for Computation and Mathematics in Electrical and Electronic Engineering vol. 31, no. 3, pp. 858-869, 2012

[84]Q.-L. Deng, F. Xiao, W.-T. Huang, “Design of New-type Axial Flux Permanent Magnet in-Wheel Machine,” IEEE International Conference on Electrical and Control Engineering 2010, pp. 5831-5834, 2010

[85]M. T. Abolhassani, H. A. Toliyat, “Fault Tolerant Permanent Magnet Motor Drives for Electric Vehicles,” IEEE International Electric Machines and Drives Conference, 2009. IEMDC '09, Miami, Florida, 3- May 2009

[86]A.M. EL-Refaie, T.M. Jahns, ”Optimal Flux Weakening in Surface PM Machines Using Concentrated Windings,” 39th IEEE IAS Annual Meeting Industry Applications Conference, 2004. Conference Record of the 2004. Pp. 1038 – 1047, vol.2, 3-7 Oct. 2004

[87]112-2004- IEEE Standard Test Procedure for Polyphase Induction Motors and Generators, 2004

[88]G. V. Cvetkovski, and L. B. Petkovska, Weight Reduction of Permanent Magnet Disc Motor For Electric Vehicle Using Genetic Algorithm Optimal Design Procedure,” IEEE International Conference EUROCON 2009, pp. 881-888, 18-23 , St. Petesburg May 2009,